INDUCED POLARIZATION:

A GEOPHYSICAL METHOD

FOR

DETECTING METAL CONTAMINATED GROUND WATER

A Thesis

Presented in Partial Fulfillment of the Requirements for the

DEGREE OF MASTER OF SCIENCE

with a

Major in Geological Engineering

in the

GRADUATE SCHOOL

UNIVERSITY OF IDAHO

by

THOMAS D. KROM

May, 1988

AUTHORIZATION TO SUBMIT

THESIS

This Thesis of Thomas D. Krom, submitted for the degree of Master of Science with a major in Geological Engineering and titled "Induced Polarization: A Geophysical Method for Detecting Metal Contaminated Ground Water," has been reviewed in final form and approved, as indicated by the signatures and dates given below. Permission is now granted to submit final copies to the Graduate School for approval.

Major Professor Kenneth F Sprenke Date 6/6/88

Committee Members Roy E. Williams Date 5/30/88

Date 6/3/88

Department Administrator John Bush Date 6-6-88

College Dean R W Bartlett Date 6/7/88

GRADUATE SCHOOL FINAL APPROVAL AND ACCEPTANCE:

Graduate School Dean Jeanine M. Shreve Date 6/27/88

ABSTRACT

Induced polarization (IP) is a useful geophysical method for investigating metal contaminated ground water. Laboratory experiments show zinc, copper, and lead contaminated ground water produce induced polarization and/or resistivity anomalies. Field testing at Smelterville Flats, Cataldo Flats, and Bunker Hill Ltd.'s East Tailings Pond in the Coeur d'Alene River Drainage in Northern Idaho demonstrates usefulness of the technique in field studies. The field sites are contaminated by controlled, uncontrolled, and abandoned mineral resource wastes, jig and flotation tailings. IP response is different in coarse sediments and wastes, clay sized wastes, and clay sized natural sediments; furthermore, IP and resistivity responses are affected by man made debris and saturation variations. The geologic complexity of the river deposited wastes and sediments has confounded many investigations at the Smelterville Flats site. Sediment and ground water contaminant concentrations interact in controlling IP response. Further laboratory experiments and field tests incorporating bore-hole control are recommended to fully develop the potential of induced polarization in remedial waste investigations.

ACKNOWLEDGMENTS

First and foremost I wish to acknowledge the support and guidance from my major professor, Ken Sprenke. This work would not have been possible without the generous support of the University of Idaho Seed Grant Program, the Idaho Mining and Mineral Resource Research Institute, and U.S. Bureau of Mines Cooperative Agreement Number CO278001. Dr. Roy Williams was instrumental in arranging the latter source of support. Last, but certainly not least, I wish to thank all those who have helped me throughout my thesis work.

TABLE OF CONTENTS

LIST OF FIGURES AND TABLES

INTRODUCTION

Problem Definition

Recent increased demand within our society for clean water resources, both for public consumption and fisheries, points out many locations with contaminated water resources. A need exists for a geophysical technique that can detect metal contamination in hydrogeologic terrains. Dobecki and Romig (1985) stated in their review of geohydraulic applications of geophysics that ground water geologists will demand ground water quality from geophysicists. Further, they believe that environmental, economic, toxic waste storage, and underground storage tank stability investigations will dominate the future of engineering and ground water geophysics.

In the last hundred years, mining activities have contaminated ground water in locations throughout the Western United States. Resource Conservation and Reclamation Act (Super-fund or RCRA) legislation is evidence of public concern over fresh water resources. The serious problems associated with mining activities are demonstrated at Butte, Montana where tailings were deposited into the river drainage contaminating many miles of river valley ground and surface water. However, mining activities in the Western U.S.A. are not the only producers of metal contamination within the States. Metal plating facilities in eastern portions of the U.S. are common metal contamination sources. Induced Polarization (IP), an electrical geophysical technique, may be able to detect metal contaminated ground water.

IP may be more cost effective than conventional testing procedures. Resistivity, a related geophysical method, frequently does not provide useful information about subsurface contamination. The resistivity method is:

> "observing the direct current (DC) electric potential and current potential at the earths surface to detect subsurface variations in resistivity which may be related to ..., ground water quality,..., etc. (American Geologic Institute, 1976)."

Induced Polarization is most useful when the contamination problem is within an alluvial environment. These environments generally have an abundance of unevenly distributed clays and clay-sized deposits (fines). Fines, which usually have low resistivities, hinder resistivity surveys attempting to outline metal contamination, also indicated by low resistivity.

Point samples, drill holes or trenches, provide no information about the contamination between sample sites. IP may alleviate this problem. IP data will help correlate the information between point samples. Preliminary IP surveys will allow better choices when sampling sites are eventually required.

History of the Technique

IP has been used to map salt water intrusions (Ogilvy and Kuz'mina, 1972 and Seara and Granda, 1987) The technique responds to chemical and physical reactions produced by a dynamic electric field in the subsurface. Membrane polarization and electrode polarization are processes that account for most of the IP response (Marshall and Madden, 1959). Membrane polarization is a mechanism where an impedance is produced within the pores. Electrode polarization produces an impedance as current flows from pore walls into or out of the pore. Resistivity and IP are closely allied, IP is a measure of the dependance of the resistivity of a material on the alternating current frequency at which it is measured. Detecting metal contamination is an outgrowth of other hydrogeologic uses of IP. Vacquier and others (1957) used IP in ground water geophysical surveys. A long hiatus followed in the U.S.A. before further investigations on IP applications in ground water appeared. Ogilvy and Kuz'mina (1972) published their very

important paper on IP for saline water detection. Since Ogilvy and Kuz'mina's paper, numerous authors, here and abroad, have investigated and refined IP use in saline ground water investigations. Theoretical explanations of the IP response to saline contamination motivated my attempt to use IP to detect metal contamination. Roy and Elliott (1980) stated that IP is sensitive to an increased concentrations of active cations, which includes contaminant metals, and is insensitive to anion species concentration and type. This led to the hypothesis that IP can detect metal contamination.

IP measurements can be made in the phase domain, frequency domain, or time domain. Phase domain is a measurement of the phase delay of the measured voltage with respect to the applied current (rad.). Two frequencies are input to the ground at different times, a ratio of the transient voltages (%) is the frequency effect. Integrating the transient voltage versus time after the current is shut off is the time domain (msec.) (Van Blaricom, 1980). The time domain method is used in this study, mainly due to equipment availability. DC Resistivity and chargeability, the time domain voltage transient at 0.5 Hertz (IP effect), are the data collected in this time domain IP survey. IP measurements are made with an array of four electrodes. The electric field is established between two current electrodes. Observations are made at the two potential electrodes. The four electrodes can be arranged in several different configurations (Sumner, 1976). Each arrangement has advantages and disadvantages. The dipole-dipole array, a current and potential pair (dipole) with equal spacings, is used in this study. The dipole-dipole array is superior for defining horizontal changes which is more fully discussed below (figure 1).

Experimental Method

Two sets of tests compose this investigation. First, a series of lab experiments demonstrate that contaminated pore-water produces an IP anomaly.

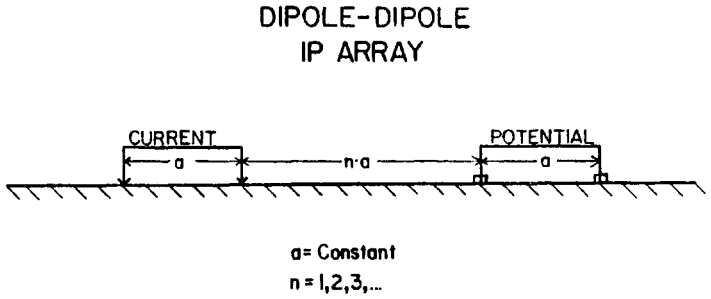

Figure 1. A-spacing and n description for a dipole-dipole IP/resistivity array

Second, field investigations in mineral resource wastes in the Coeur d'Alene Mining District in Northern Idaho show IP discriminates contaminated water in alluvial systems. Laboratory experiments in a scaled model show IP behavior in a controlled environment. The field investigations demonstrate the method's practicality in an actual contamination situation. Three types of mineral resource wastes are observed: waste contained within a waste containment facility (controlled tailings), waste material that was held in a waste containment facility and that have been abandoned (abandoned tailings), and material that was never held in a waste containment facility (uncontrolled tailings). The Coeur d'Alene Mining District has all three categories of wastes for testing IP. There are numerous investigations concerning the environmental hazard posed by the various wastes in the Coeur d'Alene District. Still, many active investigations are trying to characterize the complex problems in that polluted region. The extreme heterogeneity of the material deposited or reworked by the river at Smelterville Flats is why previous investigators, using point sampling techniques, encountered difficulties and arrived at different, or ambiguous,

conclusions. Monitoring wells and trenches are common point sampling methods used in hydrologic investigations to describe or determine if there is a contamination problem (a remedial investigation). These methods often do not reveal the true heterogeneity in the geologic material. IP and other geophysical methods can help prevent some of the these ambiguous conclusions.

The field data is very complex and required statistical treatment. Statistical analysis allowed me to interpret as much information as is impossible from the data. Several techniques I used were: semi-variograms, trend surfaces, contouring, and map comparison. The interpretation prior to statistical analysis could be very different from what is arrived at after analyzing the data.

Conclusions

This work is a preliminary study; however, important conclusions are reached. More laboratory and field work is needed to refine the induced polarization procedure, data collection and analysis, for work in metal contaminated areas. Secondly, a great need for improving the efficiency of investigations and monitoring programs can be realized by using IP. Finally, the contamination from mineral resource wastes is very complex in the Coeur d'Alene Mining District at Smelterville Flats.

LITERATURE REVIEW

Introduction

Vacquier and others in 1957 used induced polarization in the American Southwest for ground water exploration. They show the method is useful in geological materials with high clay content, low resistivity. They (Vacquier et al., 1957) suggested that other workers continue their efforts. Few papers concerning IP's use in ground water geophysical investigations were published in the U.S.A. until the early 1970's. Several exceptions do exist, one example is Henkel and Collins (1961). Serious development of IP for detecting saline ground water, which is the most common use for IP in hydrogeology, began with Ogilvy and Kuz'mina (1972). Recent work, 1980 to date, concerns the causes of IP responses, quantitative results from IP data, and subsurface interpretations. A significant portion of the recent literature concerns the use of IP in different materials.

Pre-Ogilvy and Kuz'mina

Vacquier and others (1957) used IP to explore for potable ground water. They observed that IP responds to changes in important aquifer system properties. They did not present any mathematical models within this 1957 paper. Vacquier and others observed that ground water, geologic media, and IP are interrelated in a complicated manner:

> "The magnitude of the induced polarization depends in a complicated way on the resistivity of the solution, on the amount and kind of clay, and on the particular cation saturating the clay. In general, when the concentration of the electrolyte is changed, the cation population is changed not only in the liquid but also in the clay. Unless the clay is saturated with the cation of the solution, the induced polarization is not a single-valued function of the electrolyte, but slowly drifts to a constant value as the clay-electrolyte equilibrium is reached. Generally the polarizability decreases with decrease in resistivity, so that clay banks and saline waters should give small effects.
>
> The dependance of polarization on the amount of clay is

> complex; for amounts greater than three percent it depends on whether the clay is flocculated or dispersed."

They observed that polarizability is "roughly" proportional to the ion exchange capacity of clays. The clay's affinity for the particular cation affects the magnitude of the polarization. Vacquier and others (1957) also noted that a complete explanation of the various mechanisms would not "be forthcoming in the near future." Experiments with cations and anions, chlorides, sulfates, phosphates, and carbonates, showed that IP is almost insensitive to anion species. However, cations do have a strong influence on the IP response. A polarization is produced at constrictions in the pores where clay coatings on sand grains and their "loosely held" cations form effective membranes, filters for flowing cations. They (Vacquier et al., 1957) described the voltage (E) across the membranes, which produces a polarization, with the Nerst equation:

$$E = \{ [(RT)/(nF)] [\ln(c_1/c_2)] \}$$

where T is temperature (Kelvin), R is the universal gas constant, n is ion valence, F is Faraday's constant, and c is the concentrations on either side of the membrane. Electrolyte concentrations do not affect the rate of decay of the polarization, only the magnitude of the polarization is altered.

Marshall and Madden (1959) presented a comprehensive review of mechanisms that produce IP effects. They compared the magnitude of the various mechanism, electro-osmotic, thermal coupling, membrane polarization, and electrode polarization. Electro-osmotic coupling is solvent flow through a capillary caused by an electric current flow (Marshall and Madden, 1959). Thermal coupling is a heat flow caused by a current flux. Marshall and Madden concluded that only the mechanisms generally referred to as membrane polarization and electrode polarization are significant. Membrane polarization occurs during diffusion coupling, flowing ions carry the

current flow in the x direction. This flow (J) is initiated by the potential gradient (E), voltage difference, between two electrodes on the surface.

$$J_p = - [D_p \, \partial p/\partial x] + u_p pE$$

$$J_n = - [D_n \, \partial n/\partial x] + u_n nE$$

U = mobility p = cation concentration

D = diffusion coefficient n = anion concentration

$t^+ = U_p/(U_p+U_n) = D_p/(D_p+D_n)$ = cation transfer number

$t^- = 1 - t^+$ = anion transfer number.

If t^+ varies in the direction of current flow, concentration gradients will build up. Retarding ion flow is an impedance to current flow. Diffusion, after current cessation, occurs to dispel the concentration gradients and produces a transient voltage, the membrane polarization effect. Electrode polarization is described as a chemical capacitance, due to an accumulation of reactant products, and Warburg impedance, a diffusion and frequency related impedance for supplying reactants to redox reactions at metallic mineral pore walls (Marshall and Madden, 1959). They stated that the separation of electrode and membrane polarization effects is generally not possible. This problem arises because both are diffusion processes and behave similarly.

Henkel and Collins (1961) studied the IP response of "saturated earth plugs" using different solution concentration. Saturated earth plugs are samples taken into a lab and subsequently saturated with known solutions for laboratory tests. They tested two models in their study. Henkel and Collins were proving a model where solution conduction paths are in parallel with a series conduction path of clays and solution (figure 2). They describe the IP mechanism as:

$$V_{op}/V_{1p} = Hr_w/[r_w + B]$$

where V_{op} is the out of phase voltage, V_{1p} is the potential difference across the sample H is a constant, r_w is solution resistivity, and B is a factor dependent on cell dimensions and clay resistivity. The out of phase voltage is a measure of the polarization. Additionally, they disproved a second model where electric dipoles associated with clays explains the IP effect. Henkel and Collins (1961) observed several factors that are important. First, parallel/series conduction path models provide a better explanation of IP phenomena than models based on polarized clay particle behavior. Second, IP phenomena does not vary linearly with respect to solution resistivity. Lastly, they questioned the validity of observations by previous investigators that low electrolyte concentrations produce large IP anomalies, deviations from a background or regional value. Henkel and Collins (1961) stated that experiments at low concentrations do not produce repeatable results. Their observations that the polarization decays according to a diffusion law supports Marshall and Madden's (1959) statement that IP mechanisms are diffusion mechanisms.

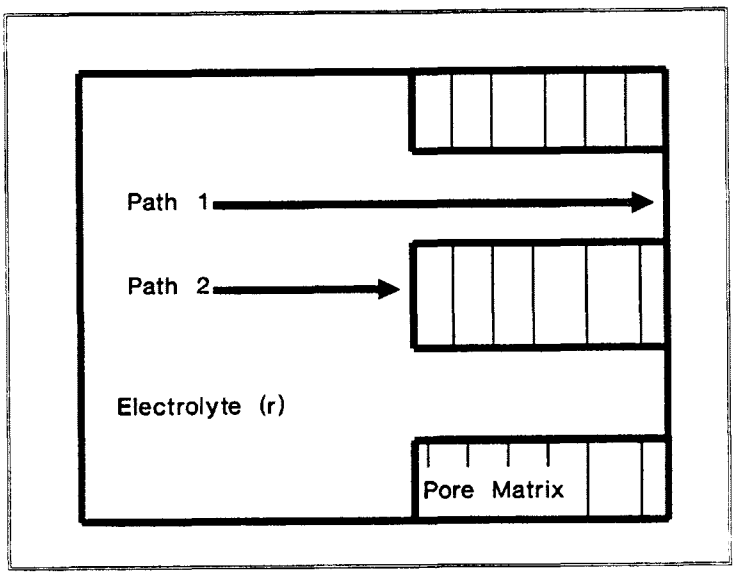

Figure 2. Parallel/Series conduction model used to simulate IP. (Henkel and Collins, 1961)

Keevil and Ward (1962) pointed out the differences between cell polarization, effects at individual point within a rock volume and rock polarization, a volumetric integration. They (Keevil and Ward, 1962) observed that it is impossible to describe the polarization at each point within a rock mass. Researchers should and can only describe processes occurring with respect to volumes of rock. Changing a parameter will affect the many IP mechanisms in different ways but have a single effect on the rock volume of interest. They showed experimentally that measures of IP are affected by electrolyte activity, or effective concentration (Hem, 1970), and the matrix material. Matrix material is the minerals and other material composing the laboratory sample or field site geology. Keevil and Ward were mainly interested in how changes in activity with depth would affect the interpretation of sulfide targets. They observed that sulfide mineral oxidation, pyrite oxidation is an example, produces significant activity gradients with depth, and consequently significant IP gradients with depth.

Bodmer and others (1968) discuss using IP to classify unconsolidated sediments in hydrogeologic investigations. Specifically they were looking to delineate clay contaminated units from non-contaminated lithologies. "The absence of an IP anomaly will therefore mean either clean gravel, dense clay, sandy clay, or perhaps gravelly clay." They compared IP field data from several sites with bore hole data to substantiate their claim.

Ogilvy and Kuz'mina (1972) took huge strides in advancing IP's usefulness in ground water investigations. Their laboratory testing showed IP discriminated between saline and potable zones within aquifers. They observed a decrease in polarizability up to 10,000 mg/L at which point their equipment could not measure the IP effect. IP decreases with an increase in cation valence. Their discussion implies that IP effects from different factors, soil moisture, salinity, cation species, grain size and shape, and

so on, are cumulative. Ogilvy and Kuz'mina (1972) recorded IP lows in response to saline contamination. Field work in areas with saline intrusion demonstrated that IP behaves similarly in the field. Unfortunately, laboratory experiments showed that many geologic variables affect the IP response. To quote the authors:

> "The laboratory experiments have proved the dependence of induced potentials of sandy-clayey media on their particle-size distribution pattern, porosity, moisture content, interporous moisture, salinity degree and temperature."

However, these observations reveal that IP could discriminate changes in each of these variables as needed in hydrologic investigations. Ogilvy and Kuz'mina (1972) noted that the maximum effect from clays occurred with clay fractions from 3 to 20 percent dry weight. These authors also observed an IP high in response to the capillary fringe, the zone above the water table with pore pressures less than atmospheric. The high due to the decreased moisture content, the capillary fringe effect, may have important consequences in ground water exploration using IP.

Post-Ogilvy and Kuz'mina

Angoran and Madden (1977) studied the effect of in-situ chemistry of electrolytes on electrode polarization. A variety of common mineral ions were tested in solution. Cupric and sulfide ions in concentrations greater than 10^{-4} N control the electrode impedance, an impedance at the pore wall which behaves similar to an electrode. Angoran and Madden describe electrode polarization as impedance mechanisms. They attribute some electrode polarization to chemical impedances produced by reactant depletion and product accumulation at the electrode, pore wall:

$$Z_i = [a_i^2/F^2n^2]\ Z_{chem\ i}$$

and

$$Z_{chem\ i} = F\ \Delta m_i\ n\ [-a_i\ i]^{-1}$$

where Z's are impedances, F is Faraday's constant, n is the number of electrons involved in redox reaction, i is current density, m_i is the chemical potential of the i^{th} species, and a_i are stoichiometric constants. The Warburg impedance (Z_W) produced by diffusion between the electrolyte and reaction sites controlling the availability of ions to redox reactions is described explicitly:

$$Z_W = RTa_i^2 \, [n^2 A_i F^2 \, \{j\Omega D\}^{0.5}]^{-1}$$

where R is the universal gas constant, T is temperature (Kelvin), A_i is the activity of the i^{th} species, Ω is frequency, D is the diffusion coefficient, and j is the square root of -1. Diffusion of ionic species of the mineral surface, to satisfy redox requirements, produces an impedance:

$$Z_{Wsurf} = \left| \frac{a_i^2 \, R \, T}{[A_i]_{surf} F^2 \, (j\Omega D_{surf})^{0.5} \tan[h(X_o(j\Omega/D_{surf})^{0.5})]} \right|$$

where X_o is the distance separating reaction zones, and the subscript surf indicates a surface property. Important to this study is Angoran and Madden's observation that pyrite and associated minerals produced no effect. Electrode polarization is not altered by the dissolution of pyrite. Ore minerals other than copper and iron were not examined.

Roy and Elliott (1980) attempted to make a qualitative judgement on aquifer salinity based on combined IP and resistivity sounding data. The most important value of this paper is large number of soundings presented in different geologic situations and the comparison of results from different sounding techniques. Their judgement is when IP drops below 3 msec. (time domain) and apparent resistivity decreases are observed this is diagnostic of saline ground water. However, Roy and Elliott show NaCl concentrations of 2000 mg/l or greater when IP values are 3 msec. and below, generally water is not potable at total dissolved solids values greater than 1000 mg/l. Also, Seara and Granda (1987) recorded data with values less than 3

msec. in zones without saline ground water. General conclusions that decreases in both IP and resistivity indicate saline zones seem reasonable; however, the 3 msec. observation probably does not have as wide spread an applicability as they suggest. Careful review of their own paper suggests this as Roy and Elliott record different time domain IP measurements at different frequencies.

Granda Sanz and Sastre Pascual (1982) reviewed ground water IP studies and presented a case history. The case history provides interesting information on IP's capabilities in site investigations. This paper, in spanish, provides a good review of the work done up to 1980/1981 and suggestions for field operations.

Klein and others (1984) studied IP phenomena to clear up questions about the active mechanisms for electrode polarization. Klein and others failed to do this when their investigation revealed both proposed mechanism can produce an IP anomaly. They successfully show that in <u>most</u> cases diffusion involving dissolved ionic species to supply ions to redox reactions are not responsible for electrode polarization; although in some cases it apparently is the dominant mechanism. Laboratory experimental equipment was designed to test diffusion layer thickness's importance. The diffusion layer is the zone along the pore wall where diffusion can occur. Klein and others laboratory apparatus could rotate the electrode surface thereby shortening the thickness of the diffusion layer. If diffusion to or from the electrolyte is important the speed of rotation will alter the polarization effect due to Warburg impedance:

$$Z_{Wrotate} = Z_W \tanh(L(j\Omega/D)^{0.5}$$

and

$$L = 0.64\ D^{1/3}\nu^{1/6}\omega^{-1/2}$$

where v is kinematic viscosity, and W is rotation speed. They observed in most cases polarization was not a function of speed of rotation. Impedances due diffusion along the surface produce the correct frequency dependance and therefore are the most common mechanisms for electrode polarization. Klein and others (1984) work demonstrated that models based on Warburg impedance are usually incorrect or incomplete descriptions of electrode polarization phenomenon. This work shows that electrolyte concentration changes will have a small effect on electrode polarization observations.

Laboratory and field tests with core samples and bore-hole control respectively produce more general conclusions on IP behavior as a function of saturation, cation valence, solute concentration, and hydraulic conductivity (Olorunfemi and Griffiths, 1985). Although some of Olorunfemi and Griffiths' work is a repeat of work done by Ogilvy and Kuz'mina they present some interesting results and information. Olorunfemi and Griffiths showed that IP response is non-linear with respect to contaminant concentration. Also, Olorunfemi and Griffiths demonstrate that IP is a function of cation valence (figure 3). Smaller valences produce larger variations with changes in concentration while larger valences tend to produce deeper IP lows at most concentrations. Olorunfemi and Griffiths state that IP and hydraulic conductivity are related by a logarithmic relation:

$$IP = m \log K + c$$

where IP is the units induced polarization measured in percent, frequency domain, m and c are regression constants, and K is hydraulic conductivity in mm/s. Hydraulic Conductivity strongly effects IP at low concentrations, less than 200 mg/L, in a laboratory setting (figure 4). Olorunfemi and Griffiths performed a linear regression analysis of hydraulic conductivity versus IP (%) effect. They found good correlations, correlation

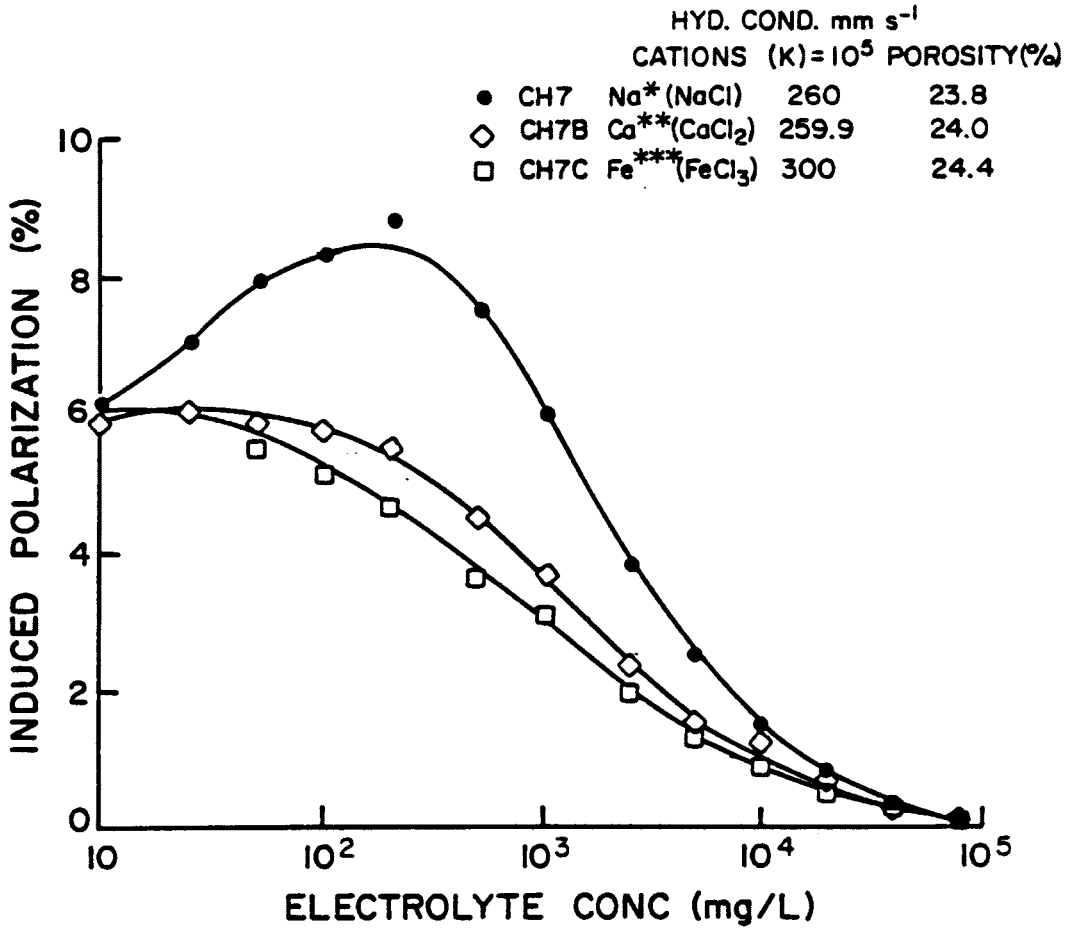

Figure 3. Shows IP is a function of cation valence in samples from the same geologic unit with similar hydraulic conductivities (Olorunfemi and Griffiths, 1985).

coefficients greater than 0.7, for concentrations of NaCl less than 100 mg/L. Correlation coefficients decrease in value as the salt concentrations increase (table 1). Cores from a bore-hole at the field site were used with varying electrolyte concentrations to form a predictive curve, conductivity versus electrolyte concentration:

$$s_w = [s_r - 10^{((IP-b)/a)}]F$$

and from their laboratory work,

$$s_w = [s_r - 10^{-0.122(IP+8.66)}]F$$

where s is conductivity in seimes, IP is frequency domain IP effect (%), F is the true formation factor, a and b are empirical constants, and the subscripts r and w represent rock and electrolyte respectively (figure 5). Field tests with bore-hole control show this relation held up moderately well.

Olhoeft (1985) in his study on the low frequency electrical properties of geologic media suggested the use of IP to detect organic chemicals contaminating the ground water. He observed organic compounds interfere with the cation exchange processes in redox reactions on clays. IP is a measure of low frequency electrical properties of geologic media. Cation exchanges for redox reactions and the oxidation-reduction reactions are also important in IP effects. Metal concentrations above or below a sites average will alter these processes producing IP anomalies. Olhoeft (1985) observed IP effects at more than 20 different frequencies for each sample, 0.001 Hz to 1 MHz, recording data on especially designed equipment. This equipment measured the real part of the complex resistivity, which is an IP effect, the phase shift between transmitter and receiver, and total harmonic distortion which is a measure of the difference in the harmonic, frequency, content of the input and output signals. While the techniques Olhoeft used are not available to this study his work in conjunction with Olorunfemi and

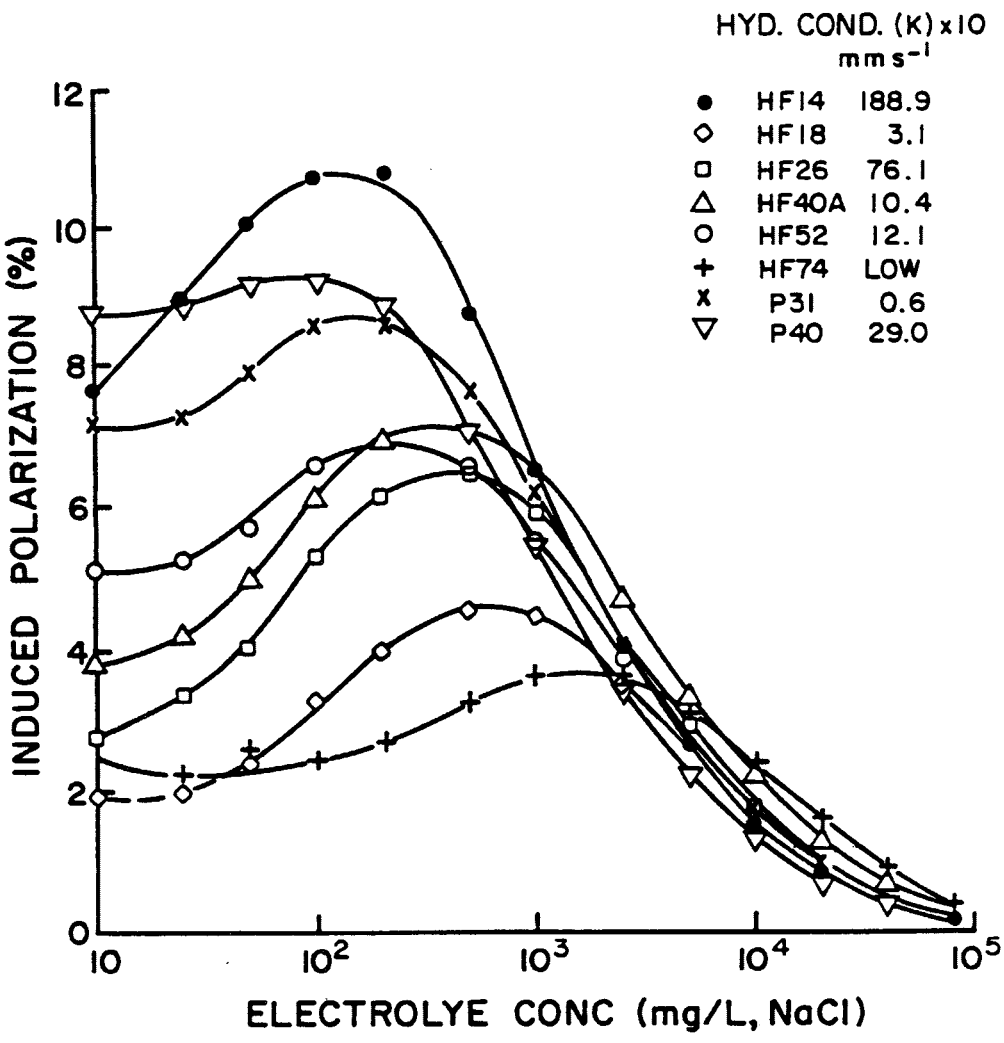

Figure 4. IP effect versus electrolyte concentrations for samples with different hydraulic conductivities (Olorunfemi and Griffiths, 1985).

Table 1. Correlation coefficients and electrolyte conductivity from Olorunfemi and Griffiths' (1985) linear regression analysis for IP versus hydraulic conductivity.

Electrolyte Concentration (mg/L NaCl)	Electrolyte Conductivity (seimes)	Correlation Coefficient
10	0.0020	0.73
25	0.0050	0.78
50	0.0096	0.76
100	0.0183	0.72
200	0.0354	0.66
500	0.0880	0.43
1000	0.1770	0.02

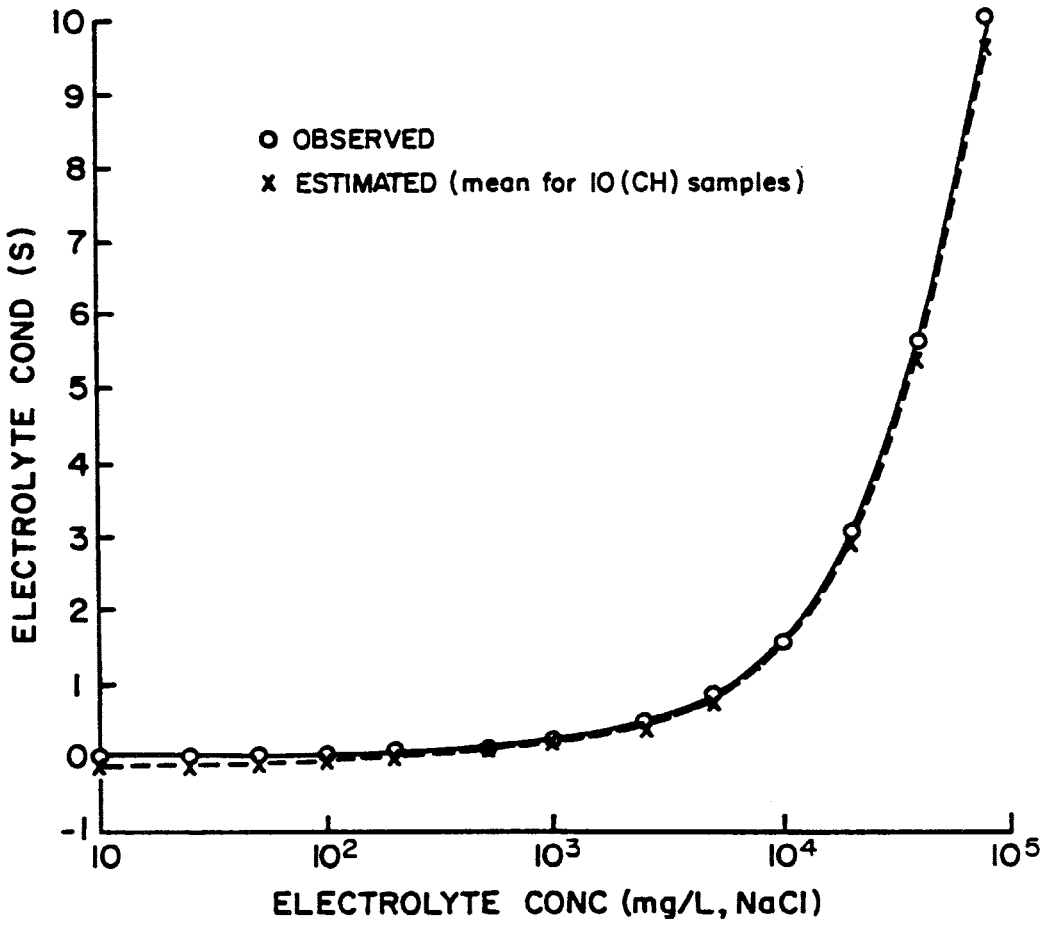

Figure 5. Graphical representation of data and theoretical curve expressing electrolyte concentration as a function of pore fluid conductivity (Olorunfemi and Griffiths, 1985).

Griffiths (1985) data provided some of the best proof that IP should detect metal contaminated ground water.

Electrolyte resistivity may not have a great affect on electrode polarization measurements made in the time domain, millivolts-seconds/volt, at low frequencies, less than 1 Hz. Mahan and others (1986) studied the IP characteristics of sulfide bearing rocks, one parameter they varied is the electrolytes' resistivity while the mineralized sample, a manufactured rock, is constant. The IP phase spectrum shifts towards higher frequencies as the electrolyte resistivity decreases. This apparently is only important at higher frequencies. However, Mahan and others (1986) data sets are not very complete at low frequencies, less than one Hz.

The importance of recent developments in IP equipment is shown in a paper by Seara and Granda (1987). These consultants performed 87 IP vertical electric soundings (IPVES) in Spain to map out salt contamination of municipal aquifers along the Mediterranean coast. IPVES is using progressively larger IP arrays with the same center point so that information is obtained about deeper conditions at a constant location. Although field data correlate well with observation well information they (Granda and Seara, 1987) stressed that information was lost because phase domain equipment was not available to their study. Phase domain curves provide a great deal on information on salt content and lithology (Ogilvy and Kuz'mina, 1972).

Induced polarization literature, concerning theoretical, laboratory, and field investigations, suggests that IP should be an excellent technique for detecting metal contaminated ground water in alluvial terrains, if not elsewhere. IP should detect metal contaminated ground water in geologic media. Recently, oil and gas exploration are utilizing IP to an ever greater extent. Phase domain induced polarization is commonly used in the

most innovative IP projects. Unfortunately phase domain equipment was not readily available for this project. The information imparted using phase domain techniques would have improved the quality of the results in this investigation.

INDUCED POLARIZATION THEORY

Introduction

Metal cations contaminating the ground water environment alter the IP effect. IP theory illustrates why this effect occurs. Induced Polarization responses from contaminant metals in the ground water are either greater or less than the regional background. Large response variations result from many physical processes within the subsurface. Understanding IP theory assists interpreting field data.

The theory of induced polarization is poorly understood. This is partially due to the numerous mechanisms which produce IP effects. A significant percentage of the observed response is produced by two mechanisms (Marshall and Madden, 1959). The dominant processes in producing IP effects are membrane polarization (Vacquier, et. al., 1959) and electrode polarization (Angoran and Madden, 1977). These two dominant processes are affected by varying any of several physical parameters. Electrolyte composition, degree of saturation, and the amount of heterogeneity exhibited in pore wall composition, are important subsurface parameters controlling IP response (Ogilvy and Kuz'mina, 1972; Marshall and Madden, 1959; Angoran and Madden, 1977; Roy and Elliott, 1980; and Olhoeft, 1985).

Ascertaining the specific physical and chemical changes that produce the observed IP response is difficult. Chemical and physical reactions in the subsurface are driven by the dynamic electric field induced by electrodes on the surface. The recorded effect is an integration of all the processes and their distribution, relative to the local current density, in the subsurface (Marshall and Madden, 1959). Interpretations of the IP response require knowing the distribution of the current density in the subsurface. Contrasting electrical properties, such as resistivity, between

layers and these layers thicknesses control the electric field distribution. (Roy and Elliott, 1981)

Membrane Polarization

Membrane polarization is an electrolyte filled pore's response to a dynamic electric field. Literature concerned with using IP for mineral exploration refers to membrane polarization as a background effect. An electric field produces an ion flux, cations and anions, in the pores (Marshall and Madden, 1959). An ion flow (J) carries the current in the x direction and is driven by the potential gradient (E) across the pore:

$$J_p = - [D_p \, \partial p/\partial x] + u_p pE$$

$$J_n = - [D_n \, \partial n/\partial x] + u_n nE$$

Diffusion, after current cessation, dispels concentration gradients that will arise due to changes in the cation transfer number along the pore. These equations did not prove very useful to my investigation, because $\partial p/\partial x$ is one parameter we are attempting to define. Ion flux is proportional to the local current density which is related to the electric field strength. The ion flux rate is controlled by changes in the pore wall material along the current flow lines. Pore wall material changes alter the cation transfer number along the pore (Sumner, 1976 and Marshall and Madden, 1959). Different pore wall materials allow different ion flow rates at a constant current density. Ion flux is a combination of both the current density and pore wall material distribution. Empirical tests show that solute concentration and solute properties affect membrane polarization (Ogilvy and Kuz'mina, 1972 and Olorunfemi and Griffiths, 1985).

The relation between solute concentration and IP response is complex. First, IP responds non-linearly to changes in solute concentration (figure 4 and 6). The geologic formation plays an important role in controlling IP response at low electrolyte concentrations (figure 4). This is not

surprising as IP is a strong function of the interaction of the pore water and lithology as is discussed above and below. An exact description of why and how changing concentrations affect membrane IP response is not available. Solute properties are involved in this too (figure 3 and 7). Cation valence is the most important solute characteristic. Comparing figures 7 and 3 reveals that the effects of cation valence are greater than those produced by hydraulic conductivity changes.

Geologic porous media do not have homogeneous pore wall mineral composition. Surface-active minerals, which allow or support redox reactions on their surface, act as membranes retarding the flow of ions. These materials which can form electrochemical membranes are clays or metals. Silica typifies minerals which can not act as membranes. However, clay or surface active mineral coatings on most any mineral may act as a membrane. Surface-active minerals reduce the ion flux causing zones with increased ion concentrations. Roy and Elliott (1980) have shown that IP is relatively insensitive to the particular anions in solution. Cessation of the electric current leaves ions unevenly distributed in the pores. These ions diffuse to a more stable distribution which generates a current. The current produces a changing voltage difference across the potential electrodes resulting in the IP effect.

Electrode Polarization

Electrode polarization is an electrochemical and physical response from current flowing from the pore wall minerals and metals into and out of the electrolyte. The observed IP effect depends on the interfaces between the pore wall and electrolyte. Important characteristics include pore wall composition, solute concentration, solute properties, and electric field strength (Olhoeft, 1985).

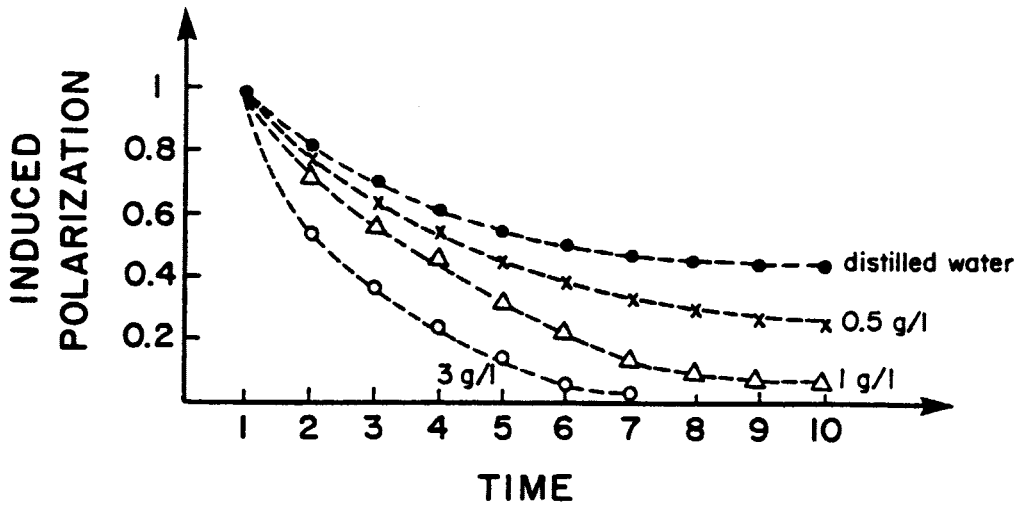

Figure 6. Induced Polarization as a function of electrolyte concentration (Ogilvy and Kuz'mina, 1972).

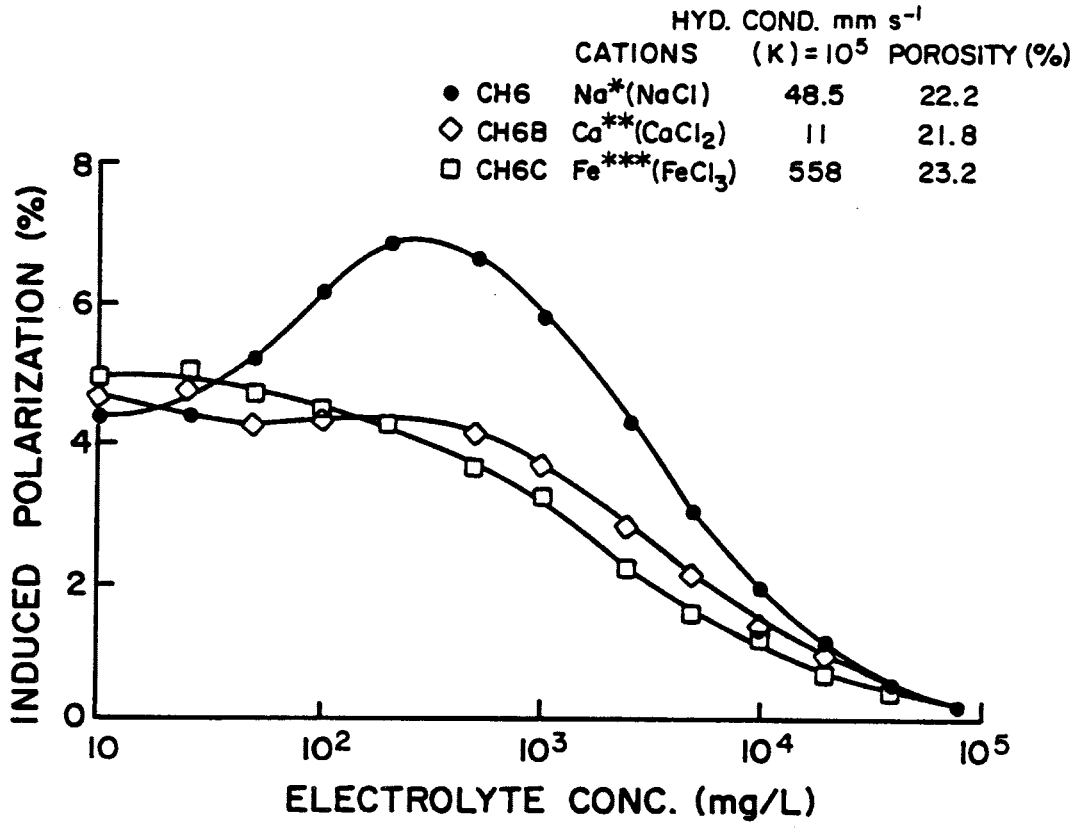

Figure 7. Shows IP is a function of cation valence in samples from the same geologic unit with different hydraulic conductivities (Olorunfemi and Griffiths, 1985).

Current flowing into or out of the wall produces the electrode polarization effect. Ions in solution and along the pore wall respond to the introduction of an electric field through oxidation-reduction reactions and diffusion at and along the pore wall (Angoran and Madden, 1977 and Klein et al., 1984). The method is insensitive to the particular anion(s) in solution (Roy and Elliott, 1980). Cation concentrations increase, at the pore wall, to provide positive ions required for the redox reactions (Olhoeft, 1985). The rate the cations go towards the pore wall is controlled by the diffusion rate. Diffusion limitations control the redox process, this produces an impedance which results in an IP effect (Angoran and Madden, 1977). The Warburg impedance produced by diffusion controlling cation flow and is described explicitly (Angoran and Madden, 1977):

$$Z_W = RT\ {}_i{}^2[n^2 A_i F^2 \{j\ D\}^{0.5}]^{-1}$$

where Z_W is the Warburg impedance, R is the gas constant, T is temperature, is a chemical property constant particular to each cation, n is the integer number of electrons in the redox reaction, A is a species chemical activity, F is Faraday's constant, j is the square root of -1, is frequency, and D is diffusivity, a measure of the diffusion rate. However, pure Warburg impedance is exhibited only when the pore wall material is pure graphite (Olhoeft, 1985). Klein and others (1984) failed to show that Warburg impedance is not the mechanism producing electrode polarization. However, they successfully showed that in most cases diffusion reactions involving aqueous species, Warburg impedance, are insufficient descriptions of electrode polarization phenomenon. Laboratory experiment design controls suggest a mechanism where diffusion layer thickness is not important, ie. surface diffusion, which has the correct frequency dependance. This work provides credence to the assumption that electrolyte concentration changes will have at best a small effect on electrode polarization observations,

especially at low frequencies (Mahan et al., 1986). Cations with different valences have different IP responses; increased valence requires fewer atoms to satisfy the redox or surface diffusion requirements. Cation reactions at the pore wall are observed as voltage gradients. These gradients relax on current cessation as a function of time. Decreasing potential gradients from cation flow generate the emf observed at the potential electrodes. Emf variation in time and magnitude and impedance relaxation are the IP effect. Chemical characteristics of the solutes occasionally control the decay of the gradient.

Current Density

The intensity of the current at the pore wall is a function of the pore wall material and the resistivity of the surrounding geologic media. The current density is a function of the resistivity of over- and under-lying geologic material. Low resistivity material overlying comparatively higher resistivity material causes most of the current to flow in the low resistivity material. This process results in low current densities at depth. Similarly, a high resistivity layer or zone overlying a low resistivity volume will restrict the amount of current entering the low resistivity unit. Roy and Elliott (1980) presented several researcher's opinions on the depth investigated versus the array size (AB). AB is the distance between the furthest electrodes. These observations vary from 1/2 AB to 1/9 AB (Evjen, 1938 and Roy and Apparao, 1971 in Roy and Elliott, 1980). The principle of reciprocity states that interchanging current and potential electrodes will produce the same results (Sumner, 1976).

Current density and voltage gradient distributions are intimately related. In homogeneous materials, current flow lines from a dipole-dipole array are ellipsoidal (figure 8). The distance between two flow lines represents the current density, smaller spacings mean a greater current

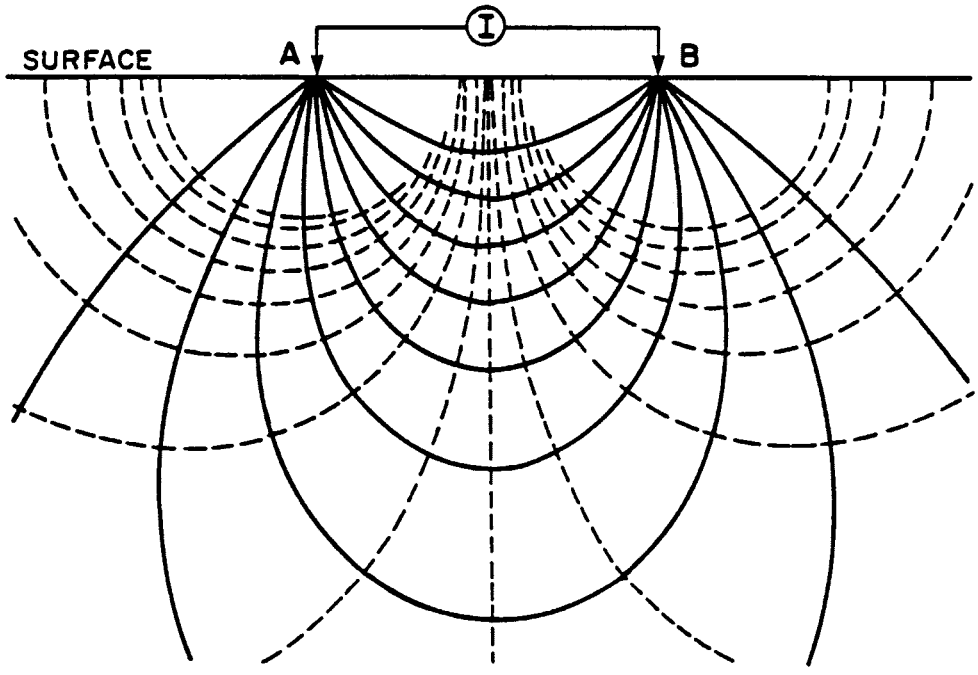

Figure 8. Current flow lines and equipotential lines in an isotropic media due to a dipole current source (Sumner, 1976).

density. Equipotential lines represent the voltage gradient. The voltage difference between any two adjacent equipotential lines is a constant (figure 8). An increased spacing between adjacent equipotential lines indicates the voltage gradient is decreased.

The effects of resistive or conductive bodies within a region of relatively constant resistivity and IP behavior is of greater interest. Figure nine A shows a conductive body within a more resistive unit. Note: the equipotential, or equivoltage, line separation increases in the body while decreasing around the body. Current flow lines are closer together within the conductive body (Sumner, 1976). Opposite behavior is observed in a resistive body in a conductive medium (figure 9b). Current density increases within a conductive body, evident by the close spacing of flow lines, while the voltage gradient deceases (figure 9a). Current density decreases while the voltage gradients increase in resistive bodies (figure 9b).

Process Integration and Other Factors

The complexity of IP chemistry and physics hinder interpretation of the field data. Determining the relative importance of the individual processes, membrane and electrode polarization, is not at all simple. Determining which factors are influencing the IP effect is nearly impossible using only time domain IP data. Hydrogeologic information is imperative for an accurate interpretation(s) of field data. The non-linear performance of IP mechanisms under changing cation concentrations is responsible for the difficult interpretations. Changes in any of the parameters affect the system in a non-linear fashion. Pore diameter is a good example, pore diameter changes alter membrane and electrode polarization. Altering pore diameter changes the surface area, significant for electrode polarization, in a complicated manner. Membrane polarization magnitude is very dependent

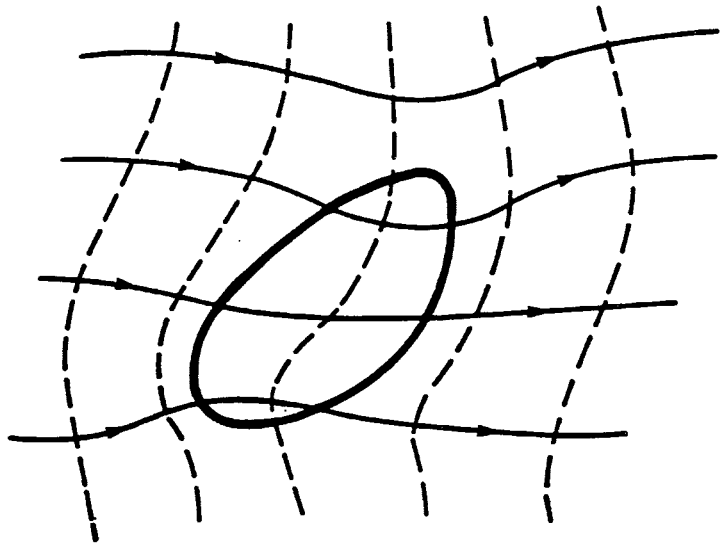

(a)

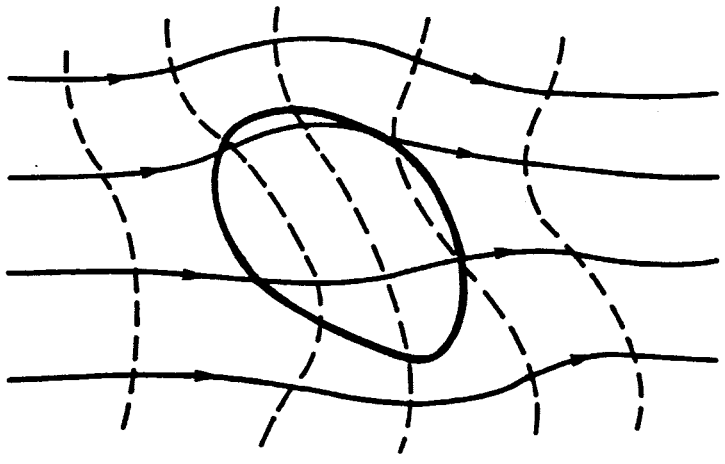

(b)

Figure 9. The effects on current and equipotential lines due to irregular conductive (a) and resistive (b) bodies (Sumner, 1976).

on the distance across the pore. Other aspects, such as pore-water flow rate, of the system are functions of grain size. Diffusion responds exponentially to system changes. To further complicate matters, all of these processes depend on the field strength distribution in the subsurface.

The resistivity and layering of the earth in conjunction with the size and type of IP array control the volume observed. The currents produced by the dynamic electric field drive the electrochemical and physical reactions discussed above. Currents in the earth produced by IP responses are observed as a voltage difference across the potential electrodes. Location and orientation of potential electrodes relative to the current electrodes determines how, and what part of, the input dynamic electric field is observed (figure 10).

A major factor controlling field distribution is layering. The electric field crosses more interfaces with thinner layers, for a given penetration depth. Each interface crossing carries a decrease in the energy available for penetrating subsequent layers and interfaces. Therefore, increased layer frequency decreases the observed volume. Resistivity contrasts between layers cause reflections and refractions of energy when the electric field lines cross boundaries between media. Reflection and refraction at the boundaries must satisfy this law:

$$r_2/r_1 = \frac{\tan \theta_1}{\tan \theta_2}$$

where θ is the angle between the current flow lines and the normal to the interface and r is resistivity (figure 11) (Sumner, 1976). The affects of the properties contrasts are directly proportional to the contrasts magnitude. Where subsurface layers exhibit low resistivity contrasts relatively greater depths can be investigated. Extreme contrasts conversely frustrate investigating substantial depths. The effective penetration can

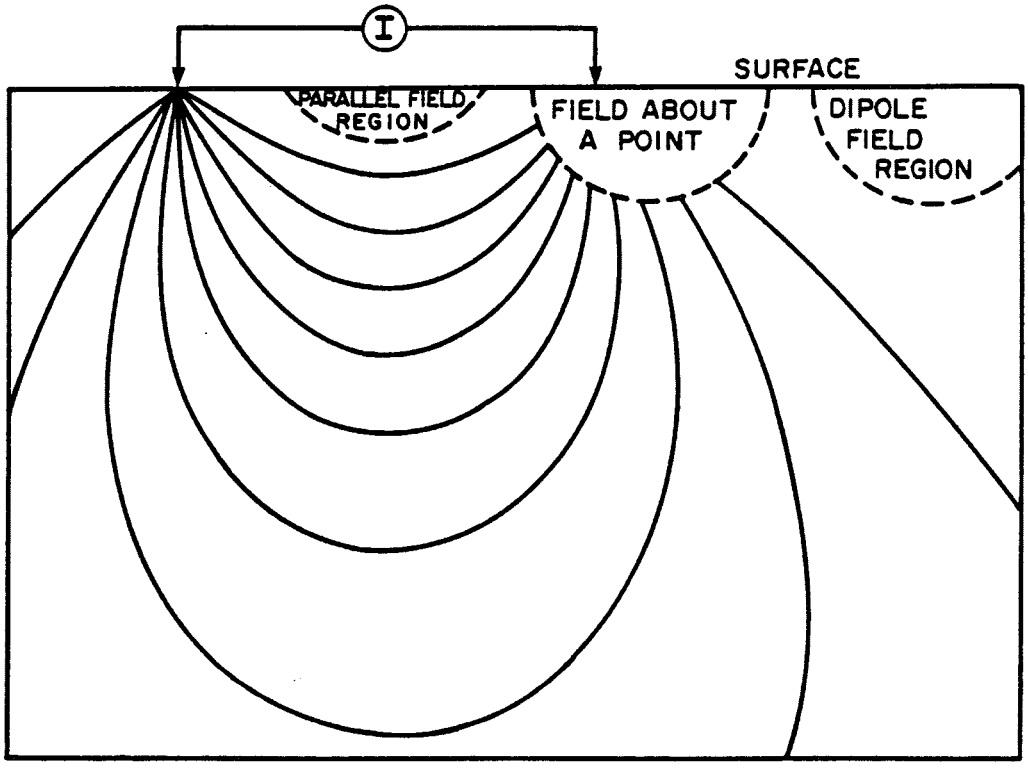

Figure 10. Portions of the dynamic electric field from a current dipole observed by differing potential dipole array locations (Sumner, 1976).

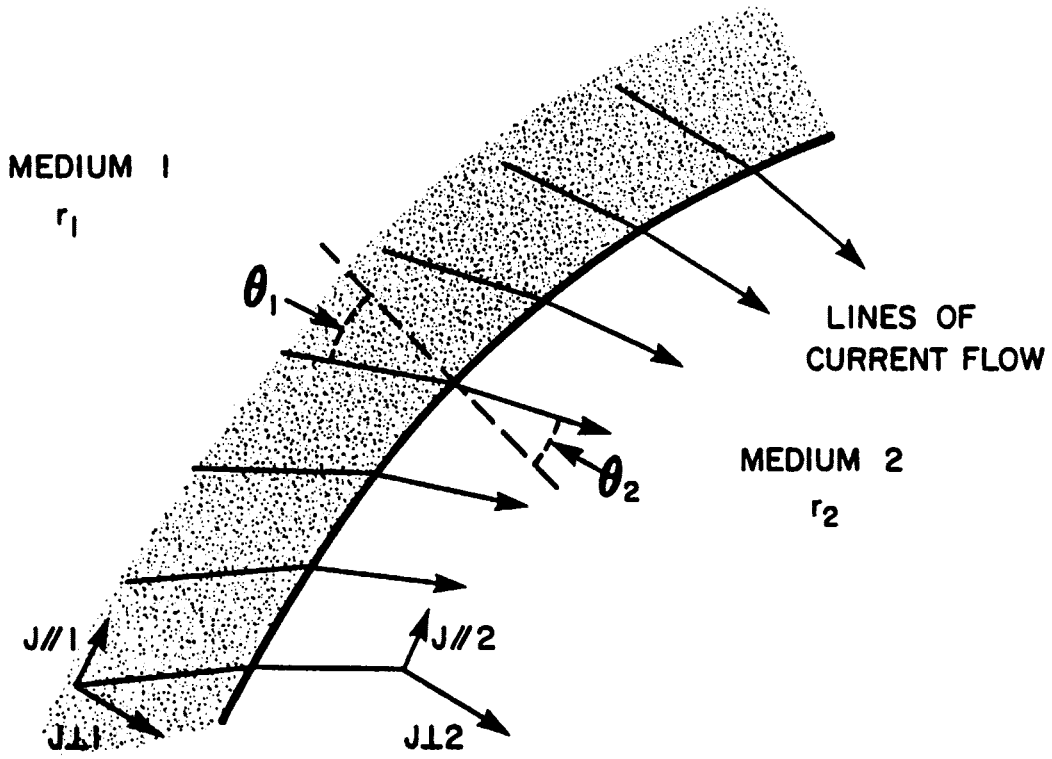

Figure 11. The effects of refraction on current flow lines when going between media with different resistivities (r) when r_2 is greater than r_1 (Sumner, 1976).

vary from an optimal 70 percent of the maximum electrode separation to 10 percent.

Estimating IP Values From Known Electrolyte Resistivities

The only predictive model in the literature is an empirical model developed by Olorunfemi and Griffiths (1985). They based their model on the observation that at concentrations less than 500 mg/L IP can be correlated to matrix conductivity (s_m):

$$IP = a \log(s_m) + b$$

where a and b are empirical constants and IP is in percent. This equation can be combined with:

$$s_r = s_m + s_w/F,$$

where s_r is the total conductivity, s_w is the electrolyte conductivity, and F is the true formation factor. After combining and rewriting one can obtain:

$$IP(\%) = b + \{a \log [s_r - s_w/F]\}.$$

This equation can be used to estimate the validity of field observations given electrolyte and total resistivity, after laboratory determination of the constants a and b. However, my investigation has several problems with this type of analysis. First and foremost a, b, and F are unknown. The values Olorunfemi and Griffiths (1985) determined for sandstone are not applicable for my field site and it was not possible to perform accurate lab tests to determine a and b. F may be estimated using depth soundings. If, I wanted to use the values for a, b, and F that they determined, the equations return IP values in percent. IP values in percent cannot be uniquely transformed into millisecond values. The final problem concerns the electrolyte data set compiled by Norton (1985).

Electrolyte conductivity estimates and standard deviations can be obtained from Norton's (1980) extensive data set. In terms of variables

used in this study, the average water resistivity is 23 ohm-meters with a standard deviation of 7 ohm-meters. The standard deviation of the unit can be estimated from these values via:

$$s'_{rt} = |\partial r_t / \partial \phi|\ s'_{\phi} + |\partial r_t / \partial r_w|\ s'_{rw},$$

where s' is standard deviation, r is resistivity, and ϕ is porosity. Unfortunately, when these values are used to determine the standard deviation of the total unit the result is 120 ohm-meters. These large values for the standard deviation imply that almost any field observation that might be recorded in an alluvial deposit can be substantiated. Analysis to determine the average and standard deviation of apparent resistivity using Norton's (1980) entire data set does not change the results very much, the average apparent resistivity is 20 ohm-meters with a standard deviation of 114 ohm-meters.

LABORATORY HYPOTHESIS TESTING

Laboratory Method

The scaled physical model used in the laboratory tests was a plywood box coated with polyurethane with interior dimensions: 100 cm x 60 cm x 60 cm high (figure 12). The middle section, perpendicular to the model's long axis, was hydrologically isolated using plywood barriers. These barriers permitted the middle section to be contaminated while the remainder of the model remained uncontaminated. Industrial grade fine white sand was used to fill the scaled physical model. Each of the three sections in the model were filled with the dry sand to predetermined levels. The center section contained the material needed to fill the volume occupied by the barriers. Equal saturations were approached in each section by adding predetermined volumes of water to each section. There were 15 cm of sand after adding the water.

Contaminated water was added to the center section. Warm water was used in all three sections. This assisted dissolving the contaminant and prevented IP effects due to temperature gradients across the model. A half hour was allowed for hydrologic gradients to decay. An IP survey with an A-spacing equal to 5 cm and n constant at one was run across the model (figure 12). Twelve readings were taken across the model. The survey line centered on the contaminated zone of the model. Resistivity and chargeability data were recorded at each of the 12 points in the model. A Scintrex IPR-8 receiver was used in conjunction with a battery powered Scintrex IP transmitter. Heavy gage copper wire was used for the current electrodes. A copper wire was inserted into the center of a number four cork to make each potential electrode (figure 13). A saturated copper sulfate solution saturated the number four corks. An array holder and a spacing guide

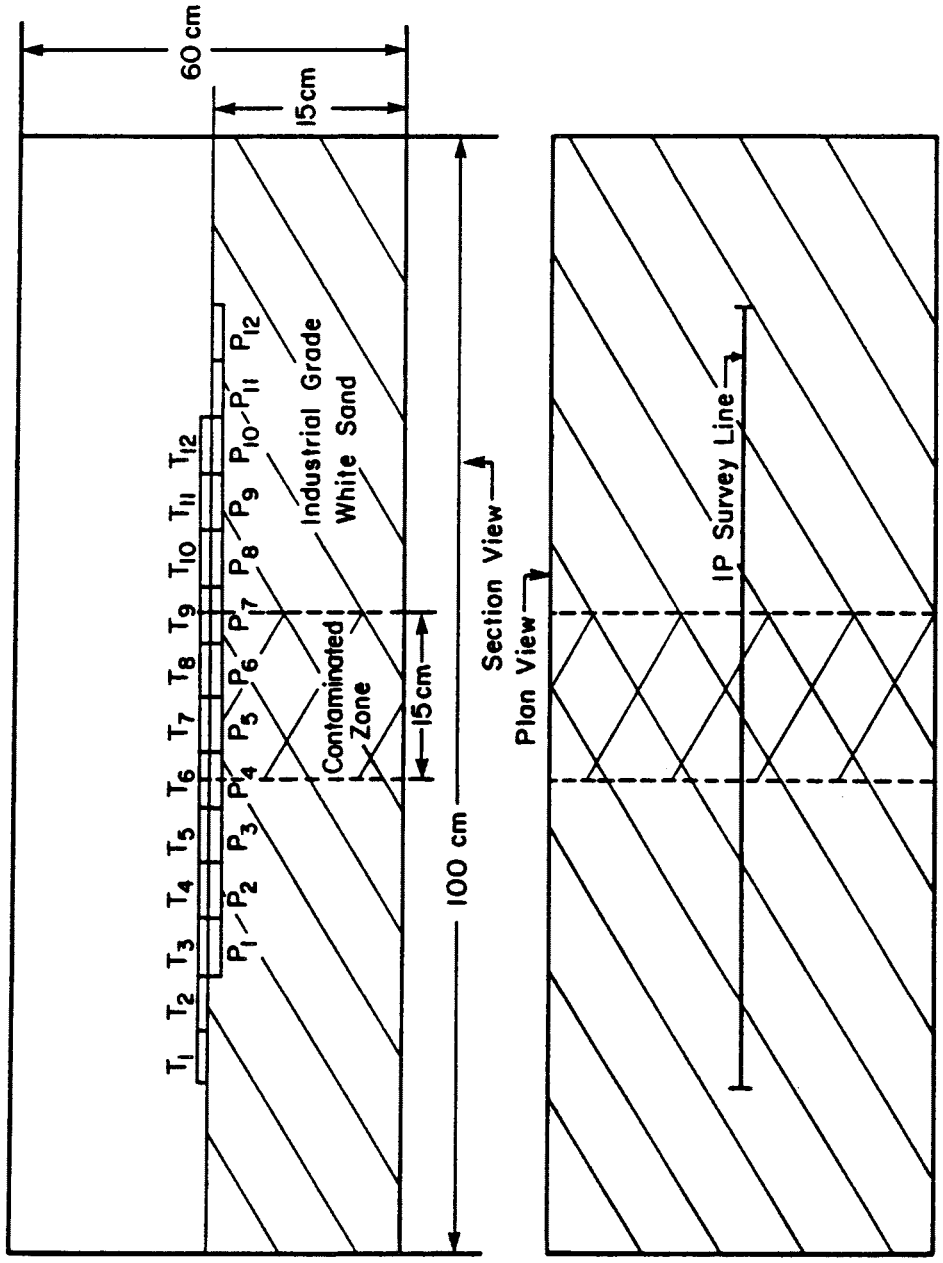

Figure 12. Sketch of the laboratory scaled physical model showing contaminated zone and dipole locations, T is for current and P is for potential electrodes.

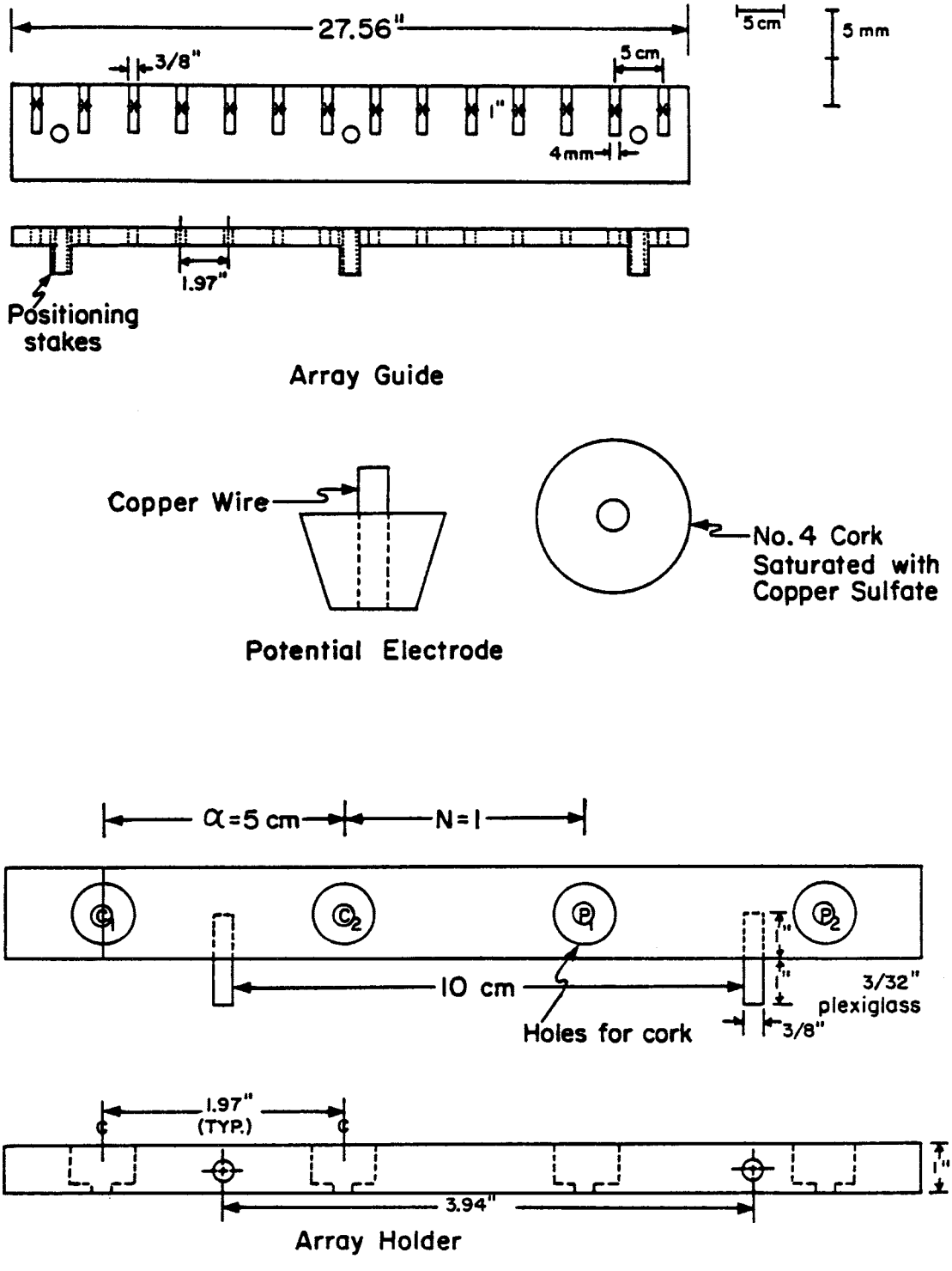

Figure 13. Diagram of Laboratory Potential Electrode, diagram of Array Holder, and Spacing Guide.

controlled electrode spacing and the surveys' progression across the scaled physical model (figure 13).

Tests were performed with zinc, lead, copper, and uncontaminated samples at different concentrations (table 2). Tests began with the weakest concentrations and proceeded to stronger concentrations. This progression minimized the probability that residual contaminants could contaminate the model. The model was thoroughly rinsed with warm water between each series of tests, contaminated and uncontaminated samples. The current shorted along the array holder as it became saturated with the contaminant solution. Shorting was a only a serious problem with the strongest 1000 mg/L, solutions.

Table 2. Metals and concentrations used in laboratory testing of induced polarization for mapping metal contaminated ground water.

Metal	Concentration (mg/L)			
Lead $Pb(NO_3)_2$.	5	20	100	1000
Copper $Cu(NO_3)_2 \cdot 3H_2O$. . . .	-	-	100	1000
Zinc $Zn(SO_4) \cdot 7H_2O$.	5	20	100	-
Blank	-	-	-	-.

The reader should recall this is a preliminary investigation and these limited laboratory tests were solely to show contaminated ground water in an uncontaminated soil produces an IP anomaly. These laboratory investigations can not and do not definitively describe induced polarizations response to all contaminant metals in their infinite combinations. Results for these metals should only be used tentatively, repeated testing and tests at more closely spaced concentrations are eventually needed.

Laboratory Results

No apparent resistivity anomaly is observed in the data set when uncontaminated water is in the middle section. However, there is a strong

IP anomaly (figure 14 a and b). The IP anomaly raises questions about any conclusions from the laboratory data. There is a distinct possibility that without a contaminant present soil disturbance alone is sufficiently important to produce a negative IP anomaly (Ogilvy and Kuz'mina, 1972) without a resistivity anomaly. The data readings are reliable for the uncontaminated sample. These results, for this uncontaminated sample, point out the need to perform additional laboratory experiments with more sophisticated equipment. Those additional experiments will provide a better understanding of the various phenomena.

I needed to determine if the observations with the different contaminant metals are different from the observations without contamination. A statistical test appears to be the best unbiased method to determine whether an observed contaminated response is different from the uncontaminated observations. Cross-correlation coefficients are a statistic showing which metal contaminant responses are from a different population than the uncontaminated samples. Observations of lead at concentrations of 1000 mg/l are inconclusive because an incomplete data set was recorded, the response was of insufficient magnitude for the instruments to record (figure 15 a and b).

I decided to use alpha from a cross-correlation analysis as an indicator of the degree of similarity between data sets. I list in table 3 the alpha values for each analysis. Alpha is:

$$\text{Alpha} = 1 - \text{confidence}.$$

The cross-correlation coefficient (r_m) and its significance (t') are described by:

$$r_m = \text{covariance}_{1,2}\ (s'_1 s'_2)^{-1}$$

and

$$t' = r_m \{ n-2\ (1 - r_m^2)^{-1} \}^{1/2}$$

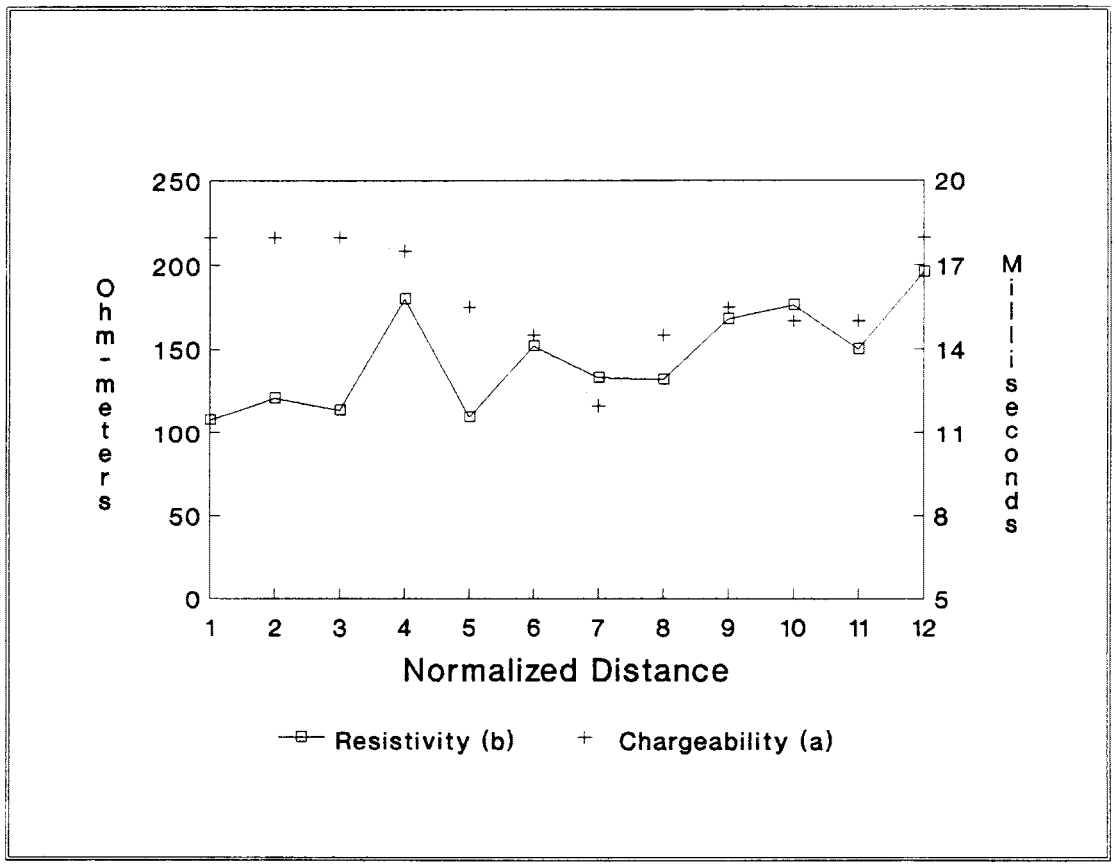

Figure 14. Laboratory data for an uncontaminated sample, where a is chargeability and b is apparent resistivity.

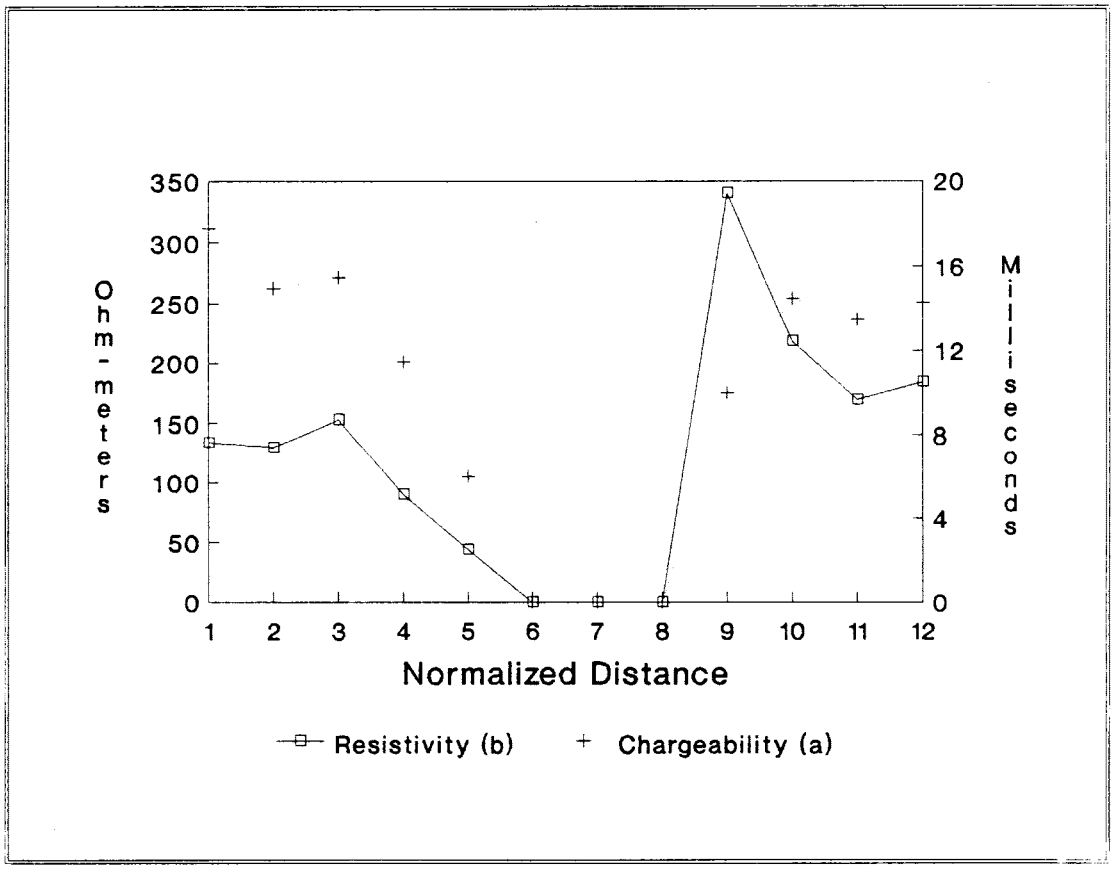

Figure 15. Laboratory Data for a sample with 1000 mg/L lead, where a is chargeability and b is apparent resistivity.

Table 3. Cross-Correlation analysis between the different contaminant metals and the uncontaminated sample in the laboratory tests.

METAL	INDUCED POLARIZATION			APPARENT RESIS.		
	r	signif.	alpha	r	signif.	alpha
ZINC:						
5 mg/L	0.59	2.59	0.14	0.76	4.87	0.000
20 mg/L	0.30	0.74	0.24	0.69	3.04	0.006
100 mg/L	-0.17	-0.54	0.70	0.59	2.31	0.02
LEAD:						
5 mg/L	-0.08	-0.23	0.59	0.52	1.9	0.04
20 mg/L	-0.39	-1.37	0.90	0.66	2.75	0.01
100 mg/L	-0.01	-0.04	0.52	0.29	0.94	0.18
10^3 mg/L	--	--	--	--	--	
COPPER:						
100 mg/L	0.62	2.48	0.02	0.35	1.2	0.13
10^3 mg/L	0.53	1.97	0.04	0.35	1.2	0.13

where n is the sample size, $covariance_{i,j}$ is the covariance between the i and j the sample sets, and s' is the standard deviation of a sample set. I am defining that the populations are the same if alpha is less than or equal to 0.10, may be different if alpha is less than 0.20 and greater than 0.10, and are different if alpha is greater than or equal to 0.20. The reader will see why I am arranging these categories.

There are no resistivity anomalies according to the statistics listed in table three (figure 16 a-e). This is most likely due to the large variability within the uncontaminated sample. Copper concentrations of 100 and 1000 mg/L and a lead concentration of 100 mg/L may have resistivity anomalies according to the aforementioned categories (figures 17 a and b and 18). However, the reason that copper at 1000 mg/L correlates better to the uncontaminated sample than lead at 100 mg/L is not intuitively obvious. My interpretation is that copper at 1000 mg/L is affected by the contaminant while the other two samples are inconclusive.

Copper at 100 mg/L and zinc at 5 mg/L do not show any IP effects from the contamination (figure 19 a and b and table 4). Zinc contaminations of 20 and 100 mg/l produces anomalies (figure 20 a and b and table 4). The reader should remember to compare the figures of contaminated samples to the uncontaminated results (figure 14). Observations of the effect of lead on the system produced the most conclusive anomalies, all three data sets (5, 20, and 100 mg/L) show different degrees of negative correlation (figure 21 a-c and table 3). A copper concentration of 1000 mg/L produces confusing IP results. Two data sets that are so different (figures 14a and 22) correlated very well. A combination of two arguments best explains this correlation. First, the trend of each data set is similar, a IP low in the center of the profile. Second, data from the experiment with copper has a large standard deviation. The standard deviation is used in calculating

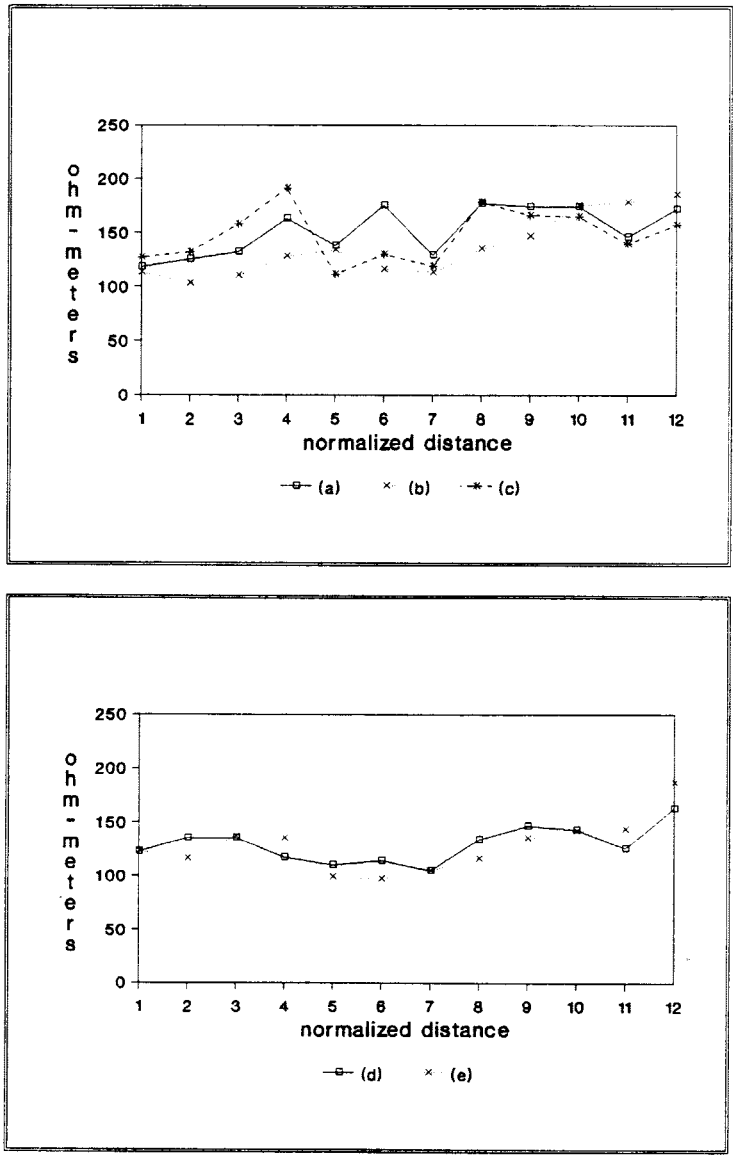

Figure 16. Resistivity data from the laboratory tests that did not have an anomalous response when compared to the uncontaminated sample, 5 mg/L zinc (a), 20 mg/L zinc (b), 100 mg/L zinc (c), 5 mg/L lead (d), and 20 mg/L lead (e).

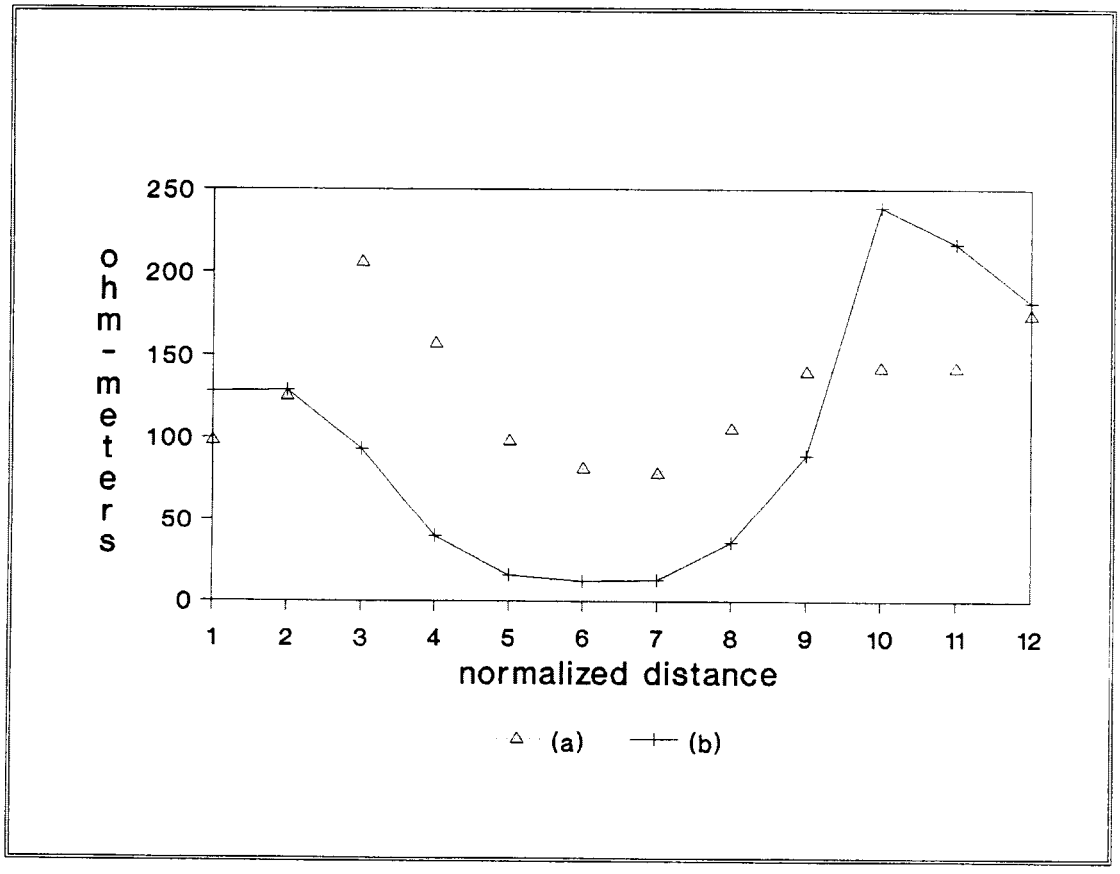

Figure 17. Resistivity data from the laboratory tests that may have an anomalous response when compared to the uncontaminated sample, copper at 100 mg/L (a) and 1000 mg/L (b).

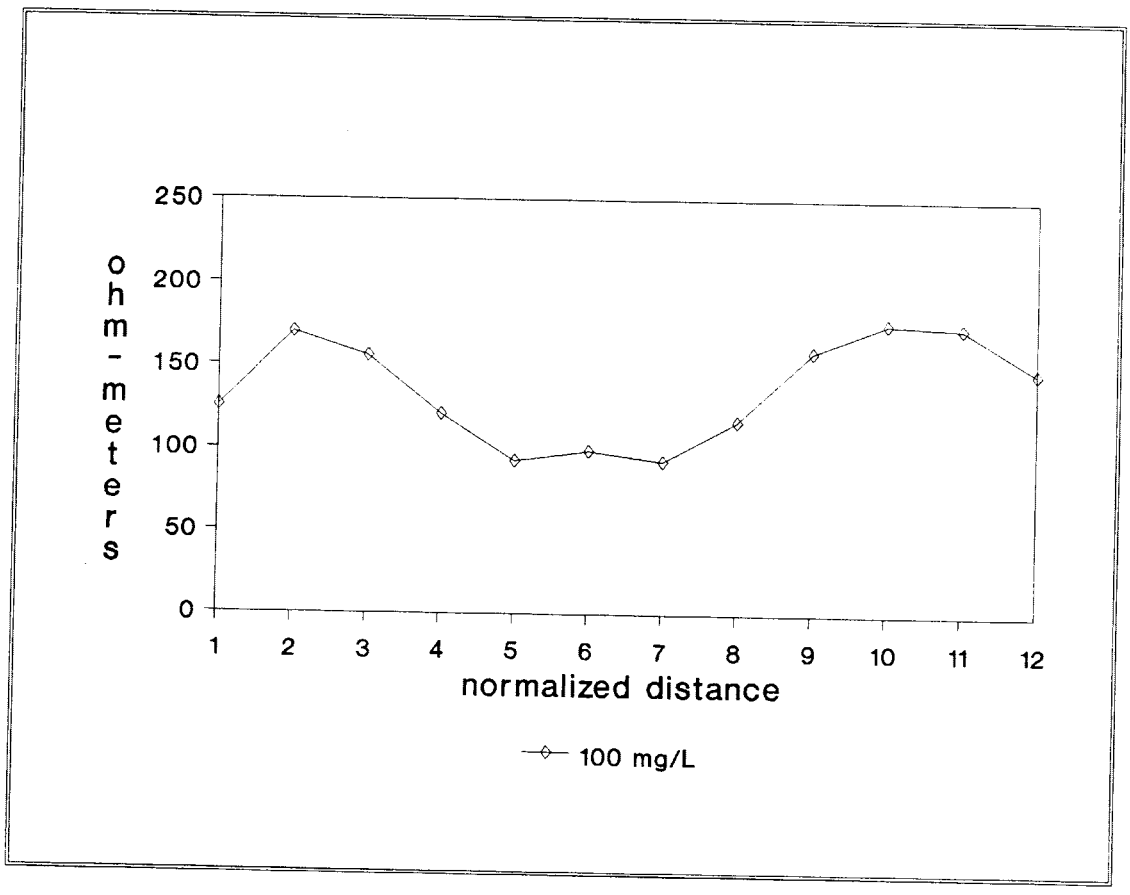

Figure 18. Resistivity data for lead at 100 mg/L from the laboratory tests which may have an anomalous response when compared to the uncontaminated sample.

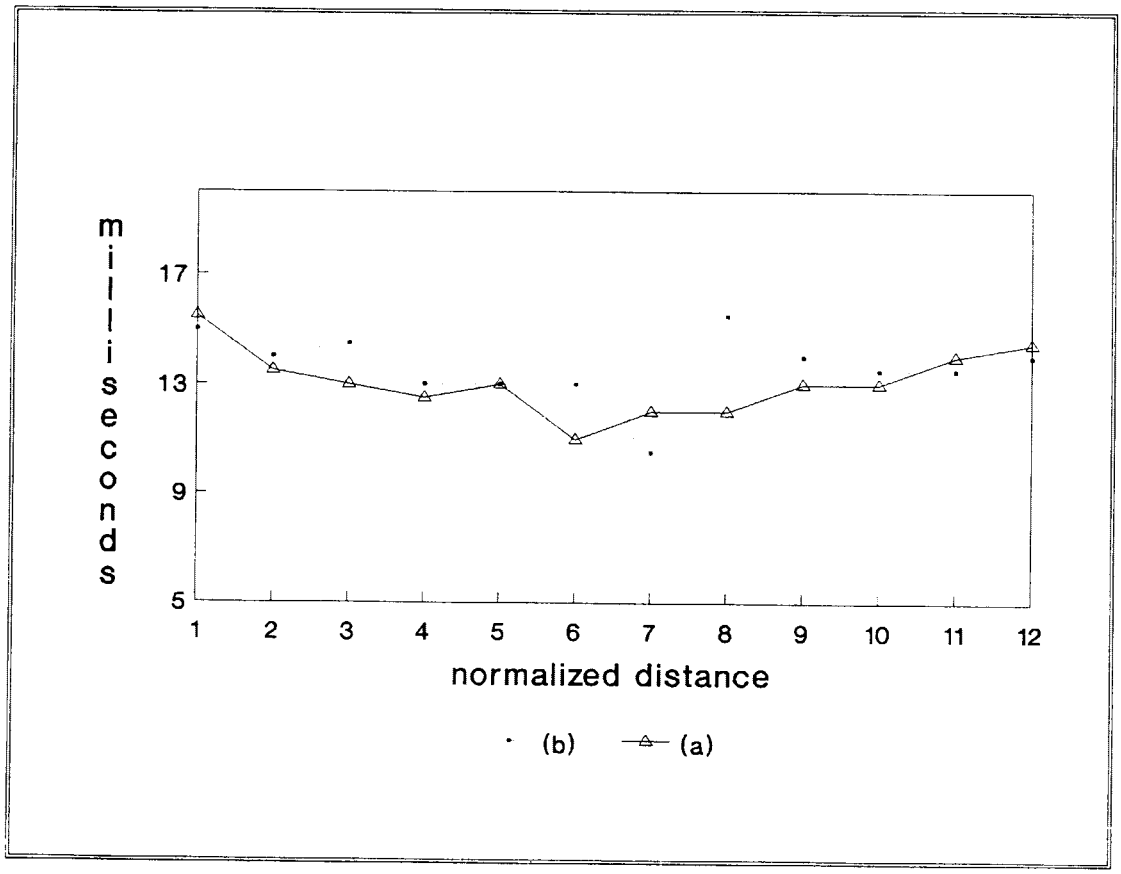

Figure 19. Copper at 100 mg/L (a) and zinc at 5 mg/L (b) do not have induced polarization anomalies when compared to the uncontaminated sample.

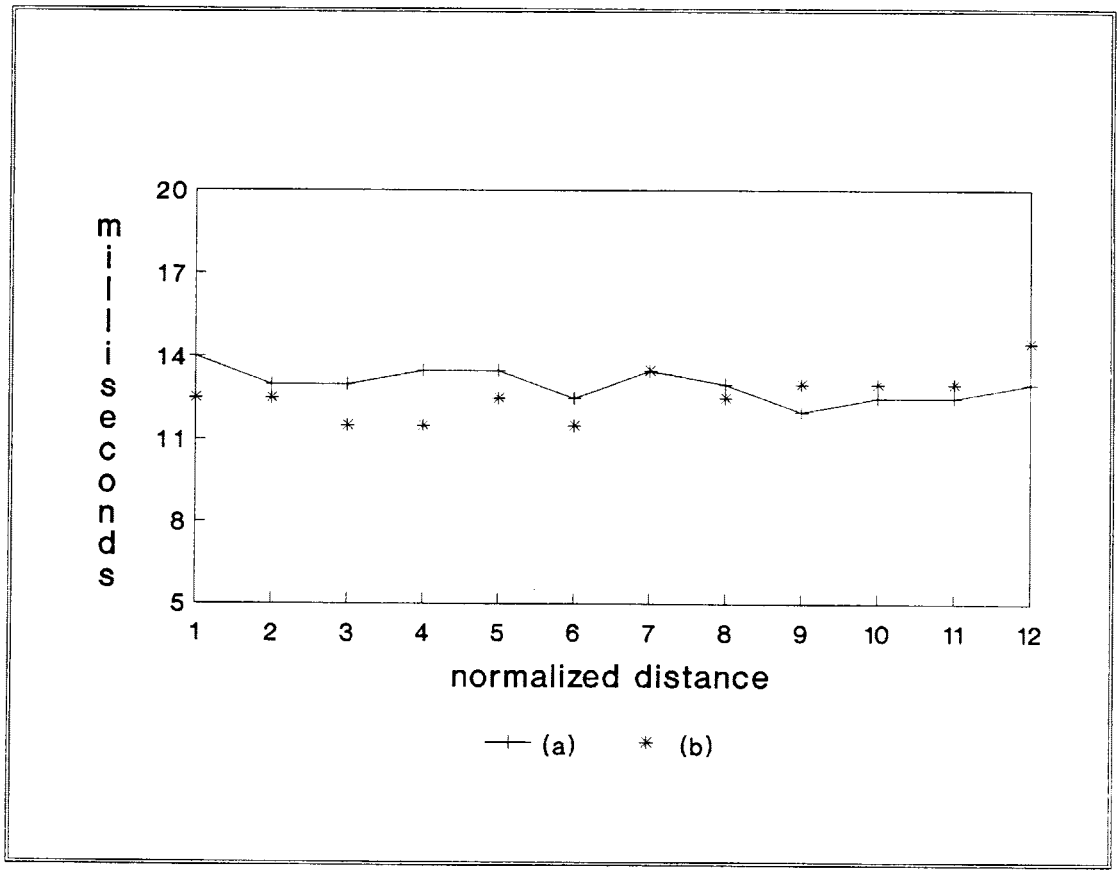

Figure 20. 20 mg/L (a) and 100 mg/L (b) zinc do produce induced polarization anomalies when compared to the uncontaminated sample.

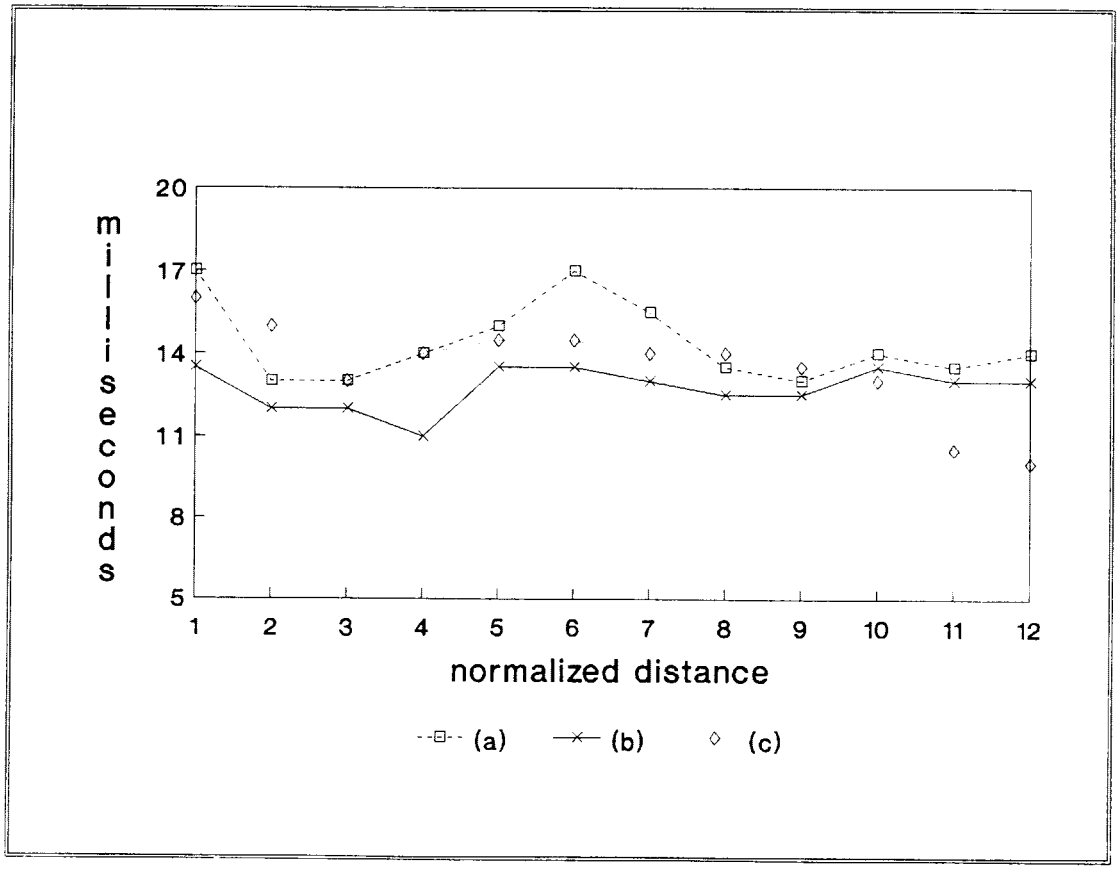

Figure 21. Lead at 5 (a), 20 (b), and 100 (c) mg/L produces an induced polarization anomaly when compared to the uncontaminated sample.

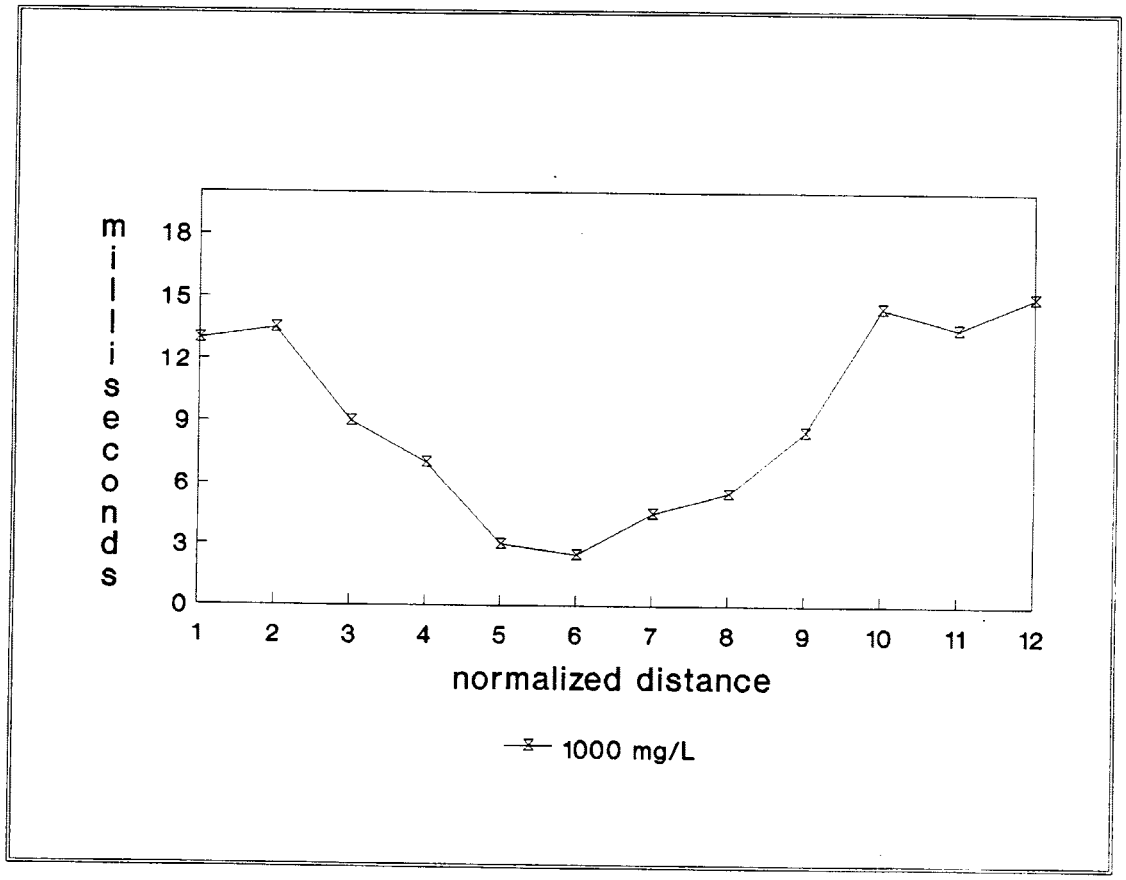

Figure 22. Copper IP laboratory data for a concentration of 1000 mg/L.

cross-correlation statistics. A combination of similar trends and a large standard deviation in one data set results in a good correlation. Although statistical calculations were performed on an HP-28c hand held calculator; these calculations were repeated twice and selectively checked on a Personal Computer using Lotus. In the case of copper contamination at 1000 mg/L I am very hesitant to state that the contamination has no affect.

In conclusion I believe that metal contamination can and does affect IP results. However, soil disturbance from removing the barriers also produces an IP anomaly. Hydraulic conductivity affects IP and the disturbance almost certainly affects the hydraulic conductivity in the model (Olorunfemi and Griffiths, 1985). I also believe that these observations, specifically lead at 5 and 20 mg/L, show IP anomalies exist when there is no apparent resistivity anomaly. In the future testing for the effects of metals on IP the entire scaled physical model should be contaminated. 20 to 30 reading should be taken in the model, at the same location for each contaminant and contaminant concentration. Large sample populations would improve the statistical analysis of the results. Observations should be in two perpendicular directions to check for anisotropy. This alternative methodology will provide a better data set to work with statistically and eliminate the effects from removing the barriers. The model should be larger for using this equipment; for although I cannot prove it, I am fairly certain some of the observations were affected by the edges of the model.

FIELD HYPOTHESIS TESTING

Field Method Introduction

The locations for field testing the induced polarization detection technique are in Coeur d'Alene Mining District of Northern Idaho (figure 23). The Mining District previously contained one of the largest lead producing mines in the free world, the Bunker Hill, and its smelter. The District is the largest silver producing region in the U.S.A., when the mines are open. Mining activities in the district commenced in 1888. Mineral resource waste disposal practices in the past were poor by current standards. These poor practices resulted in the present contamination problem, large portions of the District are designated Superfund sites. Several locations in the South and Main Forks of the Coeur d'Alene drainage are chosen as sites to test IP in realistic situations.

Regional Surficial Geology

The alluvial deposits within the Coeur d'Alene and South Fork of the Coeur d'Alene River are varied in type and thickness. Currently the South Fork is an aggraded stream (Ioannau, 1979). Generally the alluvium thickens towards the west and is up to 91 meters (300 feet) at Pinehurst. The Valley has a pronounce "V" shape with a narrow valley floor at the Kellogg and Smelterville sites. At and near Kellogg, Idaho there are approximately 30 meters (100 feet) of alluvium. The alluvium is generally river gravels with occasional clay confining layers (Ortman, 1978 and Norton, 1980) The unconsolidated alluvial sediments are progressively finer grained towards the west (Ioannau, 1979). Since the latter part of the nineteenth century mineral resource wastes characterized by jig and flotation tailings have been worked into the river sediments. This mixing results in the upper 3 to 5 meters (15 to 20 feet) of river gravels being contaminated with mineral resource wastes, tailings. The climate at Kellogg is mild summers with

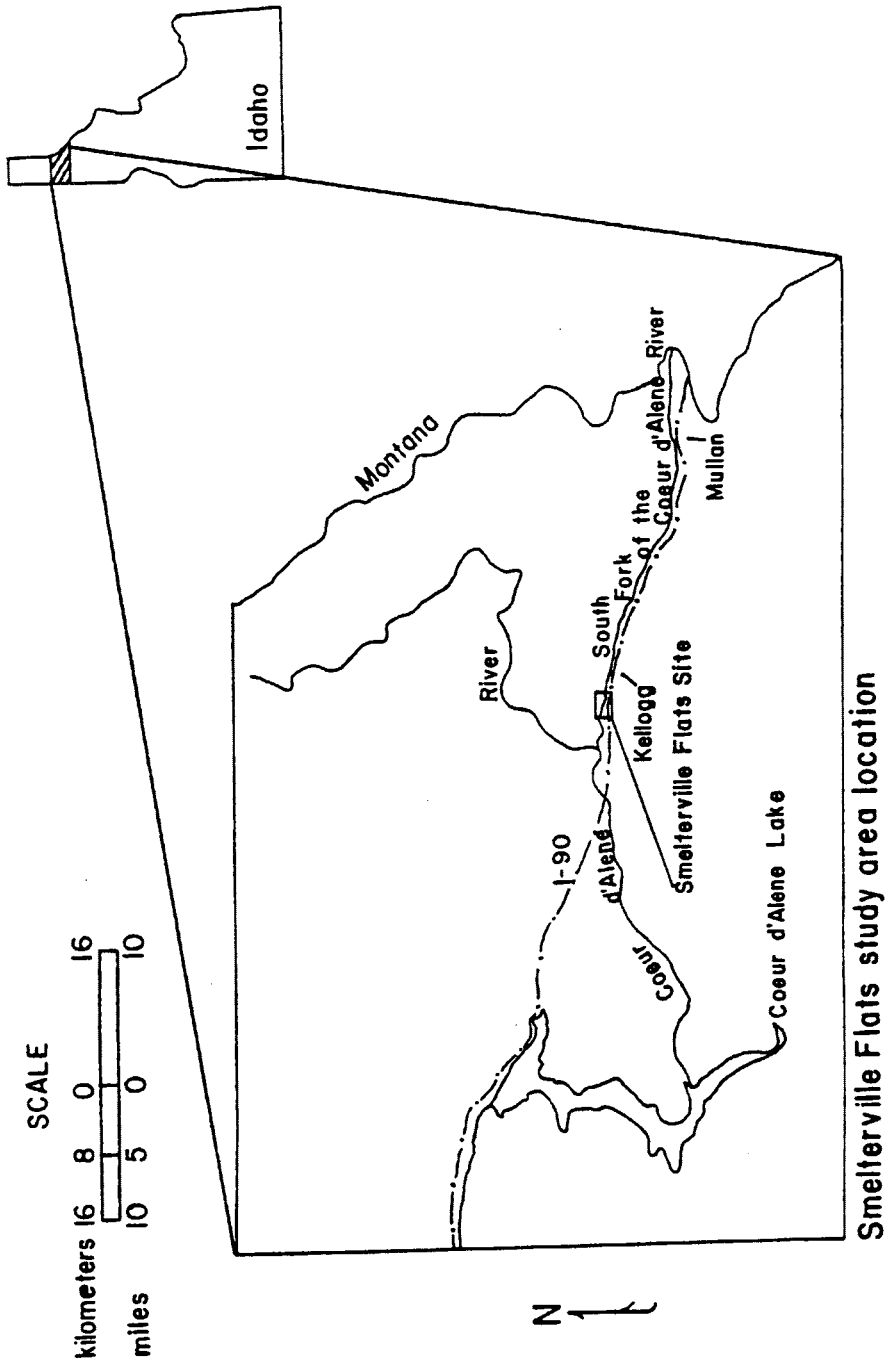

Figure 23. Map showing the locations of the three study sites within the State of Idaho.

moderately cold winters. Snow is the main source for the 0.75 meters (30 inches) of average annual precipitation at Kellogg (Ortman, 1978).

Cataldo Flats is covered with tailings, jig and flotation, dredged from the Coeur d'Alene River until 1930 (Galbraith et al., 1972). Most of the tailings at the site are jig tailings as tailings impoundments were used to some extent as early as 1901 in the Mining District. These dredged deposits are underlain by naturally deposited material that is contaminated with mineral resource wastes. Presumably these sediments are underlain by natural alluvium. Jig tailings are older and coarser, down to 1.4 mm. diameter, than most of the flotation tailings, 0.295 to 0.044 mm diameter (Ioannau, 1979).

Cataldo Flats Site

Cataldo Flats provided a site to test IP's effectiveness in uncontrolled mine wastes (figure 24). East of Fourth of July Pass and down stream along the Coeur d'Alene from Kellogg, Idaho this location is covered in dredged river deposits. Jig tailings form most of these dredged river deposits (Galbraith et al., 1972). These tailings come from the mining activities in the Coeur d'Alene Mining District. One line was surveyed with several n and A spacings to optimize n and A for this site. The abundance of buried drums, culverts, and other metal debris, interfered with the data analysis at this location. The anomalous readings produced by one large culvert prevent conclusions on the contaminant situation from most of the data. This problem persisted despite numerous analysis attempts. However, a successful series of eight soundings with an A-spacing equal to 9.1 meters (30 ft.) and n's equal to 1,2,3, and 4 were taken. These eight soundings were not affected because they were further from the portion of the site that contained the buried debris. The eight soundings produced 32 samples with two data per sample. These eight dipole-dipole soundings proceed from

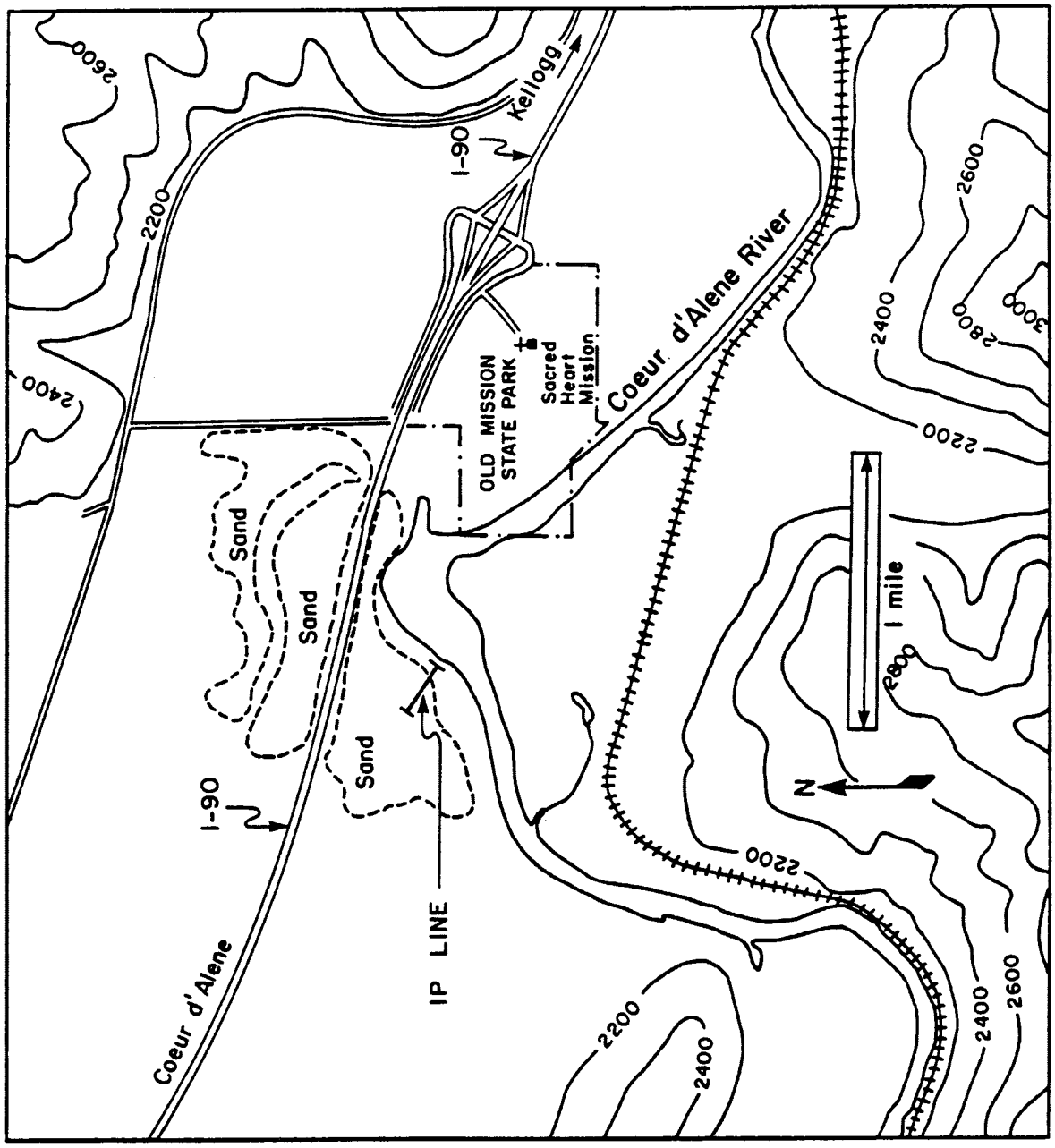

Figure 24. Location of the eight vertical electrical soundings at Cataldo (Mission) Flats, Idaho.

across the top of a small rise, approximately 7.6 meters (25 feet) above the river, down to 1 meter (3 feet) above the Coeur d'Alene River's surface. The average sounding separation is 10 meters (33 feet).

Cataldo Flats Field Data

The Cataldo (Mission) Flats Data set is full of serious problems, due to the metal garbage buried at the Flats. One line of eight depth soundings produced the only interpretable data. A pseudo-section of the data is presented in figure 25 (a and b). A pseudo-section is a diagrammatic representation of IP and apparent resistivity data designed to give the observer an impression how these properties change with depth and progression along a survey line. Pseudo-sections do not give the actual location or values of these parameters at the point where values are plotted. Figure 25a shows a chargeability anomaly half way down the gentle hill, the anomaly also persists at the deepest, n equals four, soundings. The apparent resistivity data do not reflect this anomaly structure (figure 25b). Apparent resistivity values decline from the dry sandy hill top toward the Coeur d'Alene River. Saturation changes produce this decline in apparent resistivity values, a function of distance and elevation above the Coeur d'Alene River. The degree of saturation increases in the sandy soil at Cataldo Flats as the River is approached. Chargeability anomalies are attributable to the capillary fringe. Ogilvy and Kuz'mina (1976) observed that an IP high is associated with the capillary fringe; as the geophysical investigation observes more below the water table the IP values tend to decrease, all things being equal. Olorunfemi and Griffiths (1985) performed experiments to see the effects of saturation on IP; however, their observations did not show the effect on vertical electric soundings after the water table is encountered (figure 26). This increase and subsequent decrease is what I observed in the Cataldo Flats data.

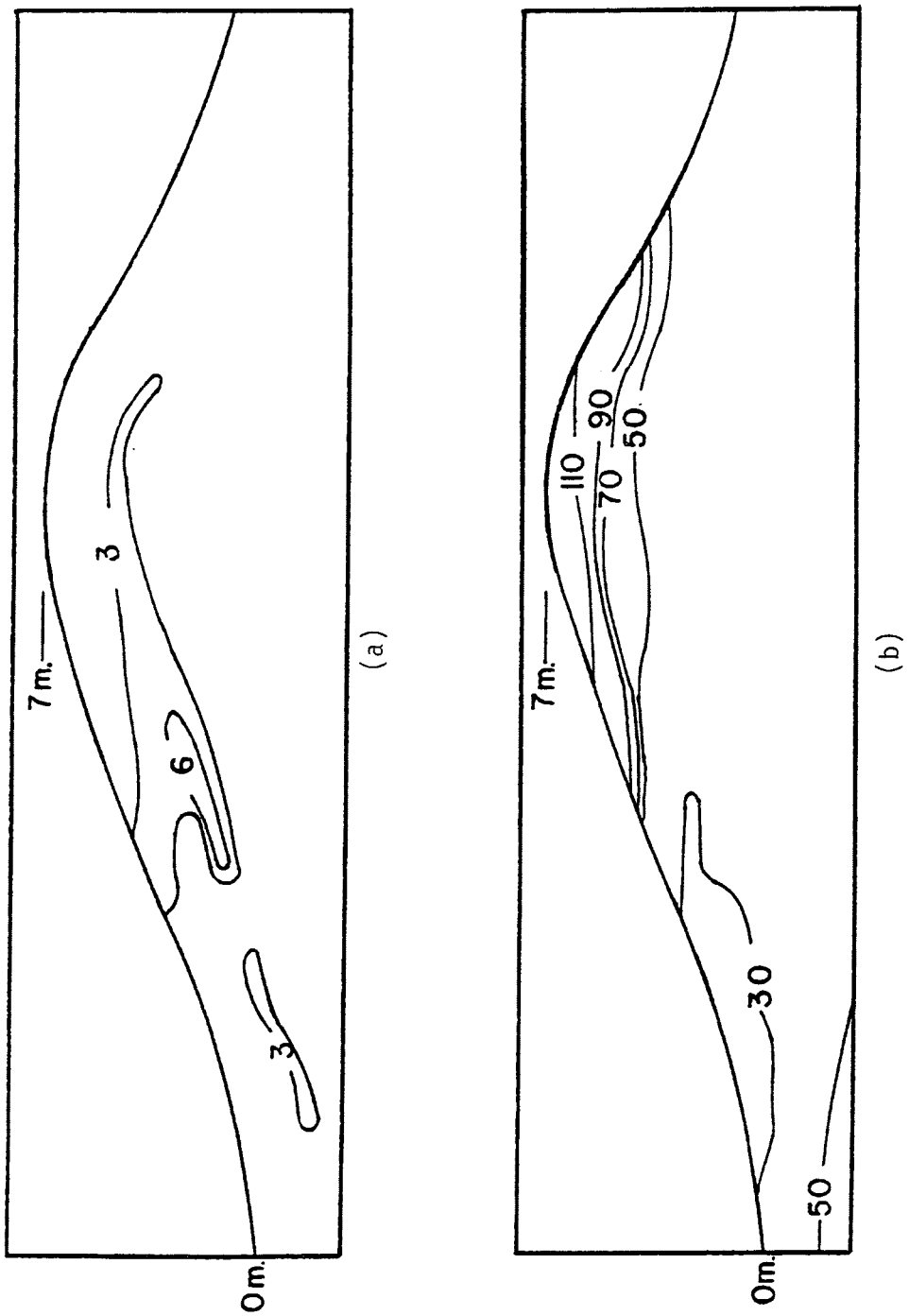

Figure 25. Chargeability (a) and apparent resistivity (b) pseudo-sections for 8 electrical depth soundings across a small hill at Cataldo Flats.

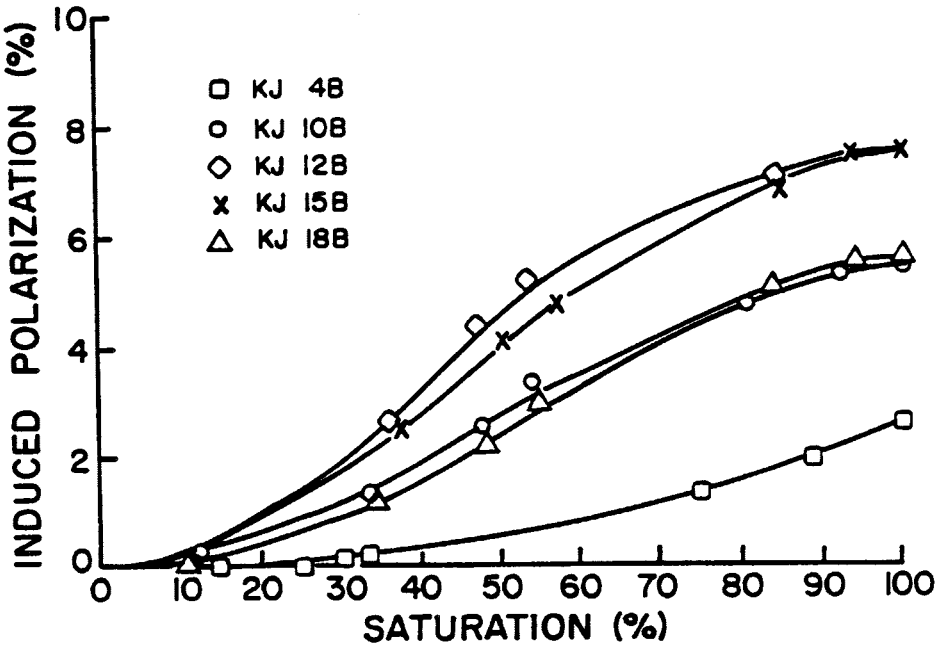

Figure 26. Saturation versus IP (%) for 5 different core samples (Olorunfemi and Griffiths, 1985).

Central Impoundment Area Site

Three short lines at the Bunker Hill Ltd.'s Central Impoundment Area (CIA), specifically the East Tailings Pond (ETP) and the slag pile, showed responses from controlled mineral resource wastes (figure 27). IP measurements in a recently active tailings pond, the ETP, obtain the response of undisturbed flotation tails. The East Tailings Pond was used as a tailings pond until the early 1980's. Water pumped from the Bunker Hill Mine which is treated for high metal loads was and is pumped in the ponds. A similar deposit of jig tails is not available, jig tailings underwent extensive reprocessing earlier in the century (Ortman, 1978). A large borrow pit, 9.15 meters or 30 feet deep, excavated in the East Tailings Pond provided fill for Interstate 90's construction (figure 27) (Ortman, 1978). The borrow pit's existence was initially revealed from data analysis. The initial results from the ETP showed an unexpected trend. Literature review and personal interviews on the ETP's history produced the information about the borrow pit. Two lines separated by a 132 degree angle in the East Tailings Pond observe any anisotropic response from typical tailing pond deposits. The measurements within the ETP have an A-spacing equal to 12 meters (40 ft.) and n's equal to 1, 2, and 3. Slag pile data produces inconclusive results. The glass rich deposit is highly resistive. The 4 kilowatt transmitter available could not produce enough power to establish a dynamic current field in the resistive slag material.

Central Impoundment Area Data

East Tailings Pond data anomalies are attributable to the filled borrow pit. Data cross-sections, chargeability and resistivity along A-A'-A", reveal a change in subsurface character approximately where the cross-section line bends (figure 28 and 29). The resistivity values change before the bend, A', in the survey line. A chargeability anomaly between 53 and 84

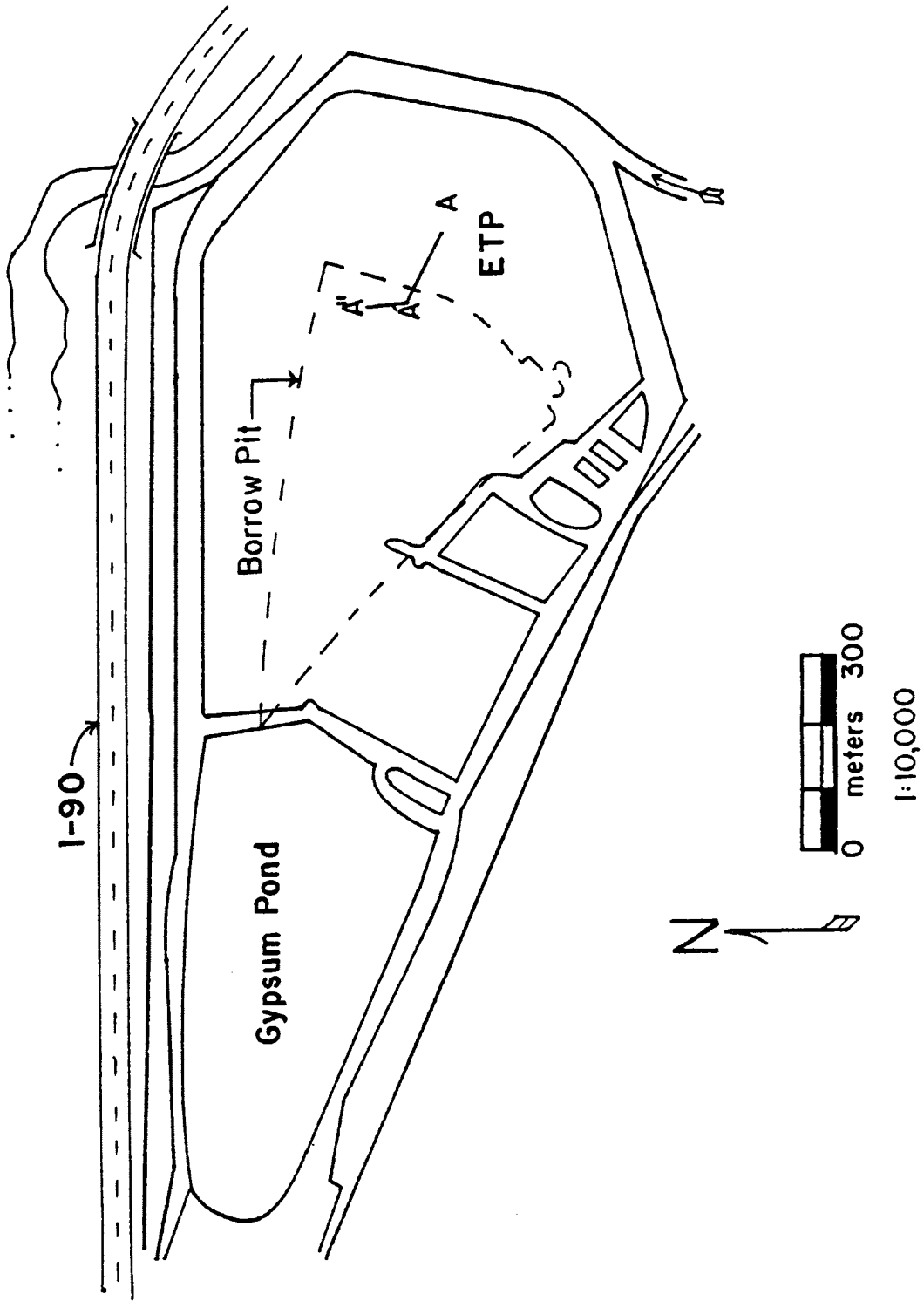

Figure 27. Map of the Central Impoundment Area at the Bunker Hill Mine complex in Kellogg Idaho. This figure shows the slag pile, ETP, borrow pit outline, and the IP/apparent resistivity survey line A-A'-A".

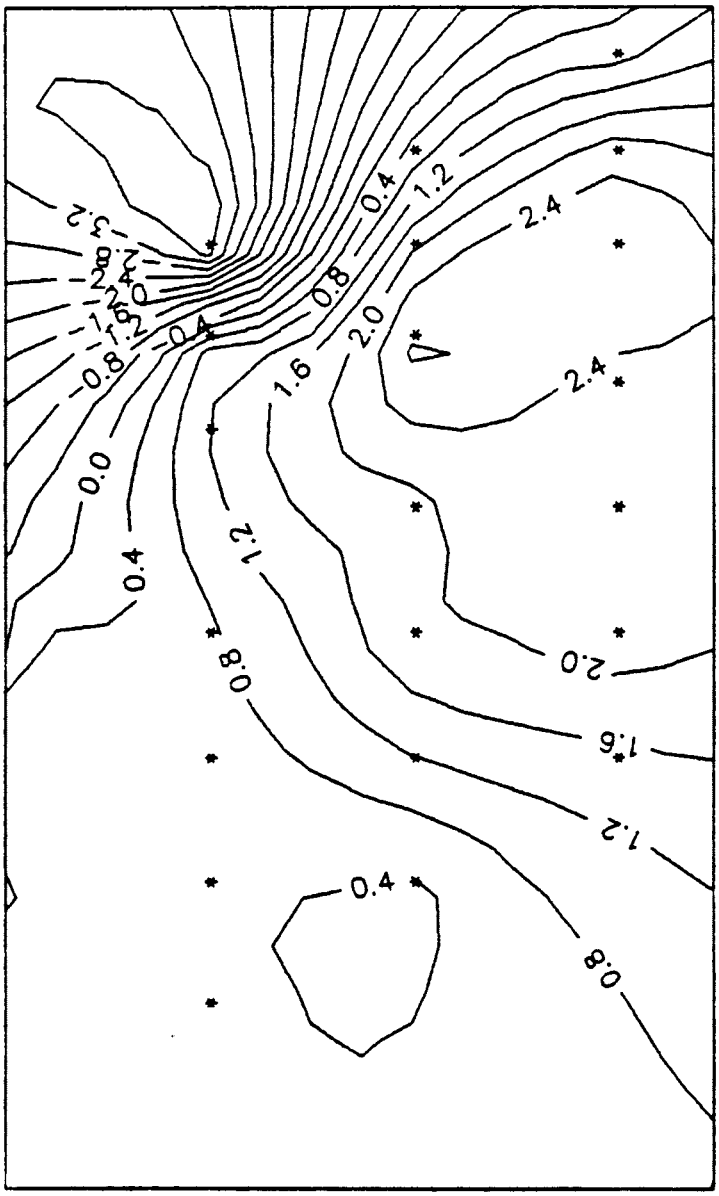

Figure 28. Contoured chargeability (milliseconds) pseudo-section for the ETP at the CIA at Kellogg's Bunker Hill Mine.

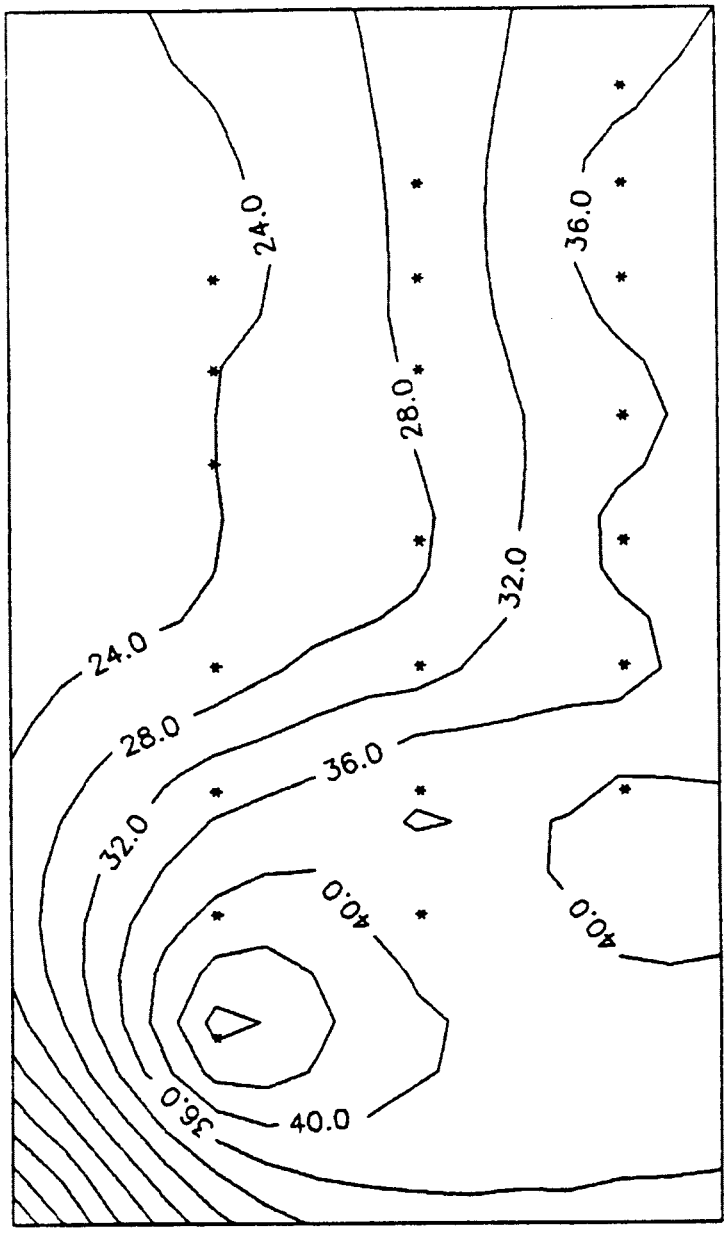

Figure 29. Contoured apparent resistivity (ohm-meters) pseudo-section for the ETP at the Central Impoundment Area at Kellogg's Bunker Hill Mine.

meters (175 to 275 feet) reflects the edge of the borrow pit. The apparent resistivity values are lower within the borrow pit region, several interpretations can be made from this. First, seepage along the plane that formed the edge ofthe borrow pit permits more efficient contaminant transport to the tails deposited as fill. A second alternative is tailings deposited as fill have a lower resistivity compared to the older unexcavated tails. Finally, dewatering of the older tailings probably occurred during the borrow pit excavation, dewatering would cause compaction within the clay size material (Freeze and Cherry, 1979). The chargeability, IP, anomaly is strongest along the edge of the filled pit. Induced Polarization is more sensitive, compared to resistivity, to pore structure or packing arrangements. Unexcavated tailings along the edge of the borrow pit would have experienced the greatest effects from dewatering. Therefore, the anomalies along the edge of the filled borrow pit are due to compaction within the unexcavated flotation tailings.

The magnitudes of the observations at the ETP are quite low, the largest IP reading is 3 millisec. and the largest apparent resistivity is 51 ohm-meters. These low values reflect the high contaminant content of the water and the very small grain size of the matrix material. These factors combine to increase the membrane polarization, decreasing the IP value. The large TDS within the pore fluid reduces the apparent resistivity. If values from salt research can be extrapolated to the ETP site concentrations within the pore fluid easily exceed 2 grams/liter (Seara and Granda, 1987 and Olorunfemi and Griffiths, 1985).

Smelterville Flats Site

Mining activities between the late 1880's and as late as 1968 deposited heavy sediment loads in the South Fork of the Coeur d'Alene River (Ioannau, 1979). Abandoned mine tailings are studied at Smelterville Flats where a

valley wide tailings pond existed from 1901 to 1933 (Norton, 1979). Subsequently, the South Fork of the Coeur d'Alene River extensively reworked the abandoned tailings (Norton, 1980). These tailing exceed the River's sediment carrying capacity whereupon mixing of mine wastes and natural sediments produces the current braided stream pattern. River migration across the valley in the last 50 years involved the entire valley floor at Smelterville Flats. Mine wastes, flotation and jig tailings are now present, not only in their original form, but also as re-sorted sediments in braided stream deposits. Long term exposure of the unconfined jig and flotation tails to the environment pollutes the South Fork of the Coeur d'Alene drainage. Grain sizes (and perhaps contaminant levels) which occur in these deposits may be reflected in the IP and resistivity results as a result of sorting processes.

Field tests at Smelterville Flats in the Coeur d'Alene Mining District of Northern Idaho (figure 30) were performed to evaluate the practicality of the IP method for discerning metal contamination. Previous hydrogeologic investigations at Smelterville Flats provided general information on the characteristics of contamination but failed to define precisely the extent of contamination on the Flats (Norton, 1980). The seriousness of the problem prompted the choice of this site. The alluvial material on the flats is rich in jig and floatation tailings; these tailings have been distributed unevenly and reworked by the South Fork of the Coeur d'Alene River (Norton, 1980). A small portion of the Flats was chosen for a detailed IP survey (figure 30). Data are collected along five IP lines trending N 5^{o} E from the abandoned Bunker pipeline toward the South Fork of the Coeur d'Alene River. Four IP/apparent resistivity lines were surveyed with an A-spacing of 12 meters (A=12 m.) (40 feet) and an A-spacing of 18 meters (A=18 m.) (60 feet) spacings for n=1 (see fig. 1). The most easterly

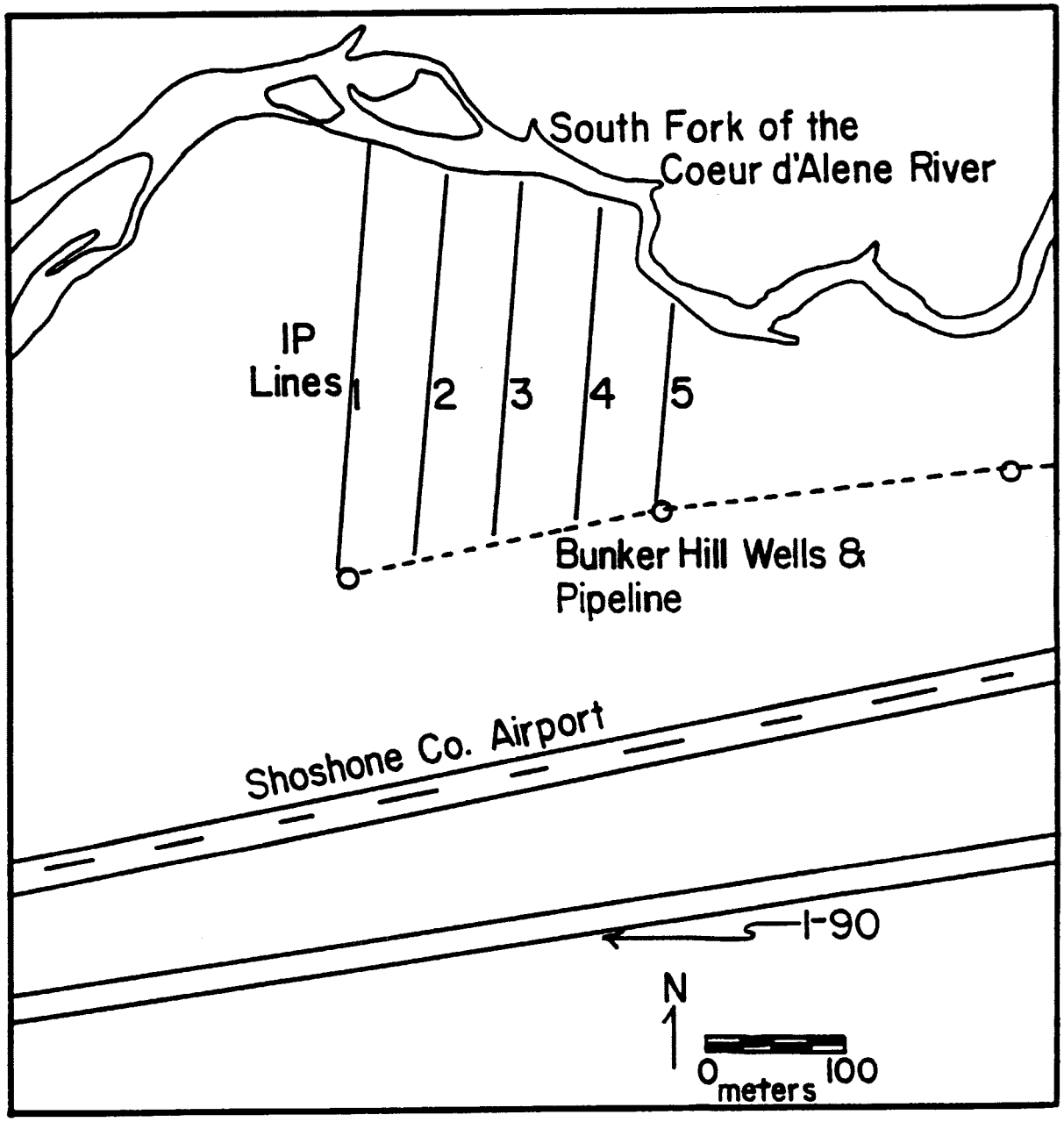

Figure 30. IP and apparent resistivity survey lines at the Smelterville Flats study site, Shoshone County, Idaho.

line, number 5, was surveyed with an A=12 meters spacing, twice at n=1 for a repeatability control, as well as at n=2 and 3 spacings. The volume sensed when A=18 meters and n=1 is nearly identical to A=12 meters and n=2 (Sumner, 1976).

Smelterville Flats Data

Smelterville Flats chargeability and apparent resistivity data and analyzed data are presented as contour maps. The A=12 meter, n=1, maps represent a shallow sampling compared to A=18 meter, n=1, maps which present information describing deeper conditions. Referred to here as the 12 and 18 meter surfaces, these values do not indicate the depth of investigation; rather the 12 meter surface is qualitatively shallower than the 18 meter surface.

The analysis of the data from the field sites require statistical treatment. Directional and omni-directional semi-variograms were calculated for the Smelterville data to determine the best direction, if any, for resistivity and chargeability data correlation. (Appendix A) (Clark, 1979). Kriging estimated values for the variables at locations where measurements were not recorded (Davis, 1986). These kriged values were used to produce contour maps over the areas of interest. Smelterville Flats data were analyzed with a fourth degree trend surface algorithm. The residuals from the trend surface analysis were treated as anomalous or a representative regional background value for the specific parameter, resistivity or chargeability (Davis, 1986). Trend residuals were normalized by the standard deviation of the residuals. This produces resistivity and chargeability data sets with identical means and standard deviations, 0 and 1 respectively. High frequency noise was removed from the normalized data sets using a fast fourier transform (FFT) technique (Press et. al., 1986). The FFT analysis incorporates a weighted average over the distance of the

line spacing, 61 meters (200 feet). The IP array crossing a boundaries between zones with different resistivities and/or chargeabilities causes high frequency noise in the data set. Statistical tests show strong positive correlation between resistivity and chargeability residuals at Smelterville Flats (figure 31 and 32), this is not true at Cataldo Flats (figure 33). Chargeability data are very variable at Cataldo Flats, especially when n equals four. The resistivity data are less variable. Appendix B contains tables listing unprocessed field and laboratory data; as well as, statistical tests performed on the various data sets.

Surface maps of the normalized 4th degree trend residuals reflect the heterogeneity and complexity in the subsurface at Smelterville Flats (figures 34-37). IP and apparent resistivity anomalies may resemble braided stream features due to reworking mineral resource wastes into braided stream deposits. The fourth degree trend surface analysis removes regional and ground water table effects within the data. Residuals from the trend analysis were normalized using the standard deviations of each data set, 12 and 18 meter chargeability and resistivity, producing chargeability and resistivity values with comparable magnitudes. Figures 34 to 37 contain a great deal of noise due to the array crossing numerous boundaries between areas with different physical, chemical, and electrical properties. The data are filtered to remove most of this noise (figures 38-41). A comparison of surfaces before and after filtering, figures 34 to 37 against 38 to 41, shows broader anomalies after filtering (figures 38-41). Figures 38 through 41 demonstrate that filtering removes single point anomalies. The filtering also reinforces originally well-defined anomalies.

The filtered data are less variable at A=12 meters than at an A spacing of 18 meters. Standard deviations of the respective data sets show this

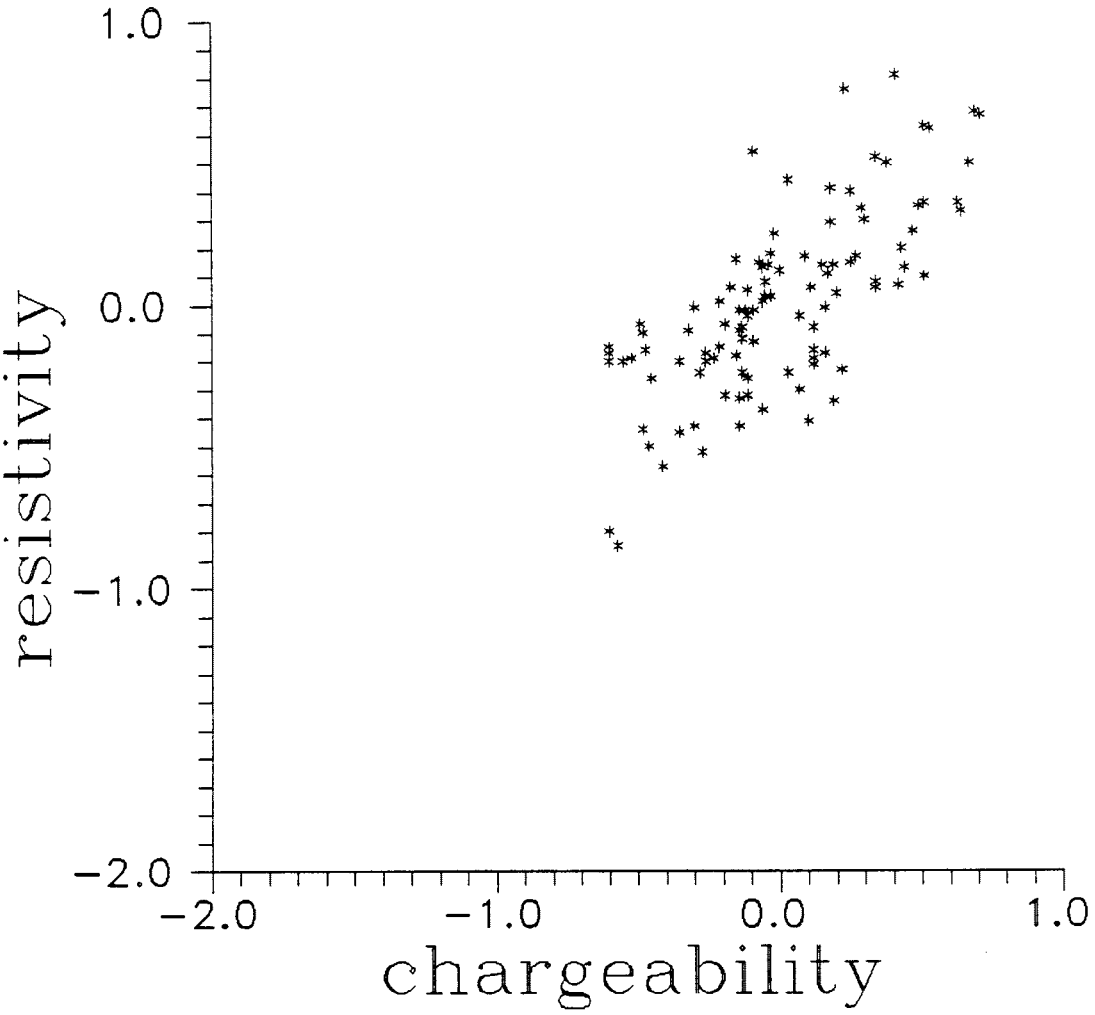

Figure 31. A-spacing = 12 meter chargeability data versus apparent resistivity data, after filtering and normalizing, from Smelterville Flats shows a 0.72 correlation.

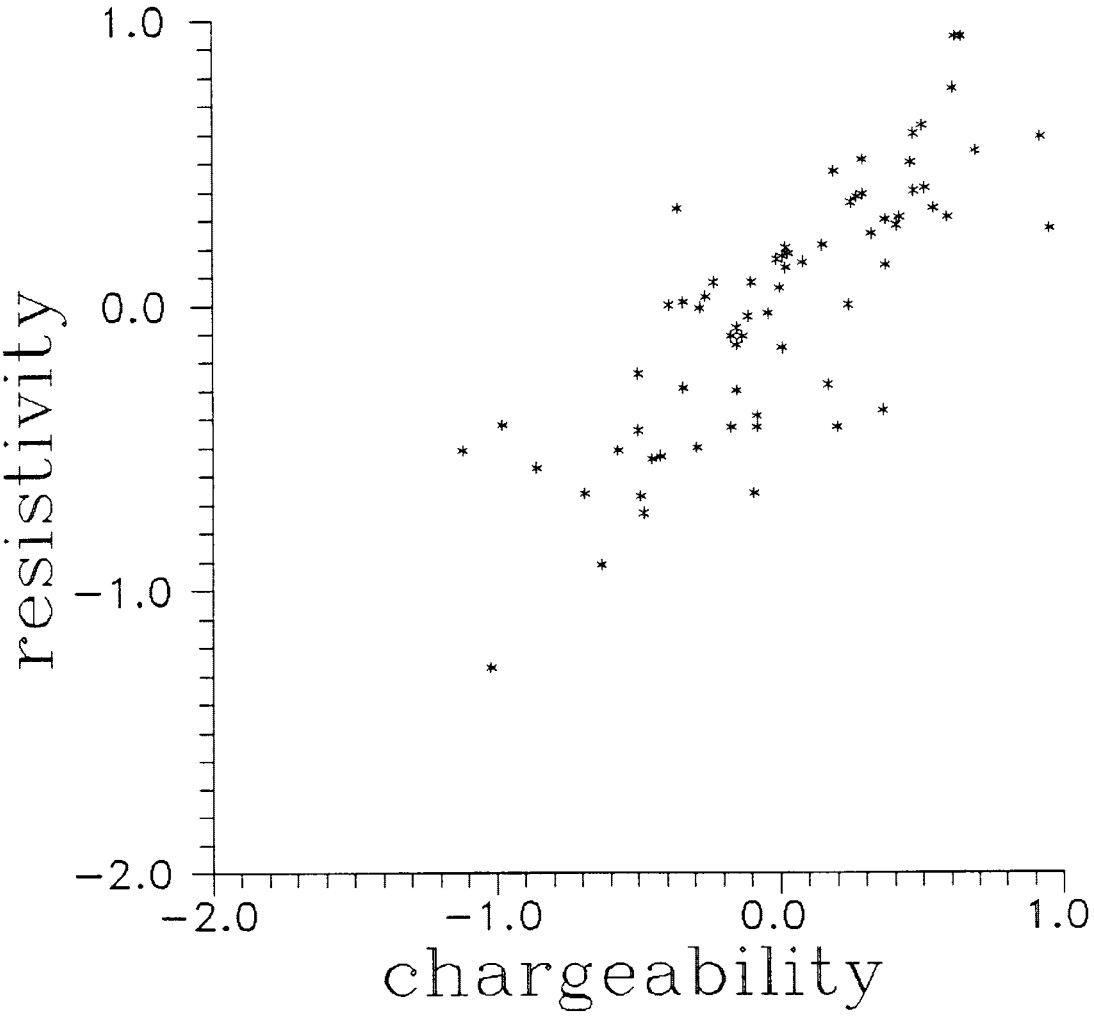

Figure 32. Chargeability data versus apparent resistivity data, after filtering and normalizing, from Smelterville Flats shows a 0.81 correlation.

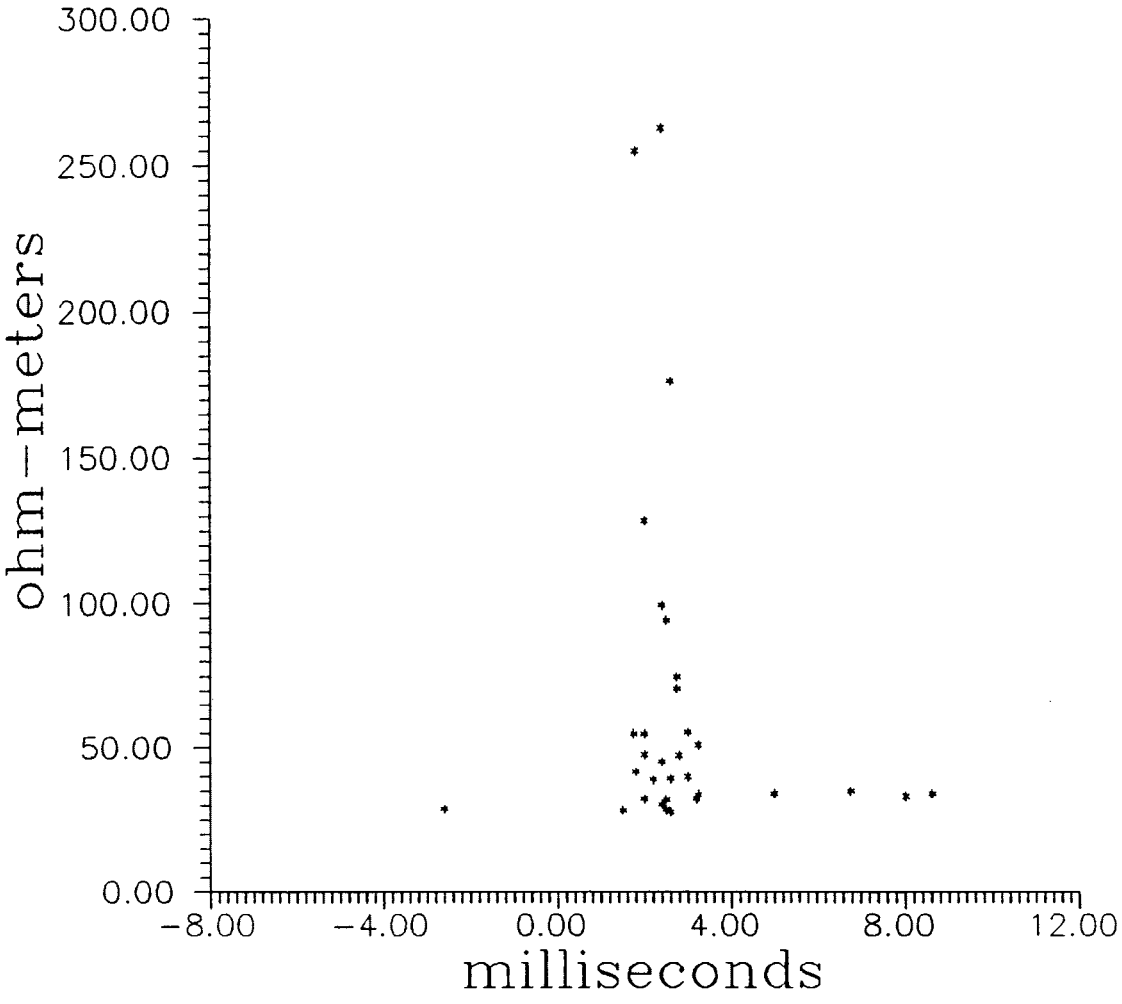

Figure 33. Chargeability plotted against apparent resistivity from Cataldo Flats shows there is no obvious correlation.

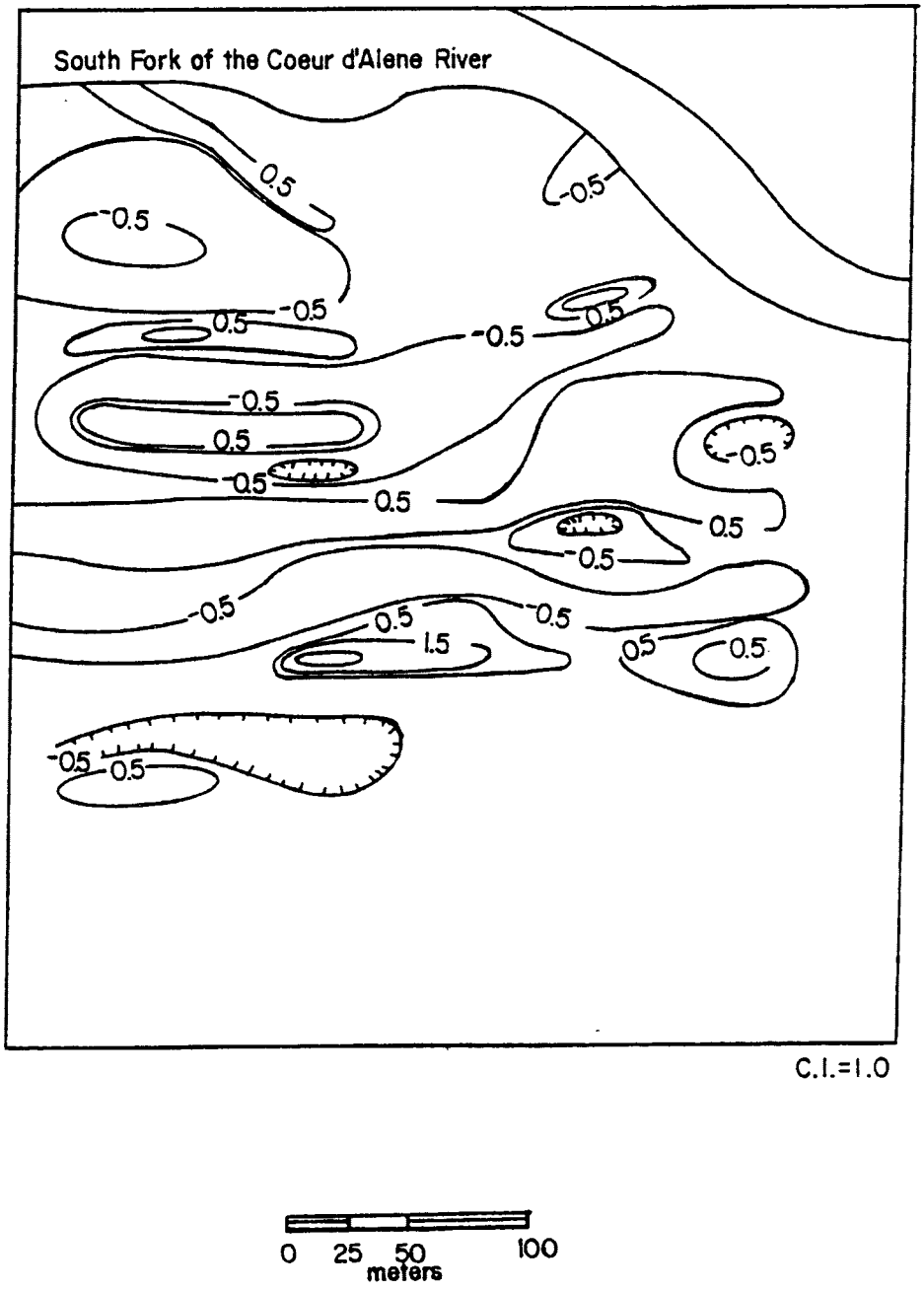

Figure 34. Contour map of kriged values based on A= 18 meter normalized IP data for the Smelterville Flats study site.

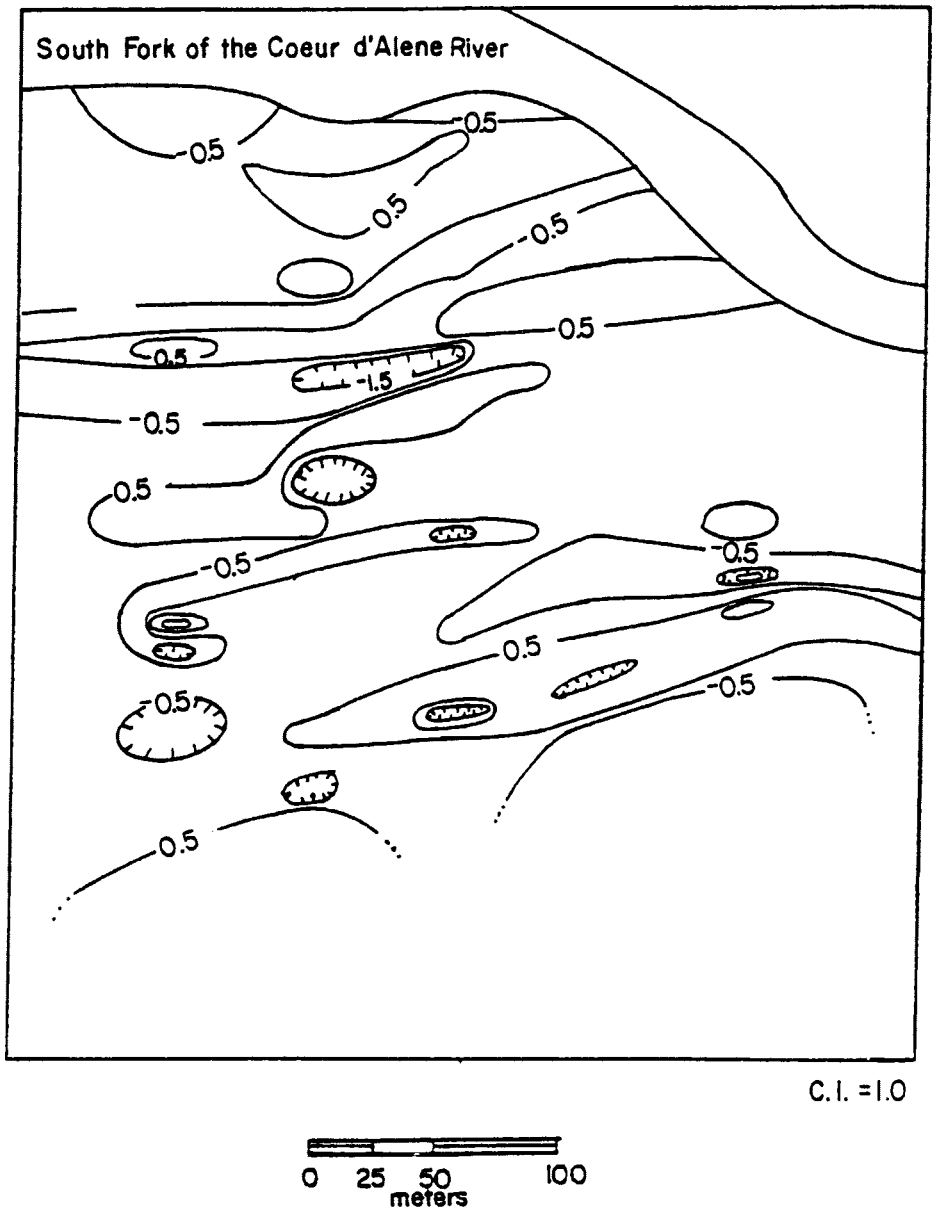

Figure 35. Contour map of kriged values based on A= 18 meter normalized apparent resistivity data for the Smelterville Flats study site.

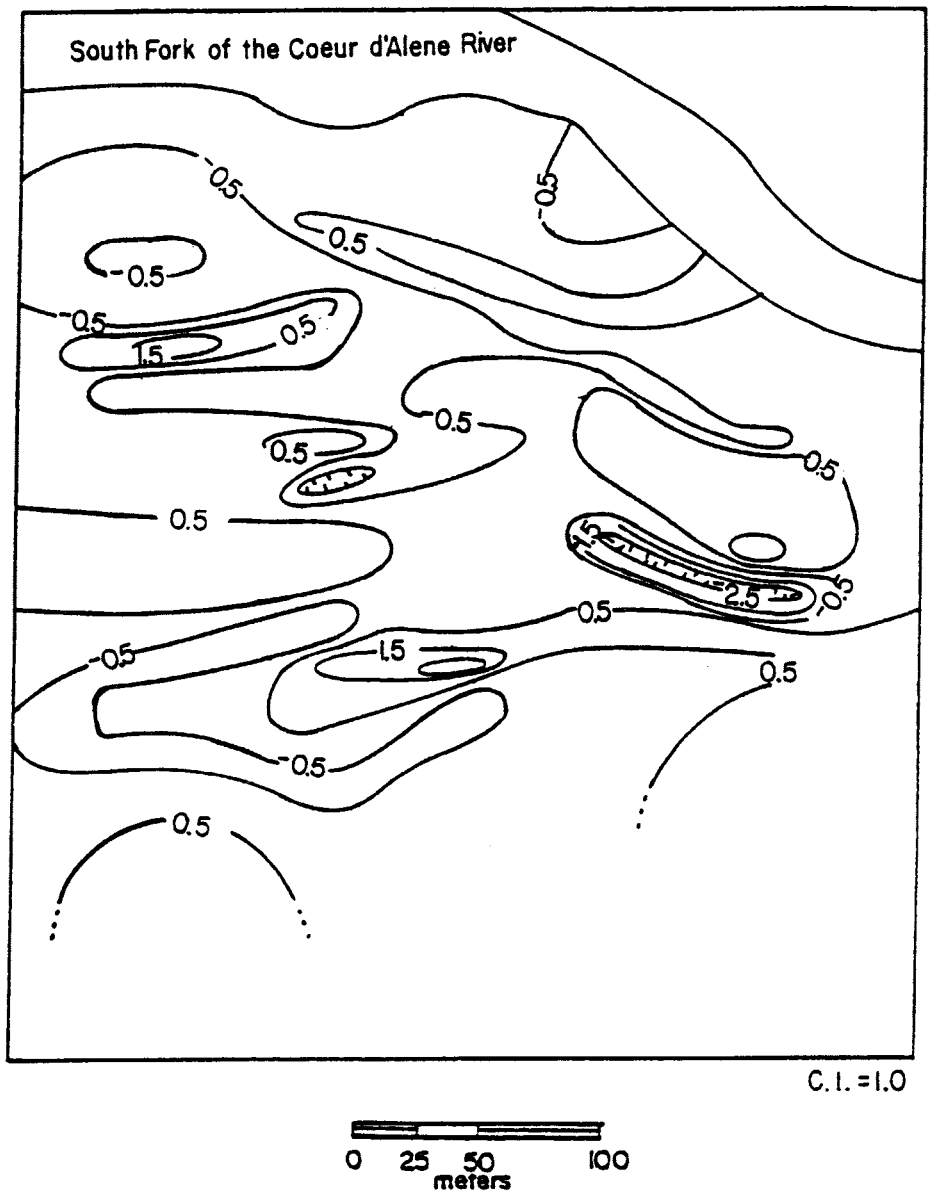

Figure 36. Contour map of kriged values based on A= 12 meter normalized IP data for the Smelterville Flats study site.

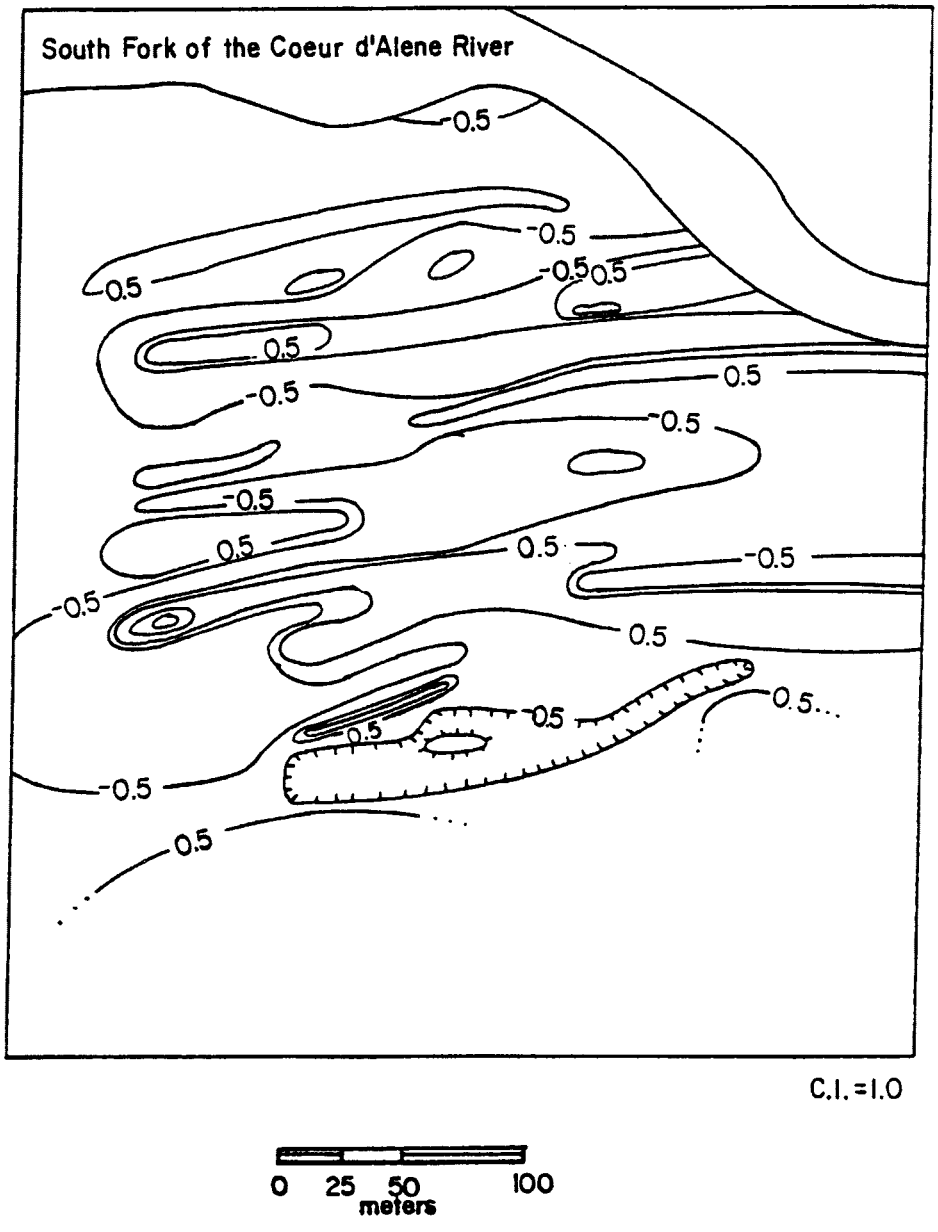

Figure 37. Contour map of kriged values based on A= 12 meter normalized apparent resistivity data for the Smelterville Flats study site.

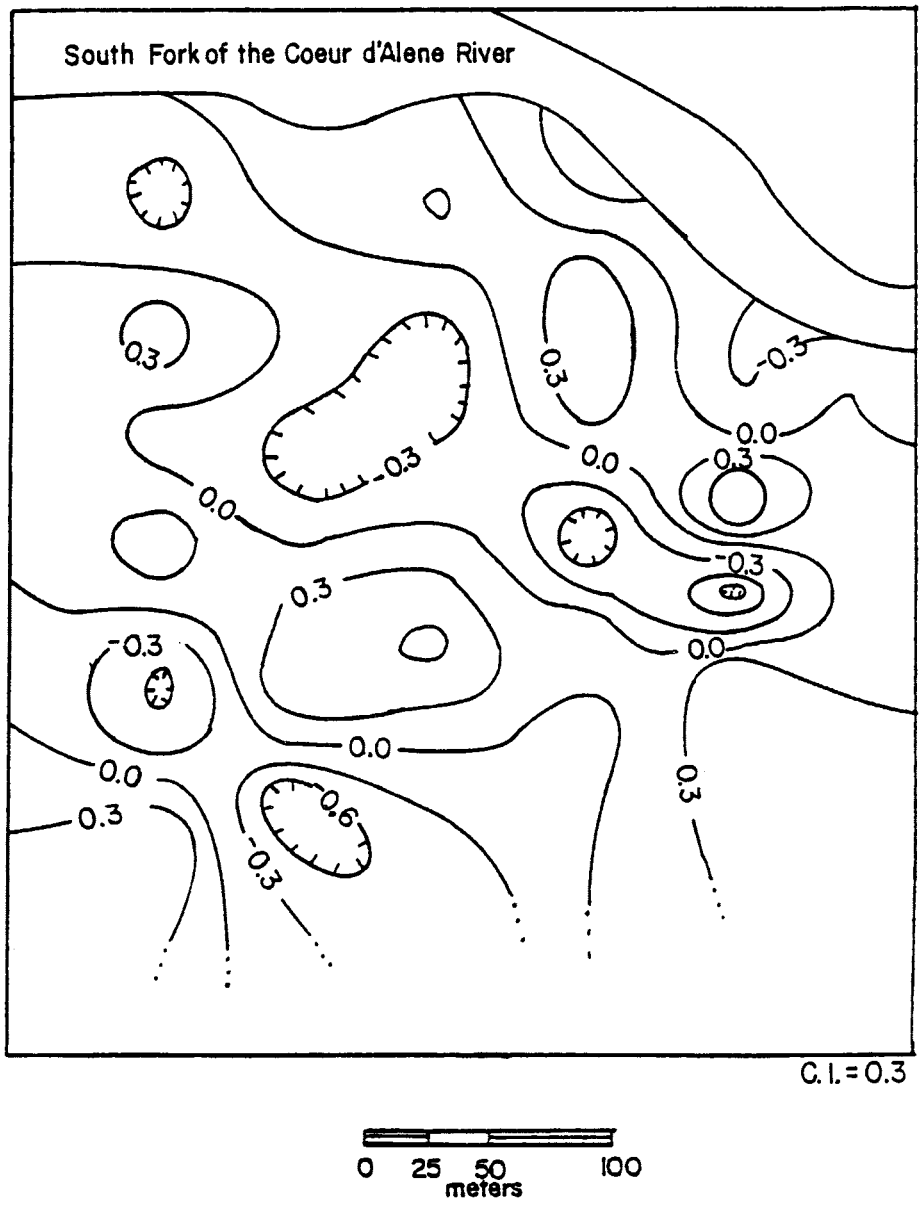

Figure 38. Contour map of kriged values based on A= 18 meter normalized and filtered IP data for the Smelterville Flats study site.

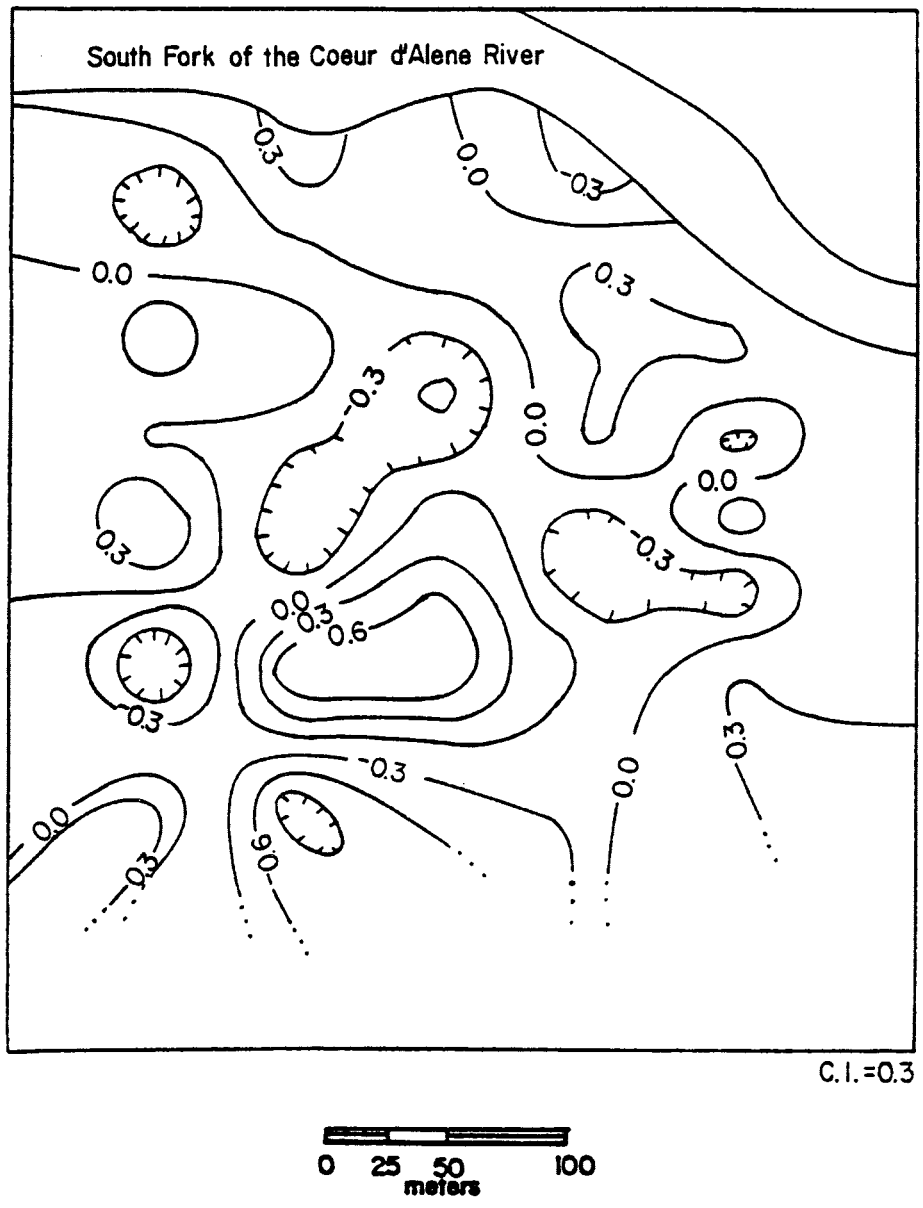

Figure 39. Contour map of kriged values based on A= 18 meter normalized and filtered apparent resistivity data for the Smelterville Flats study site.

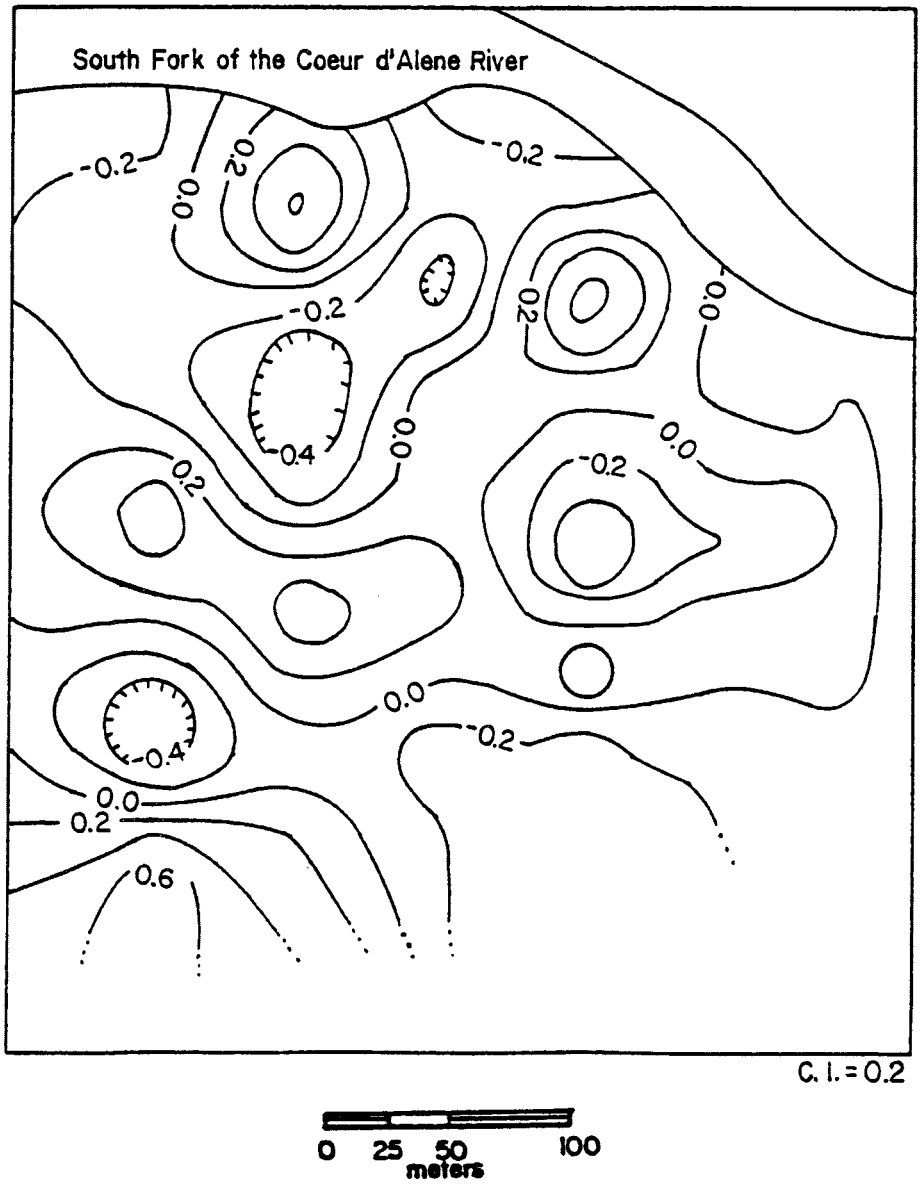

Figure 40. Contour map of kriged values based on A= 12 meter normalized and filtered IP data for the Smelterville Flats study site.

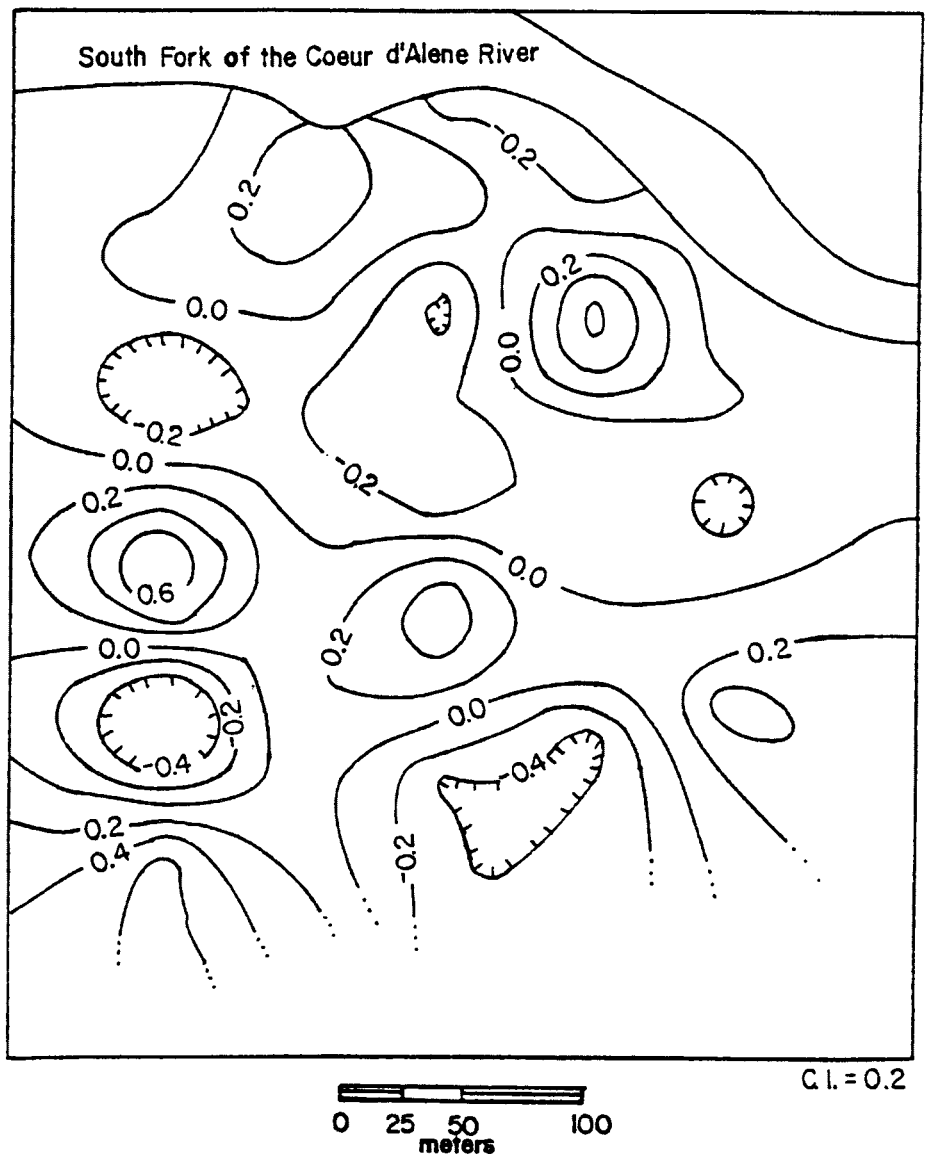

Figure 41. Contour map of kriged values based on A= 12 meter normalized and filtered apparent resistivity data for the Smelterville Flats study site.

TABLE 4. Standard deviations for the three chargeability and resistivity data surfaces, A-spacings of 12 and 18 meters, at Smelterville Flats, Idaho.

Data with Regional Trend Removed:

Data Type and A-Spacing	S.D.
12 meter resistivity:	95
12 meter chargeability:	0.87
18 meter resistivity:	60
18 meter chargeability:	0.85

Normalized Data:

12 meter resistivity:	1.00
12 meter chargeability:	1.00
18 meter resistivity:	1.00
18 meter chargeability:	1.00

Filtered and Normalized Data:

12 meter resistivity:	0.32
12 meter chargeability:	0.33
18 meter resistivity:	0.44
18 meter chargeability:	0.45.

(note: the magnitude of resistivity is much larger than chargeability) (Table 4). A 0.01 difference in the filtered data's standard deviations is not significant. The 12 meter data are more variable prior to filtering, hence the larger standard deviations. This can be produced by two processes. First, shallow alluvial material may be more variable than deeper deposits. Filtered data do not support this hypothesis. A better hypothesis is that the shorter A spacings produce more observations along each line and subsequently more readings have border crossing effects. Border effects produce a more variable unfiltered data set than the geology supports. Filtering reveals the shallow data are less variable than the slightly deeper 18 meter A-spacing data. The lesser variability in the A=12 meter filtered data set implies that the greatest contamination may be deeper than an A = 12 meters, n=1 dipole-dipole array optimally observes.

Resistivity and chargeability are well correlated. The 18 meter data surface covariance is 0.81 while the 12 meter covariance is 0.72. Deeper resistivity and chargeability anomalies, represented by the 18 meter A-spacings maps correlate more than the shallower 12 meter anomalies. The general trend and location of anomalies in the 12 and 18 meter surfaces coincide. This is readily observed by comparing figures 38 and 39 to figures 40 and 41. The 18 meter data resistivity and chargeability anomalies have the same sign and general geographic extent, which is expected with a covariance of 0.81. The 12 meter A spacing anomalies are not as distinct as those determined from the 18 meter A spacings. At A spacings of 12 meters chargeability appears more sensitive to contamination than resistivity as broader and more distinct chargeability anomalies are observed (figures 40 and 41). Laboratory work shows that IP can be more sensitive to the contaminant than resistivity in

cases with low contaminant levels. The high correlation between resistivity and chargeability may show that the arrays are observing effects below the water table. Chargeability reaches its maximum in the capillary fringe (Ogilvy and Kuz'mina, 1972). Resistivity varies inversely with saturation and would increase as saturation decreases. However, the capillary fringe will be larger in zones containing finer sediments and these finer sediments will have a greater degree of saturation and lower resistivity. Large volumes of slightly unsaturated fines should produce strong IP highs. The apparent resistivity values that would be recorded are not easily predicted, however these readings would most likely be weak lows due to a greater volume with higher saturation and the smaller grain size. Data conforming to this description is not very prevalent in either the 18 or 12 meter data sets.

The resistivity values measured on Smelterville Flats are controlled by porosity, water quality, and the degree of saturation. Because the water table is shallow, the dominant controlling factor for water content is porosity, which in turn is controlled by grain size. Flotation tailing at Smelterville Flats are composed of clay-sized particles, and should have a high degree of saturation and relatively low resistivity. Jig tailings and natural sediments are coarser and should show comparatively higher resistivities due to their lower degree of saturation and coarser grain size. Apparent resistivity and water quality are inversely related, a higher total dissolved solids (TDS) corresponds to a lower apparent resistivity.

Bodmer and others (1968) found that clean gravels, dense clays, sandy clays, and gravely clays do not produce IP anomalies. They (Bodmer et. al., 1968) avoided saline and contaminated ground water in their work. Ogilvy and Kuz'mina (1972) found the maximum IP effect in non-saline and uncontaminated deposits containing 5 to 20 percent clay. The wide range of

clay percentages is attributable to the wide range of ion exchange rates found in different clays. Low clay percentages, 5 to 30 percent, do not produce apparent resistivity anomalies.

Two different contaminant regimes are described by the four filtered data surfaces (figures 38-41). Jig tailings indicated by IP-apparent resistivity highs and flotation tailings indicated by IP-apparent resistivity lows (figure 42). These tailings are wastes products from mineral ore processing. Jig tailings originated from the older less efficient jigging process and contain relatively large amounts of contaminant metals. The finer flotation tailings have a comparatively lower metal content with much more surface area to allow metal lixiviation.

Many apparent resistivity highs coincide with IP highs. These anomalous highs probably represent jig tailings (figure 42). The high IP value could be produced by the high original metal content of jig tailings. Coarser sediments, which jig tailings typify, are generally more resistive than is greater than that of flotation tailings permitting dissolved metals to be transported from jig tails. The pore water's lower TDS causes a relatively higher apparent resistivity. IP processes in metal rich deposits, in this case jig tailings, is electrode polarization. Electrode polarization behaves opposite to membrane polarization, increased metals content increases the IP response. The data indicate that jig tailings still have high metal content. Norton (1980) observed high metal concentrations in some soil samples from soil pits on Smelterville Flats.

The resistivity lows on the filtered data maps may represent deposits of flotation tailings, natural massive clay deposits, or both. Resistivity lows associated with IP lows in both data sets, 12 and 18 meter A spacings, are defined as flotation tailing deposits (figure 42). Low IP anomalies in fine-grained tailings result from a low original metal content, their low

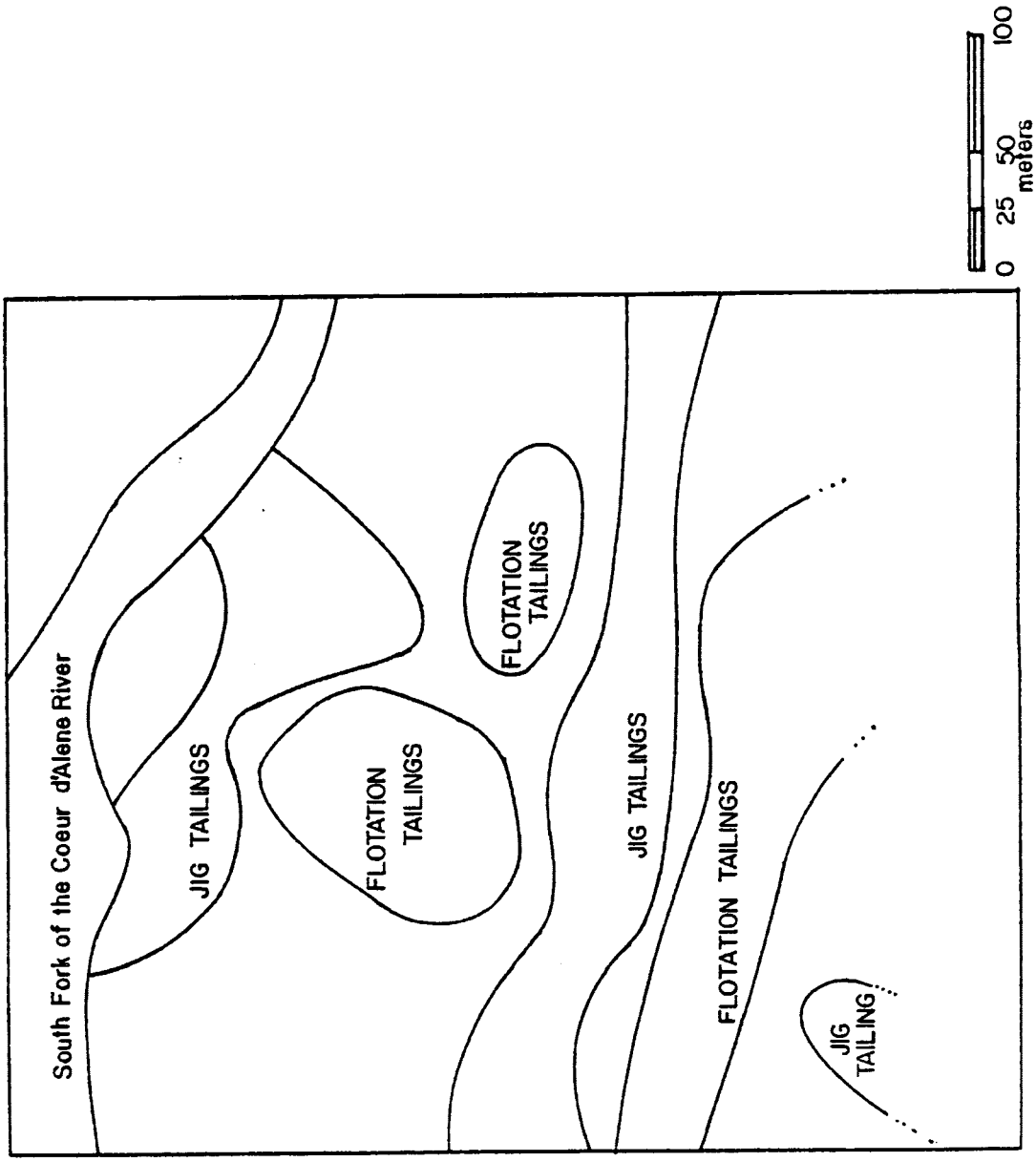

Figure 42. Estimated distribution of jig and flotation tailings at the Smelterville Flats study site based on the 12 and 18 meter A-spacing data after normalizing and filtering.

permeabilities, which can prevent liberated metal transportation, or both. Clay-sized tailing have a large surface area which permits relatively large volumes of metal liberation from the flotation tailings which produces a high TDS. A large contaminant TDS in metal poor sediments produces low apparent resistivity and chargeability. Resistivity lows in the map area not associated with significant IP anomalies probably represent natural uncontaminated low resistivity deposits.

CONCLUSIONS

Induced Polarization is a useful tool for gaining important information about the definition of ground water contamination. Laboratory work demonstrates that IP anomalies are produced by metal contaminated electrolytes in porous sediments. Field work demonstrates that IP anomalies do exist at Smelterville Flats, Cataldo Flats, and in the CIA's East Tailings Pond. Smelterville Flats anomalies are due to a contrast in sediment characteristics and ground water contamination differences. Cataldo Flats anomalies are most likely in response to changes in saturation levels. Finally, effects recorded in the East Tailings Pond are interpreted to represent physiographic changes in tailings, borrow pit effects. Studies on IP behavior in different hydrogeologic settings by previous investigators allow an estimation of the type and extent of each regime within the study areas. Phase domain instrumentation (ie. IPR-11 (Seara and Granda, 1987)) would permit more definitive conclusions at each study site. The Scintrex IPR-11 is a microprocessor controlled time domain IP receiver. This model measures 10 semi-logarithmically spaced points along the decay curve for six dipole settings simultaneously. Phase curves frequently should allow determination of metal content, grain size, and electrode versus membrane polarization.

Because IP surveys can be performed in conjunction with resistivity measurement at little additional cost, albeit three times more time on average, IP measurements should be routine in geophysical remedial evaluations. However, further study is needed in the theoretical and phenomological aspects causing the IP observations. Laboratory simulations are required with metal contamination, using expected and recorded combinations of metals and varied geologic material. Field application

studies are needed at sites with subsurface chemical, lithological, and geophysical data.

References Cited

American Geological Institute (1976). Dictionary of Geologic Terms, Revised Edition, Anchor Press/Doubleday, Garden City, New York.

Angoran, Y. and Madden, T.R. (1977). Induced Polarization: A Preliminary Study of its Chemical Basis. Geophysics Vol.42(4) pp. 788-803.

Bodmer, R., Ward, S.H., and Morrison, H.F. (1968). On Induced Electrical Polarization and Groundwater, Geophysics vol.33(5) pp. 805-821.

Clark, I. (1979). Practical Geostatistics, Elsevier Applied Science Publishers, London.

Davis, J.C. (1986). Statistics and Data Analysis in Geology, 2nd ed., John Wiley & Sons, New York.

Dobecki, T.L. and Romig, P.R. (1985). Geotechnical and Groundwater Geophysics, Geophysics, vol 50(12) pp.2621-2636

Freeze, R.A. and Cherry, J. (1979). Groundwater, Prentice Hall, Englewood Cliffs, New Jersey.

Galbraith, J.H., Williams, R.E., and Siems, P.L. (1972). Migration and Leaching of Metals from Old Mine Tailings Deposits, Ground Water vol. 10(3) pp. 33-44.

Granda Sanz, A. and Sastre Pascual, J.L. (1982). Prospeccion Geofisca Salobres en Cuencas Teciarias Analisis y Critica del Metododo Resistividad-polarizacion Inducida, Boletin Geologico y Minero T. 93(5) pp. 415-425.

Hem, J.D. (1970) Study and interpretation of the Chemical Characteristics of Natural Water, 2nd Ed., fifth printing 1983 Geological Survey Water-Supply Paper 1473, United States Government Printing Office, Washington, D.C.

Ioannau, C. (1979). Distribution, Transport, and Reclamation of Abandoned Mine Tailings along the Channel of the South Fork of the Coeur d'Alene

River and Tributaries, Idaho, Hydrology Master's Thesis, University of Idaho.

Keevil, N.B. and Ward, S.H., (1962). Electrolyte Activity: Its Effect on Induced Polarization, Geophysics vol. 27(5) pp. 677-690.

Klein, J.D., Biegler, T., and Horne, M.D., (1984). Mineral Interfacial Processes in the Method of Induced Polarization, Geophysics vol.49(7) pp. 1105-1114.

Mahan, M.K., Redman, J.D, and Strangway, D.W. (1986) Complex Resistivity of Synthetic Sulphide Bearing Rocks, Geophysical Prospecting vol. 34 pp. 743-768.

Marshall, D.J. and Madden, T.R. (1959), Induced Polarization, a Study of its Causes. Geophysics Vol. 24(4) pp. 790-816.

Norton, M.A. (1980). Hydrogeology and Potential Reclamation Procedures for an Uncontrolled Mine Waste Deposition Site, Kellogg, Idaho, Master's Thesis, University of Idaho.

Ogilvy, A.A. and Kuz'mina, E.N. (1972), Hydrogeologic and Engineering-Geologic Possibilities for Employing the Method of Induced Potentials. Geophysics Vol. 37(5) pp. 839-861.

Olhoeft, G.R. (1985), Low-frequency Electrical Properties, Geophysics Vol.50(12) pp. 2492-2503.

Olorunfemi, M.O. and Griffiths, D.H. (1985), A Laboratory Investigation of the Induced Polarization of the Triassic Sherwood Sandstone of Lancashire and its Hydrogeological Applications. Geophysical Prospecting Vol.33 pp.110-127.

Ortman, D. Controlling Seepage from the Bunker Hill Central Impoundment Area, Kellogg, Shosone County, Idaho, Hydrology Master's Thesis, University of Idaho.

Press, W.H., Flannery, B.P., Teukolsky, S.A., and Vetterling, W.T., (1986). Numerical Recipes, The Art of Scientific Computing, Cambridge University Press, Cambridge.

Roy, K.K. and Elliott, H.M. (1981), Some Observation regarding Depth of Exploration in D.C. Electrical Methods. Geoexploration Vol. 19 pp. 1-13.

Roy, K.K. and Elliott, H.M. (1980), Resistivity and IP Survey for Delineating Saline Water and Fresh Water Zones. Geoexploration Vol. 18 pp.145-162.

Seara, J.L. and Granda, A. (1987). Interpretation of I.P. Time Domain/Resistivity Soundings for Delineating Sea-Water Intrusions in Some Coastal Areas of the Northeast of Spain. Geoexploration Vol. 24 pp. 153-162.

Sumner, J.S. (1976). Principles of Induced Polarization for Geophysical Exploration, Elsevier Science Publishing Co.

Vacquier, V., Holmes, C.R., Kintzinger, P.R., and Laverge, M. (1957), Prospecting for Ground Water by Induced Electrical Polarization. Geophysics Vol.22(3) pp. 660-687.

Van Blaricom, R. (1980). Practical Geophysics for the Exploration Geologist, Northwest Mining Assoc., Spokane, Washington.

APPENDIX A

SEMI-VARIOGRAMS FOR SMELTERVILLE FLATS

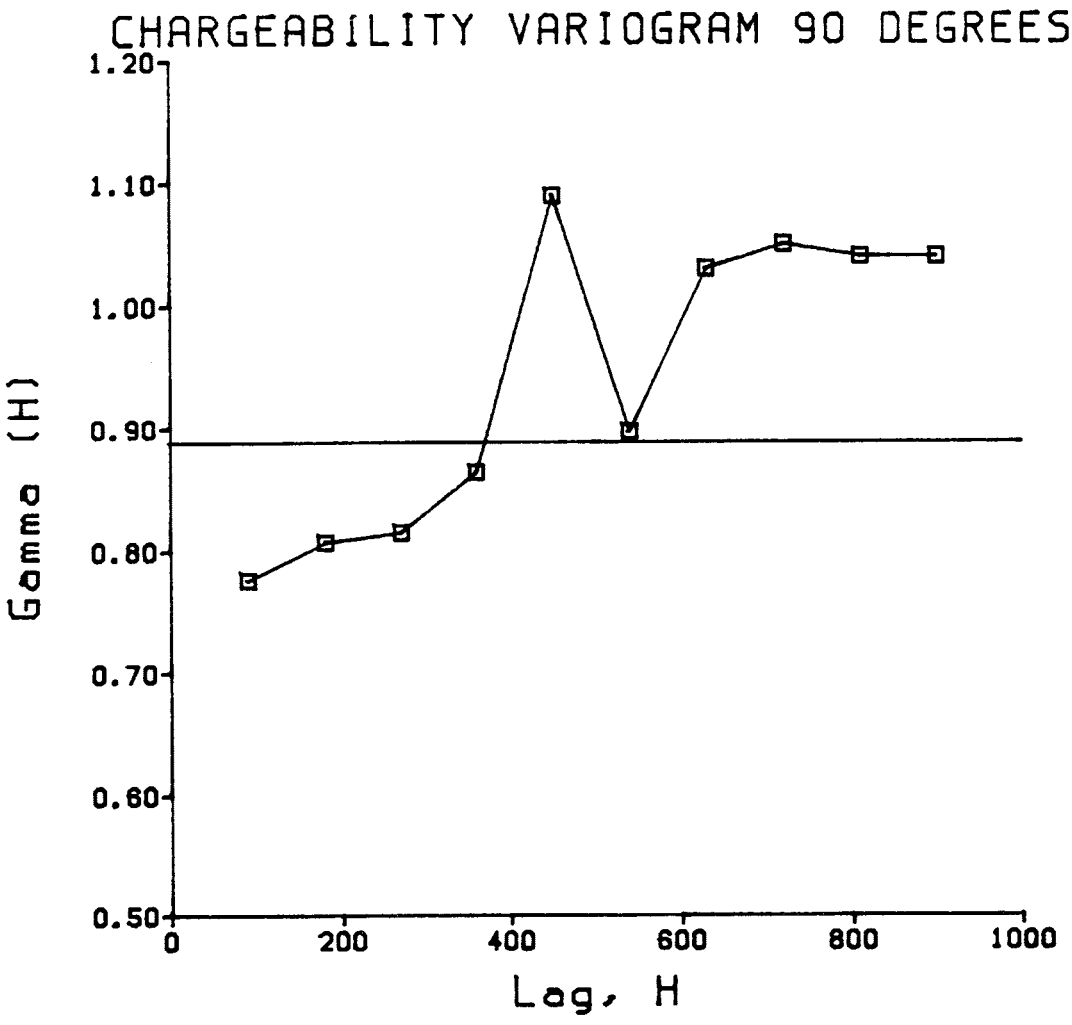
CHARGEABILITY VARIOGRAM 90 DEGREES
Gamma (H)
1.20
1.10
1.00
0.90
0.80
0.70
0.60
0.50
0
200
400
600
800
1000
Lag, H

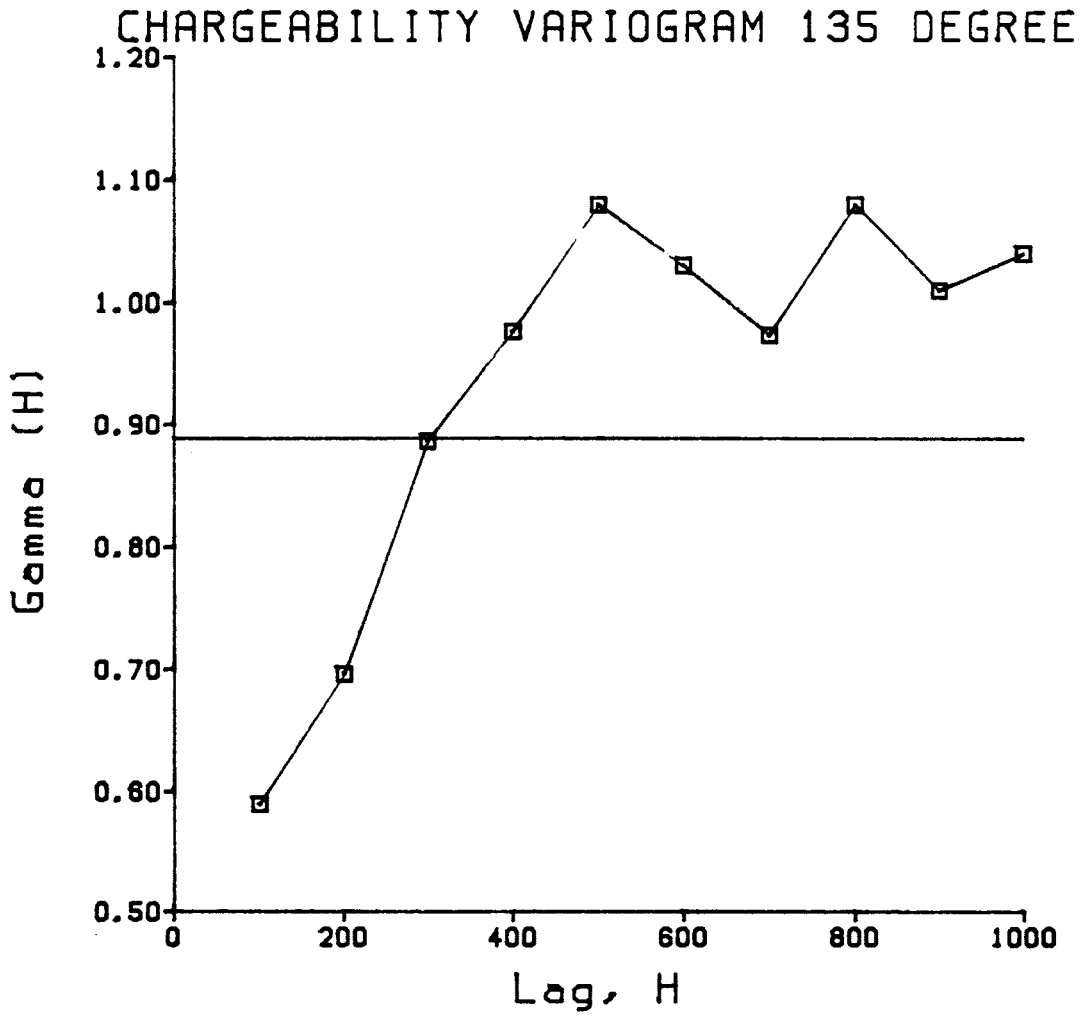
CHARGEABILITY VARIOGRAM 135 DEGREE
Gamma (H)
1.20
1.10
1.00
0.90
0.80
0.70
0.60
0.50
0
200
400
600
800
1000
Lag, H

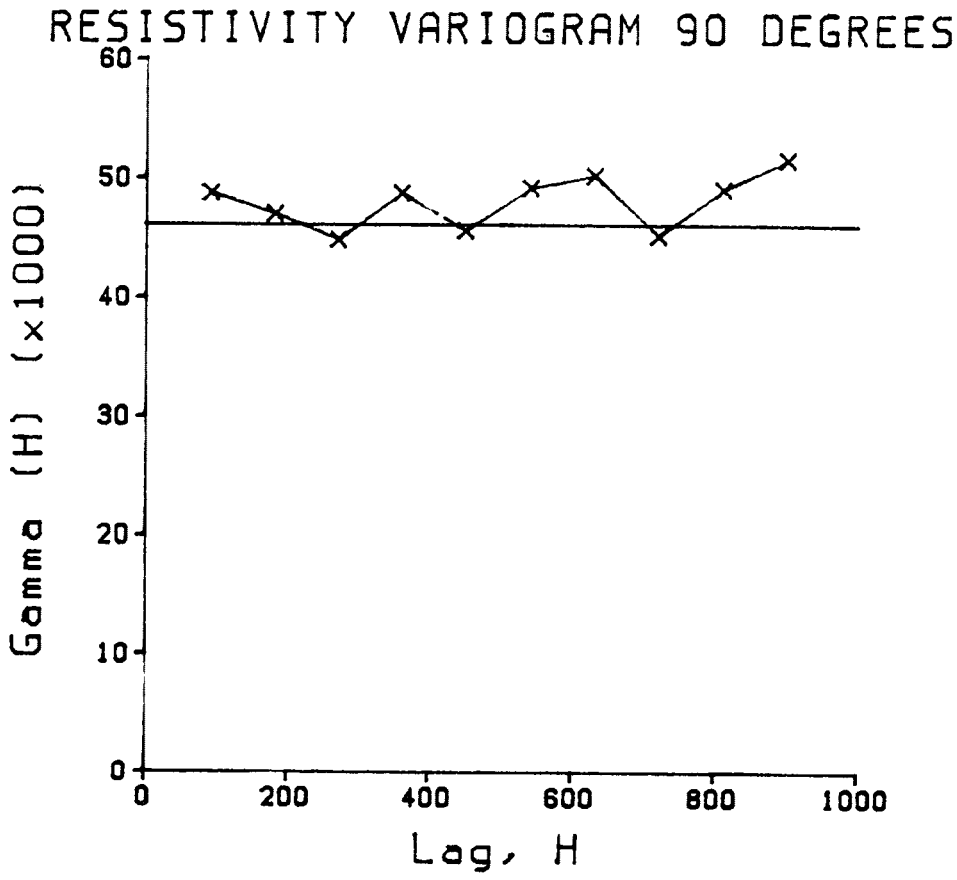
RESISTIVITY VARIOGRAM 90 DEGREES
Gamma (H) (x1000)
60
50
40
30
20
10
0
0
200
400
600
800
1000
Lag, H

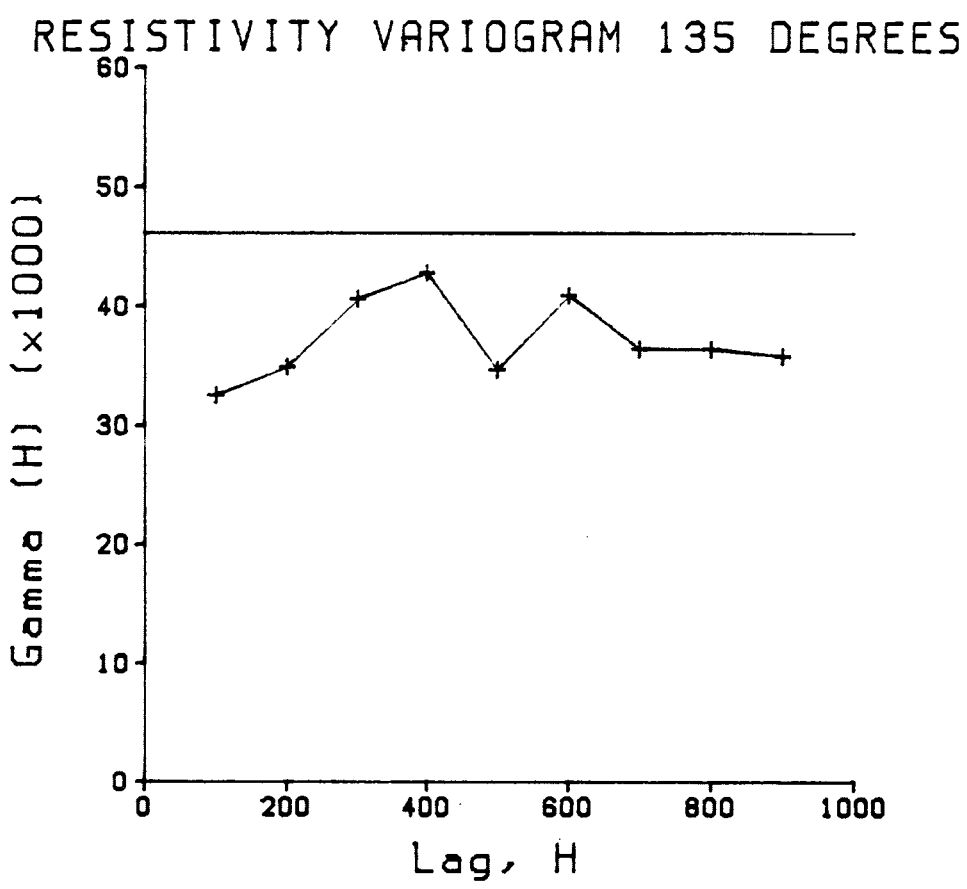
RESISTIVITY VARIOGRAM 135 DEGREES
Gamma (H) (x1000)
60
50
40
30
20
10
0
0
200
400
600
800
1000
Lag, H

APPENDIX B

FIELD DATA

AND

LABORATORY DATA

SMELTERVILLE FLATS
A = 18 METERS IP DATA

X feet	Y feet	IP effect msec.	IP effect resid.	IP effect normalized
2000	3495	4.60	0.84	0.99
2000	3555	3.80	0.01	0.01
2000	3615	3.30	-0.49	-0.58
2000	3675	3.60	-0.17	-0.20
2000	3735	2.50	-1.23	-1.45
2000	3795	3.70	0.03	0.03
2000	3855	4.40	0.80	0.94
2000	3915	4.00	0.48	0.56
2000	3975	3.20	-0.25	-0.29
2000	4035	3.50	0.12	0.14
2000	4095	2.60	-0.73	-0.86
2000	4155	5.00	1.69	1.99
2000	4215	2.75	-0.57	-0.67
2000	4275	3.70	0.32	0.38
2000	4335	2.90	-0.59	-0.70
2000	4395	3.10	-0.58	-0.68
2000	4455	4.20	0.26	0.31
2185	3545	2.10	-1.17	-1.38
2185	3605	3.40	-0.09	-0.11
2185	3665	4.20	0.55	0.65
2185	3725	5.00	1.24	1.46
2185	3785	3.10	-0.72	-0.84
2185	3845	4.60	0.77	0.91
2185	3905	4.25	0.45	0.53
2185	3965	2.00	-1.74	-2.05
2185	4025	4.50	0.85	1.00
2185	4085	2.40	-1.14	-1.35
2185	4145	3.80	0.38	0.44
2185	4205	3.75	0.45	0.53
2185	4265	2.25	-0.93	-1.10
2185	4325	3.50	0.42	0.49
2185	4385	3.25	0.24	0.29
2370	3610	3.25	0.25	0.29
2370	3670	2.20	-1.03	-1.22
2370	3730	5.50	2.10	2.48
2370	3790	3.50	0.00	0.01
2370	3850	3.50	-0.04	-0.04
2370	3910	3.70	0.18	0.21
2370	3970	3.75	0.29	0.34
2370	4030	2.40	-0.95	-1.12
2370	4090	3.25	0.04	0.05
2370	4150	2.60	-0.43	-0.51
2370	4210	2.10	-0.74	-0.87
2370	4270	3.10	0.47	0.55
2370	4330	2.75	0.33	0.39
2565	3665	3.10	-0.33	-0.38
2565	3725	3.75	0.15	0.17
2565	3785	4.30	0.57	0.68

X feet	Y feet	IP effect msec.	IP effect resid.	IP effect normalized
2565	3845	3.80	0.01	0.01
2565	3905	1.70	-2.11	-2.48
2565	3965	4.00	0.22	0.26
2565	4025	4.20	0.50	0.58
2565	4085	4.10	0.51	0.60
2565	4145	3.00	-0.46	-0.54
2565	4205	4.50	1.20	1.42
2565	4265	3.50	0.38	0.44
2565	4325	2.50	-0.45	-0.53
2565	4385	2.30	-0.47	-0.56
2760	3680	4.10	0.47	0.55
2760	3720	3.60	-0.15	-0.18
2760	3760	5.30	1.44	1.70
2760	3800	2.70	-1.25	-1.47
2760	3840	1.20	-2.82	-3.32
2760	3880	5.60	1.51	1.78
2760	3920	4.90	0.76	0.89
2760	3960	4.60	0.41	0.48
2760	4000	5.20	0.98	1.15
2760	4040	3.60	-0.65	-0.77
2760	4080	4.20	-0.08	-0.09
2760	4120	4.00	-0.30	-0.35

A = 19 METERS APPARENT RESISTIVITY DATA

X feet	Y feet	Resistivity ohm-m.	Resistivity resid.	Resistivity normalized
2000	3495	297.00	22.69	0.38
2000	3555	319.00	67.91	1.13
2000	3615	197.00	-38.76	-0.65
2000	3675	240.00	13.45	0.22
2000	3735	90.00	-131.87	-2.20
2000	3795	219.00	-1.33	-0.02
2000	3855	250.00	29.27	0.49
2000	3915	294.00	71.91	1.20
2000	3975	192.00	-31.62	-0.53
2000	4035	269.00	44.29	0.74
2000	4095	127.00	-97.98	-1.64
2000	4155	401.00	176.79	2.95
2000	4215	150.00	-72.40	-1.21
2000	4275	226.00	6.24	0.10
2000	4335	184.00	-32.68	-0.55
2000	4395	167.00	-46.74	-0.78
2000	4455	243.00	31.26	0.52
2185	3545	117.00	-82.36	-1.37
2185	3605	166.00	-35.49	-0.59
2185	3665	206.00	-0.27	0.00
2185	3725	400.00	187.73	3.13

X feet	Y feet	Resistivity ohm-m.	Resistivity resid.	Resistivity normalized
2185	3785	165.00	-53.28	-0.89
2185	3845	160.00	-63.28	-1.06
2185	3905	266.00	39.56	0.66
2185	3965	113.00	-114.15	-1.91
2185	4025	264.00	39.03	0.65
2185	4085	178.00	-41.67	-0.70
2185	4145	287.00	75.76	1.26
2185	4205	164.00	-35.83	-0.60
2185	4265	156.00	-29.81	-0.50
2185	4325	209.00	39.26	0.66
2185	4385	168.00	15.60	0.26
2370	3610	164.00	-16.71	-0.28
2370	3670	177.00	-14.10	-0.24
2370	3730	336.00	135.20	2.26
2370	3790	252.00	43.19	0.72
2370	3850	168.00	-46.34	-0.77
2370	3910	290.00	73.22	1.22
2370	3970	214.00	-1.73	-0.03
2370	4030	152.00	-58.98	-0.98
2370	4090	160.00	-42.53	-0.71
2370	4150	163.00	-27.55	-0.46
2370	4210	177.00	1.55	0.03
2370	4270	175.00	17.19	0.29
2370	4330	143.00	4.59	0.08
2565	3665	166.00	-18.91	-0.32
2565	3725	221.00	25.56	0.43
2565	3785	177.00	-27.55	-0.46
2565	3845	190.00	-21.61	-0.36
2565	3905	125.00	-91.23	-1.52
2565	3965	249.00	30.80	0.51
2565	4025	255.00	37.49	0.63
2565	4085	245.00	30.65	0.51
2565	4145	156.00	-53.11	-0.89
2565	4205	309.00	106.62	1.78
2565	4265	181.00	-13.93	-0.23
2565	4325	181.00	-6.75	-0.11
2565	4385	148.00	-34.01	-0.57
2760	3680	199.00	29.57	0.49
2760	3720	157.00	-21.20	-0.35
2760	3760	253.00	65.72	1.10
2760	3800	146.00	-50.54	-0.84
2760	3840	136.00	-69.89	-1.17
2760	3880	233.00	17.73	0.30
2760	3920	293.00	68.32	1.14
2760	3960	254.00	19.86	0.33
2760	4000	208.00	-35.72	-0.60
2760	4040	189.00	-64.52	-1.08
2760	4080	307.00	43.32	0.72
2760	4120	289.00	14.60	0.24

A = 12 METER IP DATA

X feet	Y feet	IP effect millisec.	IP effect resid	IP effect Normalized
2000	3465	3.90	0.93	1.08
2000	3505	3.10	-0.20	-0.23
2000	3545	3.75	0.17	0.20
2000	3585	3.25	-0.57	-0.65
2000	3625	3.10	-0.91	-1.05
2000	3665	3.80	-0.36	-0.41
2000	3705	4.30	0.04	0.04
2000	3745	2.75	-1.58	-1.83
2000	3785	6.25	1.88	2.17
2000	3825	3.70	-0.68	-0.78
2000	3865	4.50	0.14	0.17
2000	3905	5.00	0.69	0.79
2000	3945	5.00	0.74	0.86
2000	3985	4.50	0.31	0.36
2000	4025	4.30	0.19	0.22
2000	4065	3.60	-0.44	-0.50
2000	4105	3.40	-0.57	-0.66
2000	4145	4.75	0.83	0.96
2000	4185	3.25	-0.64	-0.74
2000	4225	3.90	0.01	0.01
2000	4265	4.10	0.17	0.20
2000	4305	3.80	-0.22	-0.25
2000	4345	4.00	-0.16	-0.19
2000	4385	4.75	0.38	0.43
2000	4425	4.25	-0.41	-0.47
2185	3515	4.60	0.68	0.78
2185	3555	2.50	-1.55	-1.78
2185	3595	4.20	0.05	0.06
2185	3635	5.00	0.78	0.90
2185	3675	4.25	-0.02	-0.02
2185	3715	4.10	-0.19	-0.22
2185	3755	4.60	0.31	0.36
2185	3795	4.25	-0.02	-0.02
2185	3835	6.50	2.27	2.62
2185	3875	3.10	-1.07	-1.24
2185	3915	4.60	0.50	0.58
2185	3955	2.90	-1.12	-1.29
2185	3995	3.10	-0.83	-0.95
2185	4035	5.10	1.27	1.46
2185	4075	2.50	-1.24	-1.43
2185	4115	2.20	-1.45	-1.67
2185	4155	3.70	0.13	0.15
2185	4195	3.00	-0.51	-0.59
2185	4235	4.25	0.77	0.89
2185	4275	3.25	-0.22	-0.25
2185	4315	4.50	1.00	1.15
2185	4355	4.30	0.73	0.84
2185	4395	4.00	0.30	0.34

X feet	Y feet	IP effect millisec.	IP effect resid	IP effect Normalized
2370	3580	4.50	-0.29	-0.33
2370	3620	4.80	0.01	0.01
2370	3660	3.60	-1.18	-1.36
2370	3700	5.90	1.13	1.31
2370	3740	5.00	0.26	0.30
2370	3780	4.00	-0.71	-0.82
2370	3820	4.60	-0.07	-0.08
2370	3860	7.40	2.79	3.21
2370	3900	3.10	-1.45	-1.67
2370	3940	4.25	-0.23	-0.26
2370	3980	4.50	0.10	0.11
2370	4020	4.30	-0.02	-0.03
2370	4060	5.50	1.26	1.45
2370	4100	4.60	0.44	0.51
2370	4140	2.25	-1.83	-2.11
2370	4180	4.50	0.49	0.56
2370	4220	4.00	0.05	0.05
2370	4260	3.10	-0.81	-0.94
2370	4300	3.25	-0.64	-0.74
2370	4340	4.00	0.10	0.12
2370	4380	3.90	-0.04	-0.05
2370	4420	4.50	0.48	0.55
2370	4460	3.60	-0.54	-0.63
2565	3635	4.10	-0.90	-1.03
2565	3675	6.25	1.33	1.54
2565	3715	4.90	0.06	0.07
2565	3755	5.25	0.48	0.55
2565	3795	4.90	0.19	0.22
2565	3835	3.25	-1.39	-1.60
2565	3875	4.10	-0.47	-0.55
2565	3915	4.20	-0.30	-0.35
2565	3955	4.30	-0.13	-0.15
2565	3995	4.00	-0.35	-0.40
2565	4035	4.25	-0.02	-0.02
2565	4075	4.00	-0.19	-0.21
2565	4115	4.30	0.20	0.23
2565	4155	4.00	-0.01	-0.02
2565	4195	5.60	1.67	1.93
2565	4235	4.30	0.45	0.52
2565	4275	3.90	0.13	0.15
2565	4315	4.10	0.39	0.45
2565	4355	3.10	-0.55	-0.64
2565	4395	3.50	-0.12	-0.14
2760	3680	4.60	-0.40	-0.47
2760	3720	4.70	-0.12	-0.14
2760	3760	5.25	0.60	0.69
2760	3800	7.00	2.51	2.89
2760	3840	1.25	-3.10	-3.57
2760	3880	4.00	-0.21	-0.24
2760	3920	5.00	0.93	1.07

X feet	Y feet	IP effect millisec.	IP effect resid	IP effect Normalized
2760	3960	4.00	0.07	0.08
2760	4000	3.70	-0.09	-0.11
2760	4040	3.70	0.05	0.06
2760	4080	3.50	0.00	0.00
2760	4120	3.10	-0.25	-0.29
2760	4160	3.10	-0.09	-0.10

A = 12 METERS APPARENT RESISTIVITY DATA

X feet	Y feet	Resistivity ohm-meters	Resistivity resid	Resistivity Normalized
2000	3465	312	100.84	1.06
2000	3505	212	-20.71	-0.22
2000	3545	265	11.10	0.12
2000	3585	221	-53.09	-0.56
2000	3625	233	-59.72	-0.63
2000	3665	219	-90.33	-0.95
2000	3705	193	-130.54	-1.37
2000	3745	215	-120.10	-1.26
2000	3785	659	315.18	3.32
2000	3825	286	-63.62	-0.67
2000	3865	471	118.47	1.25
2000	3905	471	118.34	1.25
2000	3945	240	-110.20	-1.16
2000	3985	456	110.52	1.16
2000	4025	372	33.12	0.35
2000	4065	204	-126.91	-1.34
2000	4105	222	-100.15	-1.05
2000	4145	378	64.70	0.68
2000	4185	247	-58.13	-0.61
2000	4225	295	-3.53	-0.04
2000	4265	353	58.54	0.62
2000	4305	327	32.99	0.35
2000	4345	259	-39.33	-0.41
2000	4385	304	-4.69	-0.05
2000	4425	309	-17.45	-0.18
2185	3515	341	48.31	0.51
2185	3555	200	-98.67	-1.04
2185	3595	263	-42.55	-0.45
2185	3635	503	190.42	2.00
2185	3675	218	-101.12	-1.06
2185	3715	366	41.35	0.44
2185	3755	372	43.29	0.46
2185	3795	245	-85.95	-0.90
2185	3835	469	137.89	1.45
2185	3875	189	-140.05	-1.47
2185	3915	505	180.30	1.90
2185	3955	166	-152.09	-1.60

X feet	Y feet	Resistivity ohm-meters	Resistivity resid	Resistivity Normalized
2185	3995	297	-12.36	-0.13
2185	4035	331	32.28	0.34
2185	4075	293	6.50	0.07
2185	4115	158	-115.11	-1.21
2185	4155	343	83.93	0.88
2185	4195	145	-99.99	-1.05
2185	4235	332	100.43	1.06
2185	4275	200	-19.61	-0.21
2185	4315	283	73.00	0.77
2185	4355			0.00
2185	4395	243	41.07	0.43
2370	3580	282	-72.87	-0.77
2370	3620	347	-7.94	-0.08
2370	3660	313	-43.85	-0.46
2370	3700	637	277.19	2.92
2370	3740	144	-219.16	-2.31
2370	3780	403	36.70	0.39
2370	3820	536	167.25	1.76
2370	3860	488	117.89	1.24
2370	3900	280	-90.10	-0.95
2370	3940	294	-74.50	-0.78
2370	3980	314	-51.21	-0.54
2370	4020	303	-57.23	-0.60
2370	4060	478	124.37	1.31
2370	4100	239	-106.61	-1.12
2370	4140	278	-58.43	-0.61
2370	4180	322	-4.48	-0.05
2370	4220	254	-62.22	-0.65
2370	4260	290	-16.22	-0.17
2370	4300	222	-75.14	-0.79
2370	4340	419	129.27	1.36
2370	4380	260	-24.85	-0.26
2370	4420	317	33.54	0.35
2370	4460	235	-51.58	-0.54
2565	3635	265	-95.60	-1.01
2565	3675	384	32.18	0.34
2565	3715	377	30.85	0.32
2565	3755	353	10.26	0.11
2565	3795	404	63.17	0.66
2565	3835	205	-134.76	-1.42
2565	3875	404	65.04	0.68
2565	3915	329	-8.96	-0.09
2565	3955	283	-53.39	-0.56
2565	3995	335	1.03	0.01
2565	4035	278	-52.51	-0.55
2565	4075	364	38.06	0.40
2565	4115	379	58.75	0.62
2565	4155	268	-45.55	-0.48
2565	4195	523	216.95	2.28
2565	4235	362	63.97	0.67

X feet	Y feet	Resistivity ohm-meters	Resistivity resid	Resistivity Normalized
2565	4275	206	-83.89	-0.88
2565	4315	304	21.88	0.23
2565	4355	256	-19.30	-0.20
2565	4395	233	-37.12	-0.39
2760	3680	596	101.58	1.07
2760	3720	294	-166.89	-1.76
2760	3760	520	87.99	0.93
2760	3800	545	138.17	1.45
2760	3840	269	-115.48	-1.22
2760	3880	340	-24.21	-0.25
2760	3920	311	-34.35	-0.36
2760	3960	366	38.67	0.41
2760	4000	266	-43.67	-0.46
2760	4040	256	-35.98	-0.38
2760	4080	267	-6.99	-0.07
2760	4120	344	88.50	0.93
2760	4160	192	-44.43	-0.47

CATALDO FLATS ELECTRICAL SOUNDING DATA

X feet	Y feet	Z feet	N	IP msec.	Resistivity ohm-m
848	1189	19	1	2.60	176
848	1189	19	2	2.75	71
848	1189	19	3	2.80	47
848	1189	19	4	2.40	45
867	1155	26	1	1.80	255
867	1155	26	2	2.00	129
867	1155	26	3	2.75	75
867	1155	26	4	3.00	55
885	1119	24	1	2.40	262
885	1119	24	2	2.50	94
885	1119	24	3	1.75	55
885	1119	24	4	3.25	51
904	1084	18	1	2.40	99
904	1084	18	2	3.00	40
904	1084	18	3	5.00	34
904	1084	18	4	8.00	33
923	1049	13	1	3.25	34
923	1049	13	2	2.50	29
923	1049	13	3	2.00	32
923	1049	13	4	8.60	34
941	1014	7	1	2.60	28
941	1014	7	2	-2.60	29
941	1014	7	3	3.20	32
941	1014	7	4	2.60	39
960	974	3	1	1.50	28
960	974	3	2	2.40	30
960	974	3	3	2.50	32
960	974	3	4	6.75	35
979	944	0	1	2.20	39
979	944	0	2	1.80	42
979	944	0	3	2.00	48
979	944	0	4	2.00	55

A = 12 meters

X feet	Y feet	N spacing	IP msec.	Resis. ohm-m.
60	0	1	0.5	51
60	0	2	0.3	37
60	0	3	1.5	41
100	0	1	0.4	41
100	0	2	1.2	41
100	0	3	2.25	34
140	0	1	0.6	35
140	0	2	2	30
140	0	3	2.1	38
180	0	1	0.7	25
180	0	2	1.9	27
180	0	3	2.25	34
245	40	1	1.25	24
245	40	2	3	29
245	40	3	2.8	38
275	67	1	0.9	24
275	67	2	2	29
275	67	3	2.25	38
304	94	1	-4.25	22
304	94	2	0.6	29
304	94	3	0.6	35

LABORATORY IP DATA

Distance	Unconta-minated	Zinc Contaminated Samples			Copper Contaminated Samples	
		5 mg/L	20 mg/L	100 mg/L	100 mg/L	1000 mg/L
1	18.0	15.0	14.0	12.5	15.5	13.0
2	18.0	14.0	13.0	12.5	13.5	13.5
3	18.0	14.5	13.0	11.5	13.0	9.0
4	17.5	13.0	13.5	11.5	12.5	7.0
5	15.5	13.0	13.5	12.5	13.0	3.0
6	14.5	13.0	12.5	11.5	11.0	2.5
7	12.0	10.5	13.5	13.5	12.0	4.5
8	14.5	15.5	13.0	12.5	12.0	5.5
9	15.5	14.0	12.0	13.0	13.0	8.5
10	15.0	13.5	12.5	13.0	13.0	14.5
11	15.0	13.5	12.5	13.0	14.0	13.5
12	18.0	14.0	13.0	14.5	14.5	15.0

Lead Contaminated Samples

Distance	5 mg/L	20 mg/L	100 mg/L	1000 mg/L
1	17.0	13.5	16.0	17.8
2	13.0	12.0	15.0	15.0
3	13.0	12.0	13.0	15.5
4	14.0	11.0	14.0	11.5
5	15.0	13.5	14.5	6.0
6	17.0	13.5	14.5	
7	15.5	13.0	14.0	
8	13.5	12.5	14.0	
9	13.0	12.5	13.5	10.0
10	14.0	13.5	13.0	14.5
11	13.5	13.0	10.5	13.5
12	14.0	13.0	10.0	14.3

NORMALIZED IP DATA

Distance	Unconta-minated	Zinc Contaminated Samples			Copper Contaminated Samples	
		5 mg/L	20 mg/L	100 mg/L	100 mg/L	1000 mg/L
1	1.000	0.833	0.778	0.694	0.861	0.722
2	1.000	0.778	0.722	0.694	0.750	0.750
3	1.000	0.806	0.722	0.639	0.722	0.500
4	1.000	0.743	0.771	0.657	0.714	0.400
5	1.000	0.839	0.871	0.806	0.839	0.194
6	1.000	0.897	0.862	0.793	0.759	0.172
7	1.000	0.875	1.125	1.125	1.000	0.375
8	1.000	1.069	0.897	0.862	0.828	0.379

9	1.000	0.903	0.774	0.839	0.839	0.548
10	1.000	0.900	0.833	0.867	0.867	0.967
11	1.000	0.900	0.833	0.867	0.933	0.900
12	1.000	0.778	0.722	0.806	0.806	0.833

Lead Contaminated Samples

Distance	5 mg/L	20 mg/L	100 mg/L	1000 mg/L
1	0.944	0.750	0.889	0.986
2	0.722	0.667	0.833	0.833
3	0.722	0.667	0.722	0.861
4	0.800	0.629	0.800	0.657
5	0.968	0.871	0.935	0.387
6	1.172	0.931	1.000	0.000
7	1.292	1.083	1.167	0.000
8	0.931	0.862	0.966	0.000
9	0.839	0.806	0.871	0.645
10	0.933	0.900	0.867	0.967
11	0.900	0.867	0.700	0.900
12	0.778	0.722	0.556	0.794

LABORATORY APPARENT RESISTIVITY DATA

Distance	Uncontaminated	Zinc Contaminated Samples			Copper Contaminated Samples	
		5 mg/L	20 mg/L	100 mg/L	100 mg/L	1000 mg/L
1	108	118	113	127	98	128
2	121	125	103	132	125	129
3	114	132	110	158	206	93
4	180	163	128	191	157	40
5	110	138	134	111	98	16
6	152	175	116	130	81	12
7	133	129	113	119	78	13
8	132	177	135	178	105	36
9	168	174	147	166	140	89
10	176	174	175	165	142	239
11	150	146	178	140	142	217
12	196	172	185	157	174	182

Lead Contaminated Samples

Distance	5 mg/L	20 mg/L	100 mg/L	1000 mg/L
1	122	123	125	134
2	135	116	170	130
3	135	137	156	153
4	117	135	121	90
5	110	99	93	44
6	114	97	99	

7	105	105	93	
8	134	116	117	
9	147	135	159	340
10	143	142	176	218
11	126	144	174	169
12	163	187	147	184

NORMALIZED APPARENT RESISTIVITY DATA

Distance	Uncontaminated	Zinc Contaminated Samples			Copper Contaminated Samples	
		5 mg/L	20 mg/L	100 mg/L	100 mg/L	1000 mg/L
1	1.000	1.093	1.046	1.176	0.907	1.185
2	1.000	1.033	0.851	1.091	1.033	1.066
3	1.000	1.158	0.965	1.386	1.807	0.816
4	1.000	0.906	0.711	1.061	0.872	0.222
5	1.000	1.255	1.218	1.009	0.891	0.145
6	1.000	1.151	0.763	0.855	0.533	0.079
7	1.000	0.970	0.850	0.895	0.586	0.098
8	1.000	1.341	1.023	1.348	0.795	0.273
9	1.000	1.036	0.875	0.988	0.833	0.530
10	1.000	0.989	0.994	0.938	0.807	1.358
11	1.000	0.973	1.187	0.933	0.947	1.447
12	1.000	0.878	0.944	0.801	0.888	0.929

Lead Normalized Samples

Distance	5 mg/L	20 mg/L	100 mg/L	1000 mg/L
1	1.130	1.139	1.157	1.241
2	1.116	0.959	1.405	1.074
3	1.184	1.202	1.368	1.342
4	0.650	0.750	0.672	0.500
5	1.000	0.900	0.845	0.400
6	0.750	0.638	0.651	0.000
7	0.789	0.789	0.699	0.000
8	1.015	0.879	0.886	0.000
9	0.875	0.804	0.946	2.024
10	0.813	0.807	1.000	1.239
11	0.840	0.960	1.160	1.127
12	0.832	0.954	0.750	0.939

APPENDIX C
ELECTROLYTE CONDUCTIVITY VALUES
FOR
SMELTERVILLE FLATS
from
(Norton, 1980)

SMELTERVILLE FLATS
ELECTROLYTE CONDUCTIVITY DATA
FROM MARCY, 1979

Sample Site Marcy,1979	Ec seimes	Sample Site Marcy,1979	Ec seimes	Sample Site Marcy,1979	Ec seimes
axa	1070	1yb	286	9w	516
	1070		328		337
	1070		385		393
	1070		405		405
	867	2ya	411		600
	949		430		670
	898		421	12w	291
	1020		355		284
	970		365		314
axb	1010		377		296
	806		367		199
	780		400		204
	730	2yb	270		286
1xa	1030		254		337
	1120		278		393
	1140		267		375
	1097		221	13w	481
	938		263		489
	898		302		377
	898		348		449
	1000		395		268
	950	3ya	306		316
1xb	622		311		347
	683		291		405
	485		303		390
	410		221	15w	338
	405		235		345
2xa	989		248		345
	1020		280		343
	1020		298		342
	1010	3yb	315		408
	806		328		449
	796		291		540
	755		311	16w	520
	790		179		592
	750		224		690
2xb	592		277		610
	383		315	17w	367
	340		360		357
	315	5ya	847		377
3xa	630		836		353
	806		561	18w	408
	836		444		530
	757		490		620

Sample Site Marcy,1979	Ec seimes	Sample Site Marcy,1979	Ec seimes	Sample Site Marcy,1979	Ec seime
	326		551		530
	309		580	1p	180
	214		650		207
	210	5yb	316		207
	210		421		198
3xb	1040		520		157
	1100		620		204
	830		730		196
4xa	867	6ya	1000		196
	908		1020		220
	847		1020	2p	530
	874		1013		505
	493		337		530
	490		323		522
	485		428		428
	520		428		592
	435		480		1040
4xb	273		420		1163
	273	6yb	1071		1460
	272		946		1470
	192		1030	3p	765
	208		1016		796
	185		592		755
6xa	571		492		772
	551		724		479
	530		704		887
	551		730		949
	365		730		110
	347	6yd	296		1180
	321		284	4p	1430
	403		303		1350
	323		294		1370
6xb	350		214		1383
	217		176		1061
	122		159		785
	168		190		765
	135		201		959
7xa	411		202		1000
	418		217		1180
	412	7ya	714		1340
	414		714	5p	1040
	314		724		1050
	275		717		1040
	328		457		1043
	311		551		959
	418		581		184
	330		620		184
7xb	173		600		225

Sample Site Marcy,1979	Ec seimes	Sample Site Marcy,1979	Ec seimes	Sample Site Marcy,1979	Ec seime
	173	7yb	745		243
	112		775	10p	1610
	140		765		1570
	103		762		1530
8xa	441		478		1570
	442		612		1438
	441		600		1663
	441		600		1930
	284	8ya	449		1980
	337		461	11p	836
	304		435		836
	413		448		816
	330		306		829
8xb	469		279		592
	194		326	13p	520
	128		321		551
	175		361		600
	120		392		640
9xb	365	8yb	734	18p	163
	356		714		208
	375		745		210
	365		731		220
	238		409	200	354
	268		444		354
	245		439		354
	345		440		354
	255		430		170
9xb	248	8yc	1000		105
	206	9ya	427		133
	150		427		107
	157		427		145
	110		427	201	592
aya	306		329		592
	309		350		602
	320		349		595
	312		368		56
	204		370		201
	286	9yb	570		151
	230		570		170
	297	10ya	359	202	469
	295		376		612
ayb	340		367		683
	350		367		550
	356		260	203	390
	349		262		387
	243		275		390
	355		280		389
	408	10yb	430		107

Sample Site Marcy,1979	Ec seimes	Sample Site Marcy,1979	Ec seimes	Sample Site Marcy,1979	Ec seime
	480		441		108
	530		393		158
1ya	298		421	205	376
	291		277		376
	274		294		376
	288		291		376
	224		312		166
	242		265		102
	255	3w	452		112
	278		439		110
	312		435		136
1yb	406		442	206	375
	375		156		367
	417		154		376
	399		102		373
	248		120		194
			115		105
		5w	352		130
			337		85
			369		135
			353	207	225
			353		227
			367	208	96
			360		149
			390		
			330		
		9w	612		
			612		
			612		
			612		